This manuscript is a preprint and has not been peer reviewed. The copyright holder has made the manuscript available under a Creative Commons Attribution 4.0 International (CC BY) license and consented to have it forwarded to EarthArXiv for public posting.

Title: Trends, cycles and seasonality in rainfall, temperature, NDVI, DMI and SOI in the Greater Mara-Serengeti Ecosystem: Insights for biodiversity conservation

Running title: Trends, cycles and seasonality in climate and vegetation in the Mara-Serengeti

Joseph O. Ogutu[1*], Gundula S. Bartzke[1], Sabyasachi Mukhopadhyay[1,2], Holly T. Dublin[3], Jully S. Senteu[4], David Gikungu[5], Isaiah Obara[6*], Hans-Peter Piepho[1]

[1]University of Hohenheim, Institute of Crop Science, Fruwirthstrasse 23, 70599 Stuttgart, Germany
[3] IUCN ESARO, Wasaa Conservation Centre,12 P.O. Box 68200, Nairobi, Kenya, 00200
[4]University of Groningen, Conservation Ecology group, the Netherlands
[5]Kenya Meteorological Department, Nairobi, Kenya
[6]Freie Universität Berlin, Institute for Parasitology and Tropical Veterinary Medicine and Veterinary Centre for Resistance Research, Department of Veterinary Medicine, Berlin, Germany.

* Corresponding author: jogutu2007@gmail.com; i.b.obara@gmail.com

This manuscript is a preprint and has not been peer reviewed. The copyright holder has made the manuscript available under a Creative Commons Attribution 4.0 International (CC BY) license and consented to have it forwarded to EarthArXiv for public posting.

Abstract

Understanding climate and vegetation trends and variations is essential for conservation planning and ecosystem management. These elements are shaped by regional manifestations of global climate change, impacting biodiversity conservation and dynamics. In the southern hemisphere, global climate change is partially reflected through trends in the hemispheric El Niño-Southern Oscillation (SOI) and regional oscillations such as the Indian Ocean Dipole Mode (DMI). These phenomena influence rainfall and temperature changes, making it crucial to understand their patterns and interdependencies. Appropriately analyzing these variables and their interrelations therefore requires a robust multivariate statistical model, a tool seldom employed to extract patterns in climate and vegetation time series. Widely used univariate statistical methods in this context fall short, as they do not account for interdependencies and covariation between multiple time series. State-space models, both univariate and multivariate, adeptly analyze structural time series by decomposing them into trends, cycles, seasonal, and irregular patterns. Multivariate state-space models, in particular, can provide deeper insights into trends and variations by accounting for interdependencies and covariation but are rarely used. We use both univariate and multivariate state models to uncover trends and variations in historic rainfall, temperature, and vegetation for the Greater Mara-Serengeti Ecosystem in Kenya and Tanzania and potential influences of oceanic and atmospheric oscillations. The univariate and multivariate patterns reveal several insights. For example, rainfall is bimodal, shows significant interannual variability but stable seasonality. Wet and dry seasons display strong, compensating quasi-cyclic oscillations, leading to stable annual averages. Rainfall was above average in both seasons from 2010-2020, influenced by global warming and the Indian Ocean Dipole. The ecosystem experienced recurrent severe droughts, erratic wet conditions and a substantial temperature rise over six decades (3.3 to 4.2 °C). The

This manuscript is a preprint and has not been peer reviewed. The copyright holder has made the manuscript available under a Creative Commons Attribution 4.0 International (CC BY) license and consented to have it forwarded to EarthArXiv for public posting.

insights gained have important implications for developing strategies to mitigate climate change impacts on ecosystems, biodiversity, and human wellfare.

Keywords: Rainfall, minimum and maximum temperatures, Normalized Difference Vegetation Index (NDVI), Indian Ocean Dipole Index (DMI), Southern Oscillation Index (SOI), Mara-Serengeti Ecosystem, univariate and multivariate state-space models.

Introduction

Global climate change and variation are now widely recognized, yet their regional manifestations and consequences for biodiversity conservation and dynamics, especially in the southern hemisphere, are less well understood. In the Southern hemisphere and particularly in East Africa, climate change is primarily manifested through fluctuations in the hemispheric El Niño-Southern Oscillation (SOI), the regional Indian Ocean Dipole Mode (DMI) and local rainfall and temperature variations. It follows that understanding trends and variation in rainfall and temperature and how these are influenced by SOI and DMI is basic to understanding regional consequences of global climate change. While many studies have focused on analyzing individual climatic components using univariate statistical methods, such analyses often overlook the potential interdependencies and covariation among these components. This is evident, for instance, in the extensive univariate research conducted on trends and variation in individual climatic components in the Greater Mara-Serengeti Ecosystem (GMSE) of Kenya and Tanzania (Griffiths and Gwynne 1963; Pennycuick and Norton-Griffiths 1976; Ogutu et al. 2008; Ritchie 2008, Bartzke et al. 2018; Mukhopadhyay et al. 2019, Mahony et al. 2021; Mtewele et al. 2023).

This manuscript is a preprint and has not been peer reviewed. The copyright holder has made the manuscript available under a Creative Commons Attribution 4.0 International (CC BY) license and consented to have it forwarded to EarthArXiv for public posting.

Whereas such univariate analyses can reveal useful and interesting patterns in trends and variation in climatic and vegetation components, they fail to account for the potentially complex interrelationships among climatic and vegetation components. Accounting for interrelationships and covariation between multiple climatic and vegetation components requires using multivariate models for temporal trends and variation. As a result, joint analyses of trends and variation in climatic and vegetation components using multivariate statistical models can reveal insights that go beyond those obtainable from univariate statistical models alone. Multivariate state-space models are a particularly powerful, flexible and useful class of models for joint analysis of trends and variation in multiple time series.

State-space models are especially well suited for analysing trends and variation in time series of climatic and vegetation variables because they decompose such series into intuitively interpretable but unobservable additive components. These include trend (level and slope), cyclical, seasonal and irregular (random) components. The trend component quantifies change, the cycles characterize periodic or quasi-periodic oscillations and can be deterministic and persistent or stochastic and transient whereas the seasonal component defines intra-annual oscillations and can be stable and persistent or time-varying. Yet, despite their intuitive appeal, utility and elegant decomposition of time series of climatic or other variable types into readily understandable components, state-space models have only rarely been used to analyse trends and variation in climatic variables, including for the GMSE (Ogutu et al. 2017; Bartzke et al. 2018; Mukhopadhyay et al. 2019; Moehlman et al. 2020).

Multivariate models for trend and variation in climatic variables can potentially reveal more subtle patterns and insights than can univariate models. For example, bivariate models can better characterize bivariate cycles in weather components, such as rainfall and temperature, which can have widely different impacts on vegetation and animals than can independent

This manuscript is a preprint and has not been peer reviewed. The copyright holder has made the manuscript available under a Creative Commons Attribution 4.0 International (CC BY) license and consented to have it forwarded to EarthArXiv for public posting.

cycles in both components. Moreover, univariate models are less likely to accurately characterize rainfall, temperature and vegetation cycles that are inextricably linked through physical processes that may have confounding interrelationships. For instance, rising air masses driven by heat can generate rainfall due to convection in the upper, cooler layers of the atmosphere (IPCC 2007). But in regions influenced by moisture influx from water bodies such as oceans or large lakes, temperature warming can entail an increase in rainfall (Trenberth and Shea 2005). In contrast, if temperatures increase but moisture influx remains low, for example, under continental weather conditions, prolonged and severe droughts may result (Trenberth and Shea 2005).

The intricate feedback mechanisms among temperature, rainfall and vegetation productivity further complicate their interrelationships, highlighting the importance of allowing for interdepndence and covariation among multiple variables. For example, temperature-driven rain cloud formation enhances the albedo effect, resulting in a greater reflectance of the solar radiation back into space in the daytime (IPCC 2007). Moreover clouds absorb infrared radiation from the Earth's Surface, resulting in higher temperatures predominantly during night time (IPCC 2007). On global scales the cooling effects of clouds predominate (IPCC 2007). Furthermore, the interplay among rainfall, temperature and vegetation can significantly impact plant productivity, rainfall and temperature with potential for both enhancement and reduction under varying conditions (Hoffmann and Jackson 2000; Lotsch et al. 2003; Oyama and Nobre 2004; Trenberth and Shea 2005).

Seasonal cycles, driven by phenomena such as the Intertropical Convergence Zone, also play a crucial role in the African savannas, affecting plant and animal populations and, consequently, biodiversity dynamics and conservation. Seasonal cycles in rainfall and plant productivity are pervasive features of many biomes including African savannas. The seasonal

This manuscript is a preprint and has not been peer reviewed. The copyright holder has made the manuscript available under a Creative Commons Attribution 4.0 International (CC BY) license and consented to have it forwarded to EarthArXiv for public posting.

fluctuations in the African savannas are driven by phenomena such as the movement of the Intertropical Convergence Zone, a belt of rising and convecting air masses around the equator (Brown and Cocheme 1973; Norton-Griffiths et al. 1975). The seasonal oscillations in solar radiation affect evaporation, convection and consequently rainfall, inducing wet and dry phases during the climatic year.

Furthermore, the GMSE is subject to both seasonal and inter-annual cycles of rainfall and temperature, which are critical in shaping the migration patterns of wildlife and the productivity of plant and animal populations. These cycles, varying in length and influenced by oceanic and atmospheric oscillations, can significantly affect the ecosystem's dynamics. In the GMSE, rainfall during the wet season is the major driver of the phenology and synchrony of reproduction in many plant and animal species (Prins and Loth 1988, Ogutu et al. 2014a,b). Seasonality and spatial gradients in rainfall in the GMSE also drive the migration of thousands of wildebeest (*Connochaetes taurinus*), zebra (*Equus quagga*), Thomson's gazelle (*Eudorca thomsoni*) and eland (*Tautragus oryx*) that track the rainfall-mediated vegetation greening to feed, give birth and raise their young (Pennycuick 1975, Musiega and Kazadi 2004, Boone et al. 2006, Holdo et al. 2010). The wet season rainfall generates most of the annual forage production but the dry season rainfall is indispensable for the survival of plants and animals in times of resource limitations (Sinclair 1975; Boutton et al. 1988a,b). Failure of the dry season rainfall is thus associated with severe food scarcity and elevated herbivore mortality (Mduma et al. 1999, Dublin and Ogutu 2015, Ogutu et al. 2017, Moehlmann et al. 2020). Cyclic relationships have also been established between rainfall and population dynamics (Ogutu and Owen-Smith 2005) and fecundity and fertility (Ogutu et al. 2014b, Ogutu etal. 2015) of African savanna ungulates. Oscillations in rainfall, temperature and

This manuscript is a preprint and has not been peer reviewed. The copyright holder has made the manuscript available under a Creative Commons Attribution 4.0 International (CC BY) license and consented to have it forwarded to EarthArXiv for public posting.

vegetation can therefore strongly influence plant and animal population dynamics, with important implications for biodiversity dynamics and conservation in savannas.

In addition to seasonal cycles, inter-annual rainfall cycles can exert major impacts on the productivity of plant and animal populations (Mills et al. 1995; Ogutu and Owen-Smith 2005). The dominant inter-annual rainfall cycle periods in East Africa typically range from 2 to 13 years but can vary markedly in space and time (Ogallo 1982, 1984, Nicholson 2000, McHugh 2006, Ogutu et al. 2017; Bartzke et al. 2018; Moehlmann et al. 2020). Thus, wet and dry phases can last as long as 10 to 20 years (Omondi et al. 2013). For minimum and maximum temperatures, cycle periods can range between 2 and 30 years (King'Uyu et al. 2000). In the GMSE in particular, dominant rainfall cycles have time-varying periods ranging between 3 and 10 years (Pennycuick and Norton-Griffiths 1976; Bartzke et al. 2018). Signals have also been detected with longer but weaker cycles with periods spanning 20 to 40 years (Pennycuick and Norton-Griffiths 1976) and 15-25 years (Prins and Loth 1988). The cycle periods are likely related to hemispheric oceanic and atmospheric oscillations that operate on time scales of less (SOI, DMI) or more (Atlantic Multidecadal Oscillation-AMO) than a decade (Behera et al. 2005, Knight et al. 2006). The oscillations are largely driven by variations in sea surface temperatures in the Indian (Saji et al. 1999), Pacific (Indeje and Semazzi 2000) and Tropical Atlantic (Mwale and Gan 2005) Oceans.

Here, we use historic station rainfall and station temperature and remotely sensed vegetation data, indexed by the Normalized Difference Vegetation Index (NDVI), to build state-space models. These models aim to detect and quantify trends and oscillations in weather and vegetation components in the GMSE. Moreover, we explore the potential influences of oceanic and atmospheric oscillations indexed by the DMI and the SOI, on regional rainfall and temperature trends and variation. As well, we test if rainfall seasonality is stable or

This manuscript is a preprint and has not been peer reviewed. The copyright holder has made the manuscript available under a Creative Commons Attribution 4.0 International (CC BY) license and consented to have it forwarded to EarthArXiv for public posting.

changing over time. We use both univariate and multivariate state-space models to uncover individual and joint trends and variation in the climatic and vegetation components and interpret their implications for biodiversity dynamics and conservation in the GMSE.

The Data

The data set includes time series of SOI (1913-2020), DMI (1913-2020), as well as average monthly minimum and maximum temperatures (1960-2020) and total monthly rainfall (1913-2020) recorded in Narok Town, southwestern Kenya. The average monthly minimum and maximum temperatures are daily records averaged for each month. The rainfall and temperature data were provided by the Kenya Meteorological Department (KMD). Each digital record of Narok Town's total monthly rainfall from April 1913 to December 2020 was cross-checked against the corresponding original, handwritten monthly data cards and ledger book from the Narok Meteorological Station. This verification process detected numerous errors in the initial digital data set from the KMD, which were subsequently corrected with KMD's assitance. Consequently, the total monthly rainfall data set for Narok Town presented here is the most accurate for the 1913-2020 period. However, the temperature data could not be similarly verified due to the unavailability of the original records. Station rainfall data were also available for 15 rain gauges in the Masai Mara Ecosystem for the various recording periods from January 1965 to August 2020. We also analyse total monthly rainfall series recorded at Seronera in the Serengeti National Park (January 1981 –December 2015) and at Ngorongoro Conservation Area Authority Headquarters (January 1963-December 2014) in northern Tanzania. We tried to verify these digital records against original paper records, but most original records were unavailable for both stations.

This manuscript is a preprint and has not been peer reviewed. The copyright holder has made the manuscript available under a Creative Commons Attribution 4.0 International (CC BY) license and consented to have it forwarded to EarthArXiv for public posting.

The SOI and DMI data sets were downloaded from http://stateoftheocean.osmc.noaa.gov/sur/. The SOI is a standardized index calculated from the observed sea level pressure differences between Tahiti and Darwin, Australia. It tracks large-scale fluctuations in sea surface air pressure across the western and eastern tropical Pacific, reflecting the state of the Southern Oscillation during El Niño and La Niña episodes. El Niño, the oscillation's warm phase, is typically associated with increased rainfall, whereas La Niña, the cold phase, often correlates with droughts in East Africa (Ogutu et al. 2008; https://www.climate.gov/enso). The SPOT NDVI data set covered 1998 to 2014 because the CHIRPS (2017) blended station-satellite minimum temperature data used in the multivariate model ended in December 2013. The multivariate model involving SPOT NDVI used the CHIRPS minimum and maximum temperature and rainfall data (predcited using spatio-temporal hierarchical Bayesain state space model, Mukhopadhyay et al. 2019) averaged over a 5 × 5 km grid in Narok County. All the data sets used in the analyses are available in S1-S8 Datas in the supplementary materials.

State-space models for trends and variation in climate and vegetation

The unobserved components model (UCM) for univariate time series

We applied the unobserved components model (UCM) to analyse trends in univariate time series of SOI and DMI from 1913 to 2020, as well as the average monthly minimum and maximum temperatures in Narok Town from 1960 to 2020. Unlike these four variables, rainfall data was previously subjected to UCM modelling for univariate time series in Bartzke et al. (2018). Therefore, we do not repeat the univariate state space analysis for rainfall in this study but instead consider aspects of the rainfall data not covered in that paper.

This manuscript is a preprint and has not been peer reviewed. The copyright holder has made the manuscript available under a Creative Commons Attribution 4.0 International (CC BY) license and consented to have it forwarded to EarthArXiv for public posting.

The UCM is a useful method for analysing temporal variations in univariate time series, which consist of observations collected at regular time intervals. This structural time series technique decomposes the series into easily interpretable additive components, including level, slope, cyclical, seasonal and irregular components. The level and slope components together form the trend component, while the irregular component represents the model's overall random error, typically modelled as a white-noise process or an autoregressive moving average (ARMA) process. The UCM's versatility and power lie in its ability to accommodate multiple cyclical components, serial autocorrelation in the residuals or auto-regression terms for the dependent variable. The parameters for the components can be fixed or time-varying, allowing considerable flexibility. In addition, the model supports explanatory covariates and handles missing values embedded in the dependent variable. But, our UCM model does not permit missing values in predictor variables.

The relationship between covariates and the dependent variable can be linear and time-invariant, linear and time-varying (random regression) or nonlinear (spline regression). Using the UCM modelling approach we searched for two main types of changes, namely additive outliers (AO) and level shifts (LS). An additive outlier is an unusual value in the series, possibly due to a data recording error or a temporary shock to the series generation process. By contrast, a level shift is a permanent shift, upward or downward shift, in the series' level. We examine different aspects of the outliers and level shifts, most notably their standard errors and statistical significance at all the time points in the series, with particular emphasis on those that are statistically significant.

This manuscript is a preprint and has not been peer reviewed. The copyright holder has made the manuscript available under a Creative Commons Attribution 4.0 International (CC BY) license and consented to have it forwarded to EarthArXiv for public posting.

We consider several special cases of the UCM including the 1) Random Walk Model, 2) Local Linear Trend Model, 3) Integrated Random Walk Model, 4) Random Walk With Drift and 5) Damped Local Linear Trend Model. The Random Walk Model consists of a stochastic or time-varying level trend component. The Local Linear Trend Model consists of both a random walk level trend and a random walk slope. The Integrated Random Walk Model, a special case of the Local Linear Trend Model, sets the disturbance variance of the level component to zero. The Random Walk With Drift is smilar to the Local Linear Trend Model, but with a constant slope, as the disturbance variance of the slope component is zero. Lastly, the Damped Local Linear Trend Model, akin to the Local Linear Trend Model, has a slope following a first-order autoregressive model (Harvey 1989, 2001, SAS UCM 15.2).

A general unobserved components Model (UCM) can be expressed as

$$r_t = \mu_t + \varphi_t + \delta_t + \partial_t + \sum_{i=1}^{p} \theta_i r_{t-i} + \sum_{j=1}^{m} \beta_j x_{jt} + \epsilon_t;\ t = 1,2,\ldots,T \quad (1)$$

where

r_t = rainfall (SOI, DMI, minimum or maximum temperature) at time t (with a maximum value T)

μ_t = level or time trend component

φ_t = cyclical component

δ_t = seasonal component

∂_t = autoregressive component

$\sum_{i=1}^{p} \theta_i r_{t-i}$ = autoregressive regression terms

β_j = regression coefficients

x_{jt} = regression covariates

This manuscript is a preprint and has not been peer reviewed. The copyright holder has made the manuscript available under a Creative Commons Attribution 4.0 International (CC BY) license and consented to have it forwarded to EarthArXiv for public posting.

$\epsilon_t \sim iidN(0,\sigma_\epsilon^2)$, i.e., a Gaussian white noise process.

We selected the best-supported model from the preceding five basic UCM models (1 to 5), considering the level and slope (both modelling time trends), cycles, seasonality, auto-regression, white noise and possibly auto-correlated residuals. The UCM assumes normal distributions for both the univariate dependent series and all the disturbance variances. The UCM model fitting is accomplished using the Diffuse Kalman Filtering and Smoothing algorithm, with parameters estimated using maximum likelihood (De Jong and Chu-Chun-Lin, 2003). We fitted the univariate UCM models to the SOI, DMI and average monthly minimum and maximum temperature series for Narok Town using the SAS UCM procedure (SAS Institute 2022).

Multivariate (General) state space models for trend and variation in climatic or other variables

The UCM is a special case of the general state space model which can be formulated in the general form as follows (SAS SSM 15.2).

$R_t = Z_t\alpha_t + X_t\beta + \varepsilon_t$ Observation equation (2)

$\alpha_{t+1} = T\alpha_t + W_{t+1}\gamma + c_{t+1} + \eta_{t+1}$ State transition Equation

$\alpha_1 = c_1 + A_1\delta + W_1\gamma + \eta_1$ Initial condition

R_t is a $p_t \cdot q$ response vector $r = (r_1,r_2,r_3,\ldots,r_q)$

This manuscript is a preprint and has not been peer reviewed. The copyright holder has made the manuscript available under a Creative Commons Attribution 4.0 International (CC BY) license and consented to have it forwarded to EarthArXiv for public posting.

The states α_t and the observation disturbances ε_t are random sequences

$\eta_t \sim N(0,Q_t)$ is the state disturbance and is independent of $\varepsilon_t \sim N\left(0,\left(\sigma_{t,1}^2,\ldots\right)\right)$

$\delta \sim N(0,\kappa\Sigma),\kappa \longrightarrow \infty$

We use the general state space model to simultaneously analyse trends, cyclical and seasonal variation in multivariate time series of two or more of the climatic and vegetation variables. A detailed exposition of the general state space model is beyond the scope of this paper, so we will focus on its key features relevant to our multivariate time series analyses. The general state space model offers the following features that generalize the capabilities of the univariate UCM model. (1) Multivariate trends, possibly correlated, among the individual series, including multivariate random walk, multivariate local linear trend, etc. (2) Multivariate cycle, possibly correlated, among the individual series. (3) Multivariate season, possibly correlated, among the individual series. (4) Multivariate white noise, possibly correlated, among the individual series, including (multivariate) vector autoregressive moving average (VARMA) models. (5) Can handle either univariate or multivariate data collected at irregular (longitudinal data) or regular (time series data) intervals. (6) Supports univariate continuous time cycle for univariate regular and irregular data. (7) Can accommodate complex nonlinear relationships between the dependent and the explanatory series. (8) Can identify outliers and level shifts and provide the corresponding standard errors and statistical significance at each time point.

We consider only multivariate versions of the basic models, including the Random Walk Model, Local Linear Trend Model, Integrated Random Walk Model, Random Walk Model with fixed slope and Damped Local Linear Trend Model, to select the best supported candidate model.

This manuscript is a preprint and has not been peer reviewed. The copyright holder has made the manuscript available under a Creative Commons Attribution 4.0 International (CC BY) license and consented to have it forwarded to EarthArXiv for public posting.

The general state space model assumes the multivariate dependent series follow a multivariate normal distribution. The general state space model is fitted using the Diffuse Kalman Filtering and Smoothing algorithm (De Jong and Chu-Chun-Lin, 2003) and maximum likelihood is used to estimate the model parameters. We fitted the multivariate state space models in the SAS SSM procedure (SAS Institute 2023), and all SAS program codes used to fit both the UCM and SSM models are included in the Supplementary materials to this paper.

We performed the following analyses. (1) Univariate unobserved components model analysis or structural time series analysis of the (*i*) SOI, (*ii*) DMI, (*iii*) average monthly minimum and (*iv*) average monthly maximum temperatures recorded at the Narok Meteorological Station in Narok Town located in Narok County in Southwestern Kenya. This extends our previous work, which only covered rainfall time series analysis (Bartzeke et al. 2018). (2) Bivariate state space model analyses of trends and cycles in the wet and dry season rainfall components in Narok Town and in the Masai Mara Ecosystem in Kenya, Ngorongoro Crater and Seronera in Serengeti National Park in Tanzania. (3) Bivariate state space analyses of trends, cycles and seasonality in Narok Town's average monthly minimum and maximum temperatures. (4) Trivariate state space models of trends, cycles and seasonality in Narok Town's average monthly minimum and maximum temperatures and total monthly rainfall. (5) Trivariate state space model analyses of trends, cycles and seasonality in SOI, DMI and total monthly rainfall for Narok Town, Masai Mara Ecosystem, Ngorongoro Crater and Seronera. (6) Pentavariate state space model analyses of trends, cycles and seasonality in average monthly minimum and maximum temperatures and total monthly rainfall in Narok Town, SOI and DMI. (7) Tetravariate state space model analysis for trends, cycles and seasonality in monthly averages of SPOT NDVI, average monthly minimum and maximum temperatures and total monthly rainfall.

This manuscript is a preprint and has not been peer reviewed. The copyright holder has made the manuscript available under a Creative Commons Attribution 4.0 International (CC BY) license and consented to have it forwarded to EarthArXiv for public posting.

Results

Univariate Trends and Variation in station rainfall and temperature in Masai Mara Ecosystem and Narok Town of Kenya

Temporal trend and variation in monthly, seasonal and annual rainfall in Masai Mara

Rainfall in the Mara is distinctly bimodal, with a minor peak in December during the short rains (November-December) and a major peak in April during the long rains (January-June). The average total monthly rainfall during the dry season (July-October) was 57.1 ± 35.2 mm (range: 52.4 to 61.7 mm), significantly lower than the wet season months spanning November-June, which averaged 106.1 ± 62.4 mm (range: 99.8 to 111.0 mm, Fig 1a).

Rainfall seasonality is remarkably stable in the Mara despite striking temporal variation (Fig 1b). The Mara's seasonal and annual rainfall components demonstrate strong and sustained quasi-cyclic oscillations in both the wet and dry season components (Figs 1c-f). Typically, variation in the wet and dry season components are compensatory such that high dry season rainfall is associated with low wet season rainfall and vice versa, maintaining a rather stable average annual rainfall of about 1000 mm. However, from 2010 to 2020, both components were unusually in phase and above average, leading to wetter conditions more favourable for agriculture and livestock ranching (Fig 1e). This mirrors the extended and intensified phase of the 6-10-year local rainfall cycle, amplified by the Indian Ocean Dipole and global warming influences (Fig 1h). The high dry season rainfall during 2003-2020 mirrors patterns last seen

This manuscript is a preprint and has not been peer reviewed. The copyright holder has made the manuscript available under a Creative Commons Attribution 4.0 International (CC BY) license and consented to have it forwarded to EarthArXiv for public posting.

in the mid-1970s, while the high wet season rainfall is unprecedented in the last half-century and is therefore rare and transient. Notably, the wet season rainfall trended upwards between 2003 and 2020 (Fig 1c).

Despite the increase in rainfall during 2010-2020, droughts are frequent and intense in the Mara (Fig 1g). The droughts are associated with strong interannual variations in the annual and seasonal rainfall components. During 1965-2020, the total annual rainfall averaged 1062.4 ± 193.4 mm (range: 653.4 to 1506 mm). The wet season rainfall averaged 845.6 ± 196.7 mm (range: 500.7 to 1243.5 mm), whereas the dry season rainfall averaged 228.1± 79.0 mm (range: 100.0 to 465.8 mm) (Fig 1 c-f). Temporal variation in the annual and seasonal rainfall exhibited quasi-periodic cycles, with estimated cycle periods of about 3 years for the annual, wet and dry season components (Fig 1i). Based on the annual rainfall, extreme droughts occurred in 1982, 1984, 1993, 1997, 1999 and 2006 and severe droughts in 1967, 1969, 1972, 1973, 1976, 1985-1986 and 1997. In contrast, very wet to extremely wet years were 1974, 1998, 2001, 2007, 2012, 2016 and 2018 (Fig 1g).

Fig 1. a) The distribution of the total monthly rainfall (mean ± 1SD = 89.5 ± 59.4 mm) across months in the Masai Mara Ecosystem of Kenya averaged over 1965-2020. b) The decadal averages of the total monthly rainfall. The interannual variations in standardized deviates of the c) wet season rainfall (845.6 ± 196.5 mm), d) dry season rainfall (228.1 ± 79.0 mm), e) wet and dry season rainfall and f) annual rainfall (1062.4 ± 193.4 mm). The vertical needles are the standardized deviates, the solid curves are the 3-year moving averages and the dashed horizontal lines are percentiles of the frequency distributions of the rainfall deviates. g) Percentiles of the total annual, dry and wet season rainfall components used to classify years or seasons as extreme (≤ 10%), severe (10-25%) or moderate (25-40%) drought years

This manuscript is a preprint and has not been peer reviewed. The copyright holder has made the manuscript available under a Creative Commons Attribution 4.0 International (CC BY) license and consented to have it forwarded to EarthArXiv for public posting.

(seasons), normal (40-75%), wet (75-90%), very wet (90-95%) or extremely wet (95-100%) years (seasons). h) Temporal variation in the original (blue vertical needles) and smoothed (red solid curve, smoothing done using generalized semiparametric mixed model) total monthly rainfall in Masai Mara from 1965 to 2020. I) Spectral density versus period of cycles (in years) for the annual, wet and dry season rainfall components. A large value of spectral density means strong evidence for the corresponding cycle period.

Temporal trend and variation in monthly, seasonal and annual rainfall in Narok Town

Rainfall in Narok was distinctly bimodal, with a minor peak in December during the short rains (November-December) and a major peak in April, during the long rains (January-May). The total monthly rainfall during 1913-2020 averaged 61.5 ± 64.1 mm (range: 0- 419.6 mm) (Fig 2a). Decadal averages of the total monthly rainfall reveal a striking stability in rainfall seasonality over the last century (Fig 2b). The monthly, wet and dry season rainfall components all showed marked interannual variations. The wet season component averaged 620.4 ±229.3 mm (range: 256.9 to 1396.8 mm), the dry season total averaged 119.8 ±57.8 mm (range: 10.7-333.6 mm). The average total annual rainfall was 734.5 ± 232.0 mmm (range: 341.5 to 1602.3 mm) (Fig 2c-f, h).

The seasonal rainfall components showed quasi-cyclic oscillations, with approximate cycle periods of 5.3 years for the wet season and annual rainfall and 2.2 years for the dry season. The wet season rainfall increased from 1914 to 1974 and then declined. Overall, the wet and dry season rainfall totals were below average for extended periods but above average at other times during 1913-2020 (Fig 2c-f, i). Classification of the 107 years into dry and wet years using quantiles of the frequency distribution of the annual and seasonal rainfall totals

This manuscript is a preprint and has not been peer reviewed. The copyright holder has made the manuscript available under a Creative Commons Attribution 4.0 International (CC BY) license and consented to have it forwarded to EarthArXiv for public posting.

identified many extreme (1918, 1924, 1933, 1934, 1938, 1943, 1949, 1953, 1976, 1984 and 2000) and severe (1915, 1928, 1929, 1941, 1944, 1946, 1948, 1961, 1965, 1986, 1991, 1992, 1999, 2005, 2009 and 2019) drought years, a few very wet (1917, 1942, 1957, 1963 and 1978) and extremely wet (1930, 1962, 1964, 1998 and 2003) years (Fig 2g). This demonstrates droughts are recurrent and often severe or extreme in Narok.

Fig 2. The distribution of the total monthly rainfall (mean ± 1SD = 61.5 ± 64.1 mm) across months in the Narok Town of Kenya averaged over 1913-2020. b) The decadal averages of the total monthly rainfall. The interannual variations in standardized deviates of the c) wet season rainfall (620.4 ± 230.3 mm), d) dry season rainfall (119.0 ± 58.0 mm), e) wet and dry season rainfall and f) annual rainfall (734.5 ± 233.0 mm). The vertical needles are the standardized deviates, the solid curves are the 5-year moving averages for the annual and wet season rainfall and 2-years for the dry season and the dashed horizontal lines are percentiles of the frequency distributions of the rainfall deviates. g) Percentiles of the total annual, dry and wet season rainfall components used to classify years or seasons as extreme (≤ 10%), severe (10-25%) or moderate (25-40%) drought years (seasons), normal (40-75%), wet (75-90%), very wet (90-95%) or extremely (95-100%) wet years (seasons). h) Temporal variation in the original (blue vertical needles) and smoothed (red solid curve, smoothing done using generalized semiparametric mixed model) total monthly rainfall in Narok Town. I) Spectral density versus period of cycles (in years) for the annual, wet and dry season rainfall components. A large value of spectral density indicates strong evidence for the corresponding cycle period.

Temporal trend and variation in station temperature in Narok Town of Kenya

This manuscript is a preprint and has not been peer reviewed. The copyright holder has made the manuscript available under a Creative Commons Attribution 4.0 International (CC BY) license and consented to have it forwarded to EarthArXiv for public posting.

Monthly temperatures are rising in Narok Town, particularly the minimum component, which increased markedly from 7.1 °C (95% CL: 6.6 to 7.5 °C) in July 1960 to 11.3 °C (95% CL: 10.4 to 12.3 °C) in July 2020. It initially rose from 7.1 °C in January 1960 to 11.4 °C in May 1967 and then decreased steadily to a global low of 3.3 °C in September 1973. Thereafter, it increased persistently, reaching 11.3 °C in July 2020. This represents a rise of 4.2 °C over the six decades from 1960 to 2020 (Fig 2). Concurrently, the monthly maximum temperature varied widely, rising above average (25 °C), when the minimum temperature dropped to the lowest levels and showing a more stable average thereafter (Fig 2). The monthly minimum temperature averaged across all the months in each season increased consistently over time, rising in the wet season from 8.0 °C in 1960 to 12.2 °C in 2020 and in the dry season from 7.8 °C in 1960 to 11.1 °C in 2020. Similarly, the monthly maximum temperature increased persistently in the wet season from 25.1 °C in 1960 to 26.1 °C in 2020 and in the dry season from 23.1 °C in 1960 to 24.1 °C in 2020 (Fig 3).

Fig 3. Trend in average monthly maximum temperatures (cadet blue points) during the dry (left panel) and wet (right panel) seasons in Narok Town, Kenya, from 1960 to 2020. The red solid curve is the penalized spline smoothed temperature trend whereas the golden band is the approximate 95% pointwise confidence band.

Univariate unobserved components model analysis of the SOI series

The SOI values for the 1295 months spanning January 1913-November 2020, with no missing values, averaged -0.08063 ± 1.08358 (1 SD, range -3.46 to 4.07). The best UCM model for

This manuscript is a preprint and has not been peer reviewed. The copyright holder has made the manuscript available under a Creative Commons Attribution 4.0 International (CC BY) license and consented to have it forwarded to EarthArXiv for public posting.

the trend in the SOI series included a stochastic level, cycle and irregular components. S1 Table shows the fit statistics for this model, including an adjusted r^2= 0.4189.

The residual statistics for the UCM model fit to the SOI time series (S1 Fig) and the flat loess (locally weighted least squares) smoothed residuals (S2 Fig) suggest a reasonable model fit. The estimated model parameters, the associated standard errors and t-tests of the hypothesis that a given estimate is equal to zero are provided in Table 1a. The t-tests show that the disturbance variance of the level component is not significant but that the error variances for the longer cycle and irregular components are, indicating that the latter two components are stochastic. Generally, the t-values reported in all the tables of parameter estimates for the univariate UCMs are approximations and their accuracy is conditional on the validity of the model, the nature of the model and the length of the observed series. The distributional properties of the maximum likelihood estimate of the general UCMs are yet to be fully studied. As a result, the probability values that correspond to a t distribution ought to be interpreted cautiously, as they can be potentially misleading, especially for parameters near the boundary of the parameter space (Harvey 1989, 2001). For certain parameters, such as the cycle period, the t-values in the UCM parameter estimates are uninformative because it is

This manuscript is a preprint and has not been peer reviewed. The copyright holder has made the manuscript available under a Creative Commons Attribution 4.0 International (CC BY) license and consented to have it forwarded to EarthArXiv for public posting.

never necessary to compare the estimated parameter with zero. In such cases, both the *t* values and their probability values should be simply disregarded.

The estimated cycle period is 29.4 months (2.5 years) for cycle 1 and 63.1 months (5.3 years) for Cycle 2. Towards the end of the estimation span, the chi-square tests with approximate p-values indicates the irregular, level and both cycle components are insignificant (Table 1b).

Table 1a. The Southern Oscillation Index (SOI) parameter estimates from the univariate UCM.

Model Component	Parameter	Estimate	Standard Error	t Value	Approx Pr >|t|
Irregular	Error Variance	0.41495	0.02734181	15.18	<0.0001
Level	Error Variance	0.00000283	0.00004249	0.07	0.947
Cycle_1	Damping Factor	0.99489	0.00534378	186.18	<0.0001
Cycle_1	Period	29.35667	0.72861947	40.29	<0.0001
Cycle_1	Error Variance	0.00077068	0.00051467	1.5	0.1343
Cycle_2	Damping Factor	0.9182	0.01720422	53.37	<0.0001
Cycle_2	Period	63.05988	12.6914084	4.97	<0.0001
Cycle_2	Error Variance	0.10819	0.01473964	7.34	<0.0001

This manuscript is a preprint and has not been peer reviewed. The copyright holder has made the manuscript available under a Creative Commons Attribution 4.0 International (CC BY) license and consented to have it forwarded to EarthArXiv for public posting.

Table 1b. Southern Oscillation Index (SOI) components significance tests. These are tests of the significance of each component at the end of the estimation span.

Component	Degrees of Freedom	Chi-Square	Approx Pr > Chi-Square
Irregular	1	0.38	0.5365
Level	1	1.03	0.3100
Cycle1	2	1.01	0.6039
Cycle2	2	1.47	0.4797

The SOI series showed a gradually decreasing albeit insignificant level trend (Fig 4a), an insignificant cycle with a period of 2.5 years(Fig. 4b) and stochastic oscillations with an estimated cycle period of 5.3 years (Fig. 4c). The level trend decreased persistently from 1913 to 1990 before levelling off between 1990 and 2020. Both cycles are quasi-periodic and characterized by time-varying amplitudes and phases. The smoothed level trend component superimposed on the observed SOI series (Fig. 4d) shows the slight but apparently insignificant declining trend in SOI during 1913-2020.

Fig 4a. Smoothed level trend component for the Southern Oscillation Index (SOI) series.

Fig 4b. Smoothed cycle 1 component (high frequency cycle) for the Southern Oscillation Index (SOI) series with a cycle period of 2.5 years (29.4 months).

This manuscript is a preprint and has not been peer reviewed. The copyright holder has made the manuscript available under a Creative Commons Attribution 4.0 International (CC BY) license and consented to have it forwarded to EarthArXiv for public posting.

Fig 4c. Smoothed cycle 2 component (low frequency cycle) for the Southern Oscillation Index (SOI) series with a cycle period of 5.3 years (63 months).

Fig 4d. Smoothed level trend superimposed on the Southern Oscillation Index (SOI) series.

Univariate unobserved components model analysis of the Indian Ocean Dipole Mode Index (DMI)

Likewise to the SOI, we analysed 1298 records of the DMI, with no missing values, covering January 1913 to February 2021. The DMI values averaged -0.07991± 0.33598 (1SD, range (range -1.461 to 1.402). The UCM model fit to the DMI time series has an adjusted $r^2 =$ 0.56209 (S2 Table). The residual diagnostics plots (S3 Fig) and the almost perfectly flat loess smoothed residuals for DMI (S4 Fig further support a good model fit. The parameter estimates for the UCM model components comprising level, slope, cycle and autoregressive irregular components (Table 2a) and their t-tests show that the disturbance variances of the cyclical component and the autoregressive irregular component are significant and that the cycle is stochastic. But the error variances of the level and slope components are insignificant (Table 2a), suggesting they are deterministic.

Table 2a. The Dipole Model Index (DMI) Parameter estimates.

This manuscript is a preprint and has not been peer reviewed. The copyright holder has made the manuscript available under a Creative Commons Attribution 4.0 International (CC BY) license and consented to have it forwarded to EarthArXiv for public posting.

Component	Parameter	Estimate	Standard Value	Error	t	Approx Pr >|t|
Irregular	Error Variance	0.00307	0.00281208		1.09	0.2752
Level	Error Variance	2.90E-10	1.15E-07		0	0.9980
Slope	Error Variance	3.17E-10	4.29E-10		0.74	0.4604
Cycle	Damping Factor	0.74997	0.03002805		24.98	<0.0001
Cycle	Period	32.03793	8.49710533		3.77	0.0002
Cycle	Error Variance	0.0417	0.00321307		12.98	<0.0001

However, towards the end of the estimation span of the DMI series, the level, slope and cyclical components become significant, indicating that the level and slope are deterministic and significant (Table 2b). This signifies that both the level and slope components, which characterize the time trend in the DMI, exhibit significant and deterministic variation over time. This deterministic time trend is coupled with a significant stochastic cycle (Table 2b).

Table 2b. The Dipole Mode Index (DMI) Components significance tests.

Component	Degrees of Freedom	Chi-Square	Approx Pr >Chi-Square
Irregular	1	0.05	0.8313
Level	1	13.2	0.0003
Slope	1	5.4	0.0202
Cycle	2	1.81	0.4043

This manuscript is a preprint and has not been peer reviewed. The copyright holder has made the manuscript available under a Creative Commons Attribution 4.0 International (CC BY) license and consented to have it forwarded to EarthArXiv for public posting.

The smoothed level component reveals a significant and persistent curvilinear increase in the DMI from 1913 to 2021 (Fig 5a). Similarly, the smoothed slope component also suggests a progressive increase in the DMI from 1913 to 1990, followed by a deceleration and levelling off of the rate of increase (Fig 5b).

Fig 5a. Smoothed level trend component for the Indian Ocean Dipole Mode Index (DMI) series.

The smoothed cyclical component reveals a stochastic cycle with a period of 2.7 years (32 months), time-varying amplitude and phase (Fig 5c).

Fig 5b. Smoothed slope component for the Indian Ocean Dipole Mode Index (DMI) series.

The smoothed level trend component superimposed on the DMI series confirms the curvilinear increase in the DMI values between April 1913 and February 2021 (Fig. 5d).

Fig 5c. Smoothed cycle component for the Indian Ocean Dipole Mode Index (DMI) with a cycle period of 2.7 years (32 months).

Fig 5d. Smoothed trend superimposed on to the Indian Ocean Dipole Mode Index (DMI) series.

This manuscript is a preprint and has not been peer reviewed. The copyright holder has made the manuscript available under a Creative Commons Attribution 4.0 International (CC BY) license and consented to have it forwarded to EarthArXiv for public posting.

Univariate unobserved components model analysis of the average monthly minimum temperature for Narok Town, Kenya

The 726 records of average monthly minimum temperature or Narok Town from January 1960 to June 2020 averaged 9.172 ± 2.2782 °C (±1 SD, range 0.3 to 17.4 °C). The UCM model has an adjusted r^2= 0.70279, which together with other metrics, indicate a good model fit to the minimum temperature series (S3a Table).The residual diagnostics and loess smoothed prediction error plots further support the plausibility of the selected model (S5 and S6 Figs). The components of the selected UCM model consist of a stochastic level, a deterministic slope, two stochastic cycles, a deterministic 12-month seasonal component and autoregressive errors. The t-tests confirm that all the parameters for all the model components except the slope and the seasonal components are significant and stochastic (S3b Table). Furthermore, chi-square tests of the parameter estimates towards the end of the estimation span show that the level, slope and seasonal components are significant but deterministic (S3c Table). The estimated cycle period for the subsidiary stochastic cycle (cycle1) is 2.4 years (28.5 months) whereas that for the primary cycle (cycle2) is 13.9 years (167.3 months).

The smoothed level component reveals a striking linear increase in the average monthly minimum temperature by about 4.5 °C from 7.2 °C in January 1960 to 11.7 °C in July 2020. This equates to an average increase of 0.74 °C per decade (Fig 6a). Unlike the level component, the smoothed slope component is best represented by a constant throughout the estimation span (Fig 6b).

This manuscript is a preprint and has not been peer reviewed. The copyright holder has made the manuscript available under a Creative Commons Attribution 4.0 International (CC BY) license and consented to have it forwarded to EarthArXiv for public posting.

Figure 6a. Smoothed level trend component for the average monthly minimum temperature for Narok Town, Kenya.

Figure 6b. Smoothed slope component for the average monthly minimum temperature for Narok Town, Kenya.

The subsidiary cycle (cycle1) exhibits high irregularity, with small-amplitude oscillations interrupted by short-term, large-amplitude pulses. The oscillations also have a widely time-varying phase (Fig 6c). A notable feature of the primary cycle is a remarkable drop in the minimum temperature by over 4 °C around the mid-1970s (Fig 6d). The cause of this drop, whether solely due to natural temperature variation or other factors, remains uncertain. The overlaid smoothed trend on the observed series further reinforce the strong linear increase in the minimum temperature through time in Narok Town (Fig 6e).

Fig 6c. Smoothed primary cycle component (cycle1) with a period of 2.4 years (28.5 months) for the average monthly minimum temperature for Narok Town, Kenya.

Fig 6d. Smoothed secondary cycle component (Cycle 2) with a period of 14.0 years (167.3 months) for the average monthly minimum temperature for Narok Town, Kenya.

Fig 6e. Smoothed trend superimposed over the observed average monthly minimum temperature series for Narok Town, Kenya.

This manuscript is a preprint and has not been peer reviewed. The copyright holder has made the manuscript available under a Creative Commons Attribution 4.0 International (CC BY) license and consented to have it forwarded to EarthArXiv for public posting.

Univariate unobserved components model analysis of the average monthly maximum temperature for Narok Town, Kenya

The maximum temperature series for Narok Town, comprising monthly averages of daily records, spans 726 months from January 1960 to June 2020. The maximum temperature averaged 24.9 ± 2.111 °C (±1SD, range 19.8-30.6 °C). The UCM model effectively fits this series as evidenced by an adjusted r^2= 0.75738 (S4a Table). The residual diagnostics and loess smoothed residuals further support a good model fit (S7 and S8 Figs). The UCM model for the maximum temperature series consists of seven components: level, slope, two cycles, seasonal, autoregressive and irregular components. T-tests of the parameter estimates for the model components show that the autoregressive component and the secondary cycle (cycle 1) are significant (S4b Table). Towards the end of the estimation span, chi-square tests of the parameter estimates suggest that the level and seasonal components are deterministic and significant, whereas the slope component and the primary cycle (cycle 2) are not (S4b Table).

The smoothed level trend shows a marginal increase (0.05 °C) in the maximum temperature from 24.87 °C in January 1960 to 24.92 °C in July 2020 (Fig. 7a). The slope component is constant, small and insignificant (Fig. 7b). The two cycles had approximate cycle periods of 3.6 years (43.1 months) and 12.6 years (150.7 months) (Figs 7c and d). Notably, the secondary cycle in the maximum temperature shows a pronounced spike in the mid-1970s, coinciding with the lowest minimum temperatures. However, while the amplitude of the oscillations was high from 1960 to 1990, it dampened from 1990 to 2020 (Fig. 7d). A plot of the smoothed trend superimposed onto the observed maximum temperature series reveal no evident trend from 1960 to 2020 (Fig. 7e).

This manuscript is a preprint and has not been peer reviewed. The copyright holder has made the manuscript available under a Creative Commons Attribution 4.0 International (CC BY) license and consented to have it forwarded to EarthArXiv for public posting.

Fig 7a. Smoothed level trend component for the average monthly maximum temperature for Narok Town, Kenya.

Fig 7b. Smoothed slope component for the average monthly maximum temperature for Narok Town, Kenya.

Fig 7c. Smoothed primary cycle component (cycle1) for the average monthly maximum temperature for Narok Town, Kenya. Approximate cycle period is 3.6 years (43.1 months).

Fig 7d. Smoothed secondary cycle component (cycle2) for the average monthly maximum temperature for Narok Town, Kenya. Approximate cycle period is 12.6 years (150.7 months).

Fig 7e. Smoothed trend superimposed onto the observed series for the average monthly maximum temperature for Narok Town, Kenya.

Multivariate state space models with trend, cycle and seasonal components

For each multivariate model we report results of extensive model diagnostics performed to assess model fit. For each response variable we report results of model diagnostics including one-step-ahead residual analysis illustrated through various graphs. (1) residual normality plot for checking normality of residuals, (2) residual histogram, (3) residual Q-Q plot and (4) time

This manuscript is a preprint and has not been peer reviewed. The copyright holder has made the manuscript available under a Creative Commons Attribution 4.0 International (CC BY) license and consented to have it forwarded to EarthArXiv for public posting.

series plot of standardized residuals. For each response variable we also use graphs for outlier detection and structural break analysis comprising (1) prediction error normality plot for checking normality of residuals, (2) prediction error histogram, (3) prediction error Q-Q plot, (4) time series plot of standardized additive-outlier statistics and (5) time series plot of maximal state shock chi-square statistics.

For each multivariate model, we present a table summarizing the parameter estimates of the unknown elements in the model system matrices. However, for brevity, we omit several other tabular results used to asses model performance including the following (1) Convergence status of the estimation process, (2) summary of the likelihood-based fit-statistics, (3) likelihood-based information criteria, (4) estimate of the disturbance covariance, (5) elementwise state break summary, (6) overall state (e.g., level, trend, cycle, error) break summary, and (7) summary of maximal state (e.g. level, trend, cycle, error) shocks.

Bivariate state space model for wet and dry season rainfall in Narok Town, Kenya

The residual and prediction error normality diagnostics plot for the wet season and dry seasons suggest approximate normality of the one-step-ahead residuals (S9-S12 Figs). The standardized prediction error and standardized residual plots for Narok Town’s wet season rainfall (S13 and S15 Figs) identified one outlier (an exceptionally high value) in 1962 whereas that for the dry season (S14 and S16 Figs) identified three outliers, one each in 1917, 1996 and 2011.

This manuscript is a preprint and has not been peer reviewed. The copyright holder has made the manuscript available under a Creative Commons Attribution 4.0 International (CC BY) license and consented to have it forwarded to EarthArXiv for public posting.

The wet season rainfall in 1962 (1396.8 mm) was 2.3 times the average for 1914-2020. In contrast, the dry season rainfall in 1917 (312.7 mm), 1996 (272.9 mm) and 2011 (333.6 mm) was 2.6, 2.2 and 2.7 times the average for 1913-2020, respectively. The maximal shock statistics plot (with reference line at the 90th percentile) identified structural breaks in Narok Town's rainfall series in 2017. The parameter estimates for the bivariate model for the wet and dry season rainfall show a negative correlation between the two cycles for the two rainfall components (-0.00185) and that the bivariate cycle period is 9.3 years. The damping factor for this bivariate cycle is 1, indicating it is persistent over time (S5 Table).

The smoothed bivariate random walk trends for both wet and the dry season rainfall, positively correlated, suggest an initial decline in rainfall from 1913 to a low between 1930 and 1940. This was followed by an increase peaking in 1969-1976, a subsequent decline until the mid-1980s, and then a relatively stable average level, before another increase from 2000 to 2020 (Fig 8a).

Fig 8a. Smoothed bivariate random walk trends for the wet and dry season rainfall components (each divided by its mean) during 1913-2020 in Narok Town, Kenya.

The opposing oscillations in wet and dry season rainfall are consistent with the negative correlation between their cycles (Fig 8b). This indicates that an increase in wet season rainfall typically corresponds to a decrease in dry season rainfall, and vice versa. Furthermore, the amplitude of these rainfall oscillations remained rather stable during 1913-2020 (Fig 8b).

This manuscript is a preprint and has not been peer reviewed. The copyright holder has made the manuscript available under a Creative Commons Attribution 4.0 International (CC BY) license and consented to have it forwarded to EarthArXiv for public posting.

Fig 8b. Smoothed cycles for the bivariate random walk model for wet and dry season rainfall (each divided by its mean) in Narok Town, Kenya. The bivariate cycle has a cycle period of 9.3 years.

Bivariate state space model with stochastic level, cycle and white noise components for the wet and dry season rainfall for Masai Mara, Kenya

The residual normality (S17 and S18 Figs) and prediction error (S19 and S20 Figs) diagnostic plots show that the bivariate random walk model with trend and cycle components, effectively fits the wet and dry season rainfall trends in Masai Mara. After accounting for oscillations in rainfall in the bivariate model, no distinct directional trend is evident in either the wet or dry season rainfall components in Masai Mara (Fig 9a). Additionally, outlier diagnostics (figures not shown) did not detect any exceptionally high or low seasonal rainfall values. There is a negative correlation between the cycles of wet and dry season rainfall (S6 Table). The model suggests a bivariate cycle with an approximate period of 20.4 years, where increases in wet season rainfall correspond to decreases in dry season rainfall (Fig 9b). Remarkably, the amplitude of the oscillation is much greater in the dry season rainfall component than in the wet season (Fig 9b). The estimated damping parameter of 1.0 indicates that these oscillations are persistent over time.

This manuscript is a preprint and has not been peer reviewed. The copyright holder has made the manuscript available under a Creative Commons Attribution 4.0 International (CC BY) license and consented to have it forwarded to EarthArXiv for public posting.

Fig 9a. Smoothed bivariate random walk trends for wet and dry season rainfall components (divided by their respective means) in Masai Mara, Kenya, during 1965-2020.

Fig 9b. Smoothed cycles for bivariate random walk model for wet and dry season rainfall (each divided by its mean) in Masai Mara, Kenya, during 1965-2020. The bivariate cycle has a period of 20.0 years.

Bivariate state space model with trend and cycle components for wet and dry season rainfall for Seronera, Serengeti National Park, Tanzania

The residual normality diagnostic, standardized residual and prediction error plots (not shown) all provided evidence of good model fit. Outlier analysis identified unusually high rainfall during the El Niño floods of 1998 ($\chi^2 = 8.11$, P = 0.0044) but no outlying rainfall values were recorded for the dry season. As well, there was no evidence of a level shift in the rainfall series during 1981-2015. Trends in the wet and dry season rainfall components were negatively correlated (S7 Table). However, while the wet season rainfall component showed no evident trend during 1981-2015, the dry season rainfall component increased progressively from 1981 and surpassed the 1981-2015 average in 2010 (Fig 10a). There was also evident oscillation in the wet and dry season rainfall, with a cycle period of about 10.4 years. These oscillations were negatively correlated such that an increase in wet season rainfall is offset by a decrease in dry season rainfall (Fig 10a). Furthermore, the amplitude of oscillation in the dry season rainfall was greater than that in the wet season during 1980-2015 (Fig 10b).

This manuscript is a preprint and has not been peer reviewed. The copyright holder has made the manuscript available under a Creative Commons Attribution 4.0 International (CC BY) license and consented to have it forwarded to EarthArXiv for public posting.

Fig 10a. Smoothed bivariate random walk trends for wet and dry season rainfall in Seronera, Serengeti National Park, Tanzania.

Fig 10b. Smoothed cycles for bivariate random walk model for wet and dry season rainfall in Seronera, Serengeti National Park, Tanzania. The bivariate cycle has a period of 10.4 years.

Bivariate state space model with trend and cycle components for wet and dry season rainfall for Ngorongoro Crater, Tanzania

The residual and prediction error diagnostics for the wet and dry season rainfall components suggest reasonabl model fit (S21-S24 Figs). The standardized residuals identify only one outlier, corresponding to exceptionally high dry season rainfall in 1967, and none for the wet season rainfall component (S25-S28 Figs). The trends in the wet and dry season rainfall components were negatively correlated such that the wet season rainfall increased while the dry season rainfall decreased (S8 Table, Fig 11a). Specifically, while the wet season rainfall component increased, surpassing the 1963-2014 average in 1985, the dry season rainfall exhibited a decreasing trend (Fig 11a). Unlike for Narok and Seronera, the bivariate oscillations of the wet and dry season rainfall were positively correlated, with a cycle period of 21.4 years (S8 Table). The oscillation amplitude was larger for the dry season than for the wet season. Also, the amplitude of these oscillations in both the wet and dry season rainfall components varied little during 1963-2014 (Fig 11b).

This manuscript is a preprint and has not been peer reviewed. The copyright holder has made the manuscript available under a Creative Commons Attribution 4.0 International (CC BY) license and consented to have it forwarded to EarthArXiv for public posting.

Fig 11a. Smoothed bivariate random walk trends for wet and dry season rainfall in Ngorongoro Crater, Tanzania.

Fig 11b. Smoothed cycles for bivariate random walk model for wet and dry season rainfall in Ngorongoro Crater, Tanzania. The bivariate cycle has a period of 21.4 years.

Bivariate state space model with trend, cycle and seasonal components for the average minimum and maximum temperatures for Narok Town, Kenya

The residual (S29 and S30 Figs) and prediction error (S31 and S32 Figs) normality diagnostics for average monthly minimum and maximum temperature were largely as expected. However, six observations for minimum temperature were identified as outliers. Specifically, standardized prediction error plot for minimum temperature highlighted the six extreme observations (S33 Fig). The five additive outliers in the minimum temperature series correspond to significant temperature drops in September 1974 and Nov 2018 and rises in October 1982, July 2001 and February 2019 (S9 Table). In contrast, while the standardized prediction error plot for maximum temperature (S34 Fig) also identified three extreme observations, none were statistically significant.

Both minimum and maximum temperature series show similar upward trends, as indicated by the positive correlation between their trends (S10 Table, Fig 12). The minimum temperature reached a record low in September 1974 and has been persistently increasing since 1985,

This manuscript is a preprint and has not been peer reviewed. The copyright holder has made the manuscript available under a Creative Commons Attribution 4.0 International (CC BY) license and consented to have it forwarded to EarthArXiv for public posting.

surpassing the 1960-2020 average in November 1993 (Fig 12). The maximum temperature showed a similar, but less marked, increasing pattern and exceeded the 1960-200 average in December 1991 (Fig 12).

Fig 12. Smoothed bivariate random walk trends for average monthly minimum and maximum temperature for Narok Town, Kenya.

Trivariate state space model with trend, cycle and seasonal components for total monthly rainfall, average monthly minimum and maximum temperatures in Narok Town, Kenya

The minimum and maximum temperature series in Narok Town were positively correlated with each other but both showed a negative correlation with rainfall (S11 Table, Fig 13). Specifically, 1972 recorded the lowest rainfall coinciding with the highest maximum temperature. Further, the period 1972-1974, marked by the highest rainfall, corresponded with the lowest and below average minimum temperatures. Conversely, during 1974-1985, rainfall was below average when the minimum temperature was above average (Fig 13). Lastly, the progressive rise in minimum temperatures since 1985 has been paralleled by a declining rainfall trend during the same period (Fig 13).

Fig 13. Smoothed trivariate random walk trends for average monthly minimum and maximum temperature and total monthly rainfall for Narok Town, Kenya.

This manuscript is a preprint and has not been peer reviewed. The copyright holder has made the manuscript available under a Creative Commons Attribution 4.0 International (CC BY) license and consented to have it forwarded to EarthArXiv for public posting.

Trivariate state space model with trend, cycle and seasonal components for total monthly rainfall for Narok Town, Kenya, Southern Oscillation Index (SOI) and Dipole Mode Index (DMI)

The residual and prediction error normality diagnostic plots for total monthly rainfall in Narok Town (S35 and S38 Figs), the SOI (SS36 and S39 Figs) and the DMI (S37 and S40 Figs) indicate a reasonable model fit but a few large rainfall values tend to be underestimated. The standardized prediction error plots identified nine rainfall observations (all exceeding expectation), five SOI observations (three below and two above expectation) and one DMI observation (above expectation) as outliers or extreme values (S41-S43 Figs). The SOI series showed quasi-periodic oscillation with notable positive peaks around 1961, 1975, 1990, 2000 and 2011 and the lowest values during periods of severe drought around 1984 and 1993 (Fig 14). The rainfall oscillation was negatively associated with SOI but positively correlated with DMI. Moreover, the SOI and DMI were negatively correlated with each other (S12 Table, Fig 14), suggesting that high rainfall tends to coincide with strong El Niño (negative SOI values) and strong DMI episodes, whereas low rainfall is associated with strong La Niña (positive SOI values) and weak DMI conditions.

The trend for the rainfall series was positively correlated with both the SOI and DMI series, but the SOI and DMI trends themselves were negatively correlated (S12 Table, Fig 14). This implies that the rainfall trend mirrored those of the SOI and DMI. Spefically, the DMI series generally increased throughout 1913-2020, whereas the SOI series decreased, became more negative and more intense, in the same period. The rainfall series generally tracked the pattern of variation in the DMI, increasing alongside the DMI series, but inversely to the SOI series (Fig 14).

This manuscript is a preprint and has not been peer reviewed. The copyright holder has made the manuscript available under a Creative Commons Attribution 4.0 International (CC BY) license and consented to have it forwarded to EarthArXiv for public posting.

Fig 14. Smoothed trivariate random walk trends for total monthly rainfall for Narok Town, Kenya, Southern Oscillation Index (SOI) and Indian Ocean Dipole Model Index (DMI).

Trivariate state space model with trend, cycle and seasonal components for total monthly rainfall for Masai Mara, Kenya, Southern Oscillation Index (SOI) and Dipole Mode Index (DMI)

The residual (S44-S46 Figs) and prediction error (S47-S49 Figs) normality diagnostic plots suggest that the state space model effectively captured the trivariate patterns in rainfall, SOI and DMI. Outlier diagnostics pinpointed the total monthly rainfall in January 2001(χ_1^2 = 6.81, P = 0.0091) and 2002 (χ_1^2 = 12.89, P = 0.0003) as unusually high. The parameter estimates (S13 Table) show positive associations between the level trend components as well as between the cyclical components. From 1965 to around 1985, rainfall, SOI and DMI all decreased, followed by a consistent increase, and then plateaued out from 2010 (Fig 15). The trivariate cycles, with a period of 9.3 years and a damping factor of 0.96, suggest a decline in oscillation amplitude of all the three series after the record-breaking 1997-1998 El Niño episode (S13 Table). Throughout 1965-2020, these cycles were in phase or synchronized (Fig 16).

Fig 15. Smoothed trivariate random walk trends for total monthly rainfall for Masai Mara, Kenya, Southern Oscillation Index (SOI) and Indian Ocean Dipole Model Index (DMI).

This manuscript is a preprint and has not been peer reviewed. The copyright holder has made the manuscript available under a Creative Commons Attribution 4.0 International (CC BY) license and consented to have it forwarded to EarthArXiv for public posting.

Fig 16. Smoothed trivariate cycles for total monthly rainfall for Masai Mara, Kenya, Southern Oscillation Index (SOI) and Indian Ocean Dipole Mode Index (DMI).

Trivariate state space model with trend, cycle and seasonal components for total monthly rainfall for Seronera, Tanzania, Southern Oscillation Index (SOI) and Dipole Model Index (DMI)

The normality diagnostic plots for residual (S50-S52 Figs) and prediction error (S53-S55 Figs) indicate that the state space model accurately represented the trivariate patterns in rainfall, SOI, and DMI. Additionally, outlier diagnostics (S56-S58 Figs) highlighted exceptionally high total monthly rainfall (in Nov 1985, Apr 1988, Dec 1997, Jan 1998, and Apr 2015). From 1981 to 2015 in Seronera, Serengeti, Tanzania, both the total monthly rainfall and the DMI increased (Fig 17). However, the SOI showed distinct oscillations with peaks apparent around 1990, 2000 and 2010 (Fig 18). This pattern differs from the SOI variation in Narok (Fig 14). Overall, the pattern of temporal variation suggests that rainfall is more strongly positively correlated with variations in the DMI than with variations in the SOI (S14 Table, Fig 17).

Fig 17. Smoothed trivariate random walk trends for total monthly rainfall for Seronera, Serengeti, Tanzania, Southern Oscillation Index (SOI) and Indian Ocean Dipole Mode Index (DMI).

Fig 18. Smoothed trivariate random walk rainfall /mean (=65.9 mm), Southern Oscillation Index (SOI) and Indian Ocean Dipole Mode Index (dmi) cycles for Seronera in Serengeti National Park in northern Tanzania.

This manuscript is a preprint and has not been peer reviewed. The copyright holder has made the manuscript available under a Creative Commons Attribution 4.0 International (CC BY) license and consented to have it forwarded to EarthArXiv for public posting.

Trivariate state space model with trend, cycle and seasonal components for total monthly rainfall for Ngorongoro Crater, Tanzania, Southern Oscillation Index (SOI) and Dipole Mode Index (DMI)

The residual (S59-S61 Figs) and prediction error (S62-S64 Figs) normality diagnostic plots demonstrate that the state space model effectively captured the trivariate patterns in rainfall, SOI and DMI. Moreover, outlier diagnostics (S65-S67 Figs) identified unusually high total monthly rainfall (MAR 1974, NOV 1963, DEC 1997 and JAN 2001) and atypically low SOI (in Feb 2005). Likewise to Seronera, a quasi-periodic oscillation in SOI was evident in Ngorongoro Crater, with positive peaks around 1975, 1990, 2000 and 2010 (Fig 19). The trends in rainfall, SOI and DMI were all positively correlated. Notably, both DMI and rainfall increased during 1963-2014 (S15 Table, Fig 19).

Fig 19. Smoothed trivariate integrated random walk trends for total monthly rainfall for Ngorongoro Crater, Tanzania, Southern Oscillation Index (SOI) and Indian Ocean Dipole Mode Index (DMI).

Multivariate state space model with trend, cycle and seasonal components for total monthly rainfall, average monthly minimum and maximum temperatures for Narok Town, Kenya, Southern Oscillation Index (SOI) and Dipole Mode Index (DMI)

The residual (S68-S72 Figs) and prediction error (S73-S77 Figs) normality diagnostic plots show that the pentavariate model effectively captured total monthly rainfall, average monthly

This manuscript is a preprint and has not been peer reviewed. The copyright holder has made the manuscript available under a Creative Commons Attribution 4.0 International (CC BY) license and consented to have it forwarded to EarthArXiv for public posting.

minimum and maximum temperatures, the SOI and the DMI for Narok County. The simultaneous variations in these five series at Narok Town are provided in Fig. 20 whereas their parameter estimates are detailed in S16 Table. The salient features of the five trends in Fig 20 are largely similar to those already described, and so, are not repeated here.

Fig 20. Smoothed multivariate integrated random walk trends for total monthly rainfall, average monthly minimum and maximum temperatures for Narok Town, Kenya, Southern Oscillation Index (SOI) and Indian Ocean Dipole Model Index (DMI).

Multivariate state space model with trend, cycle and seasonal components for monthly average NDVI, total monthly rainfall, average monthly minimum and maximum temperatures for Narok Town, Kenya

The residual (S78-S81 Figs) and prediction error (S82-S85 Figs) normality diagnostic plots show that the quadrivariate model accurately captured patterns in the total monthly rainfall, average monthly minimum and maximum temperatures and monthly average of SPOT NDVI for Narok County. The trend component of the model shows that all four variables increased from 1998 to around 2003, maintained stable average levels from 2004 to about 2009, and then increased again until 2014 (Fig 21). The parameter estimates for the quadrivariate model (S17 Table) reveal positive correlations among the level trends of all variables, except for an inverse relationship between SPOT NDVI and minimum temperature. This suggests that an increase in

This manuscript is a preprint and has not been peer reviewed. The copyright holder has made the manuscript available under a Creative Commons Attribution 4.0 International (CC BY) license and consented to have it forwarded to EarthArXiv for public posting.

minimum temperatures is associated with vegetation browning. The cycle component of the model, has an estimated period of 12.7 years (S17 Table). While the cycles are generally positively correlated, rainfall and maximum temperature, and SPOT NDVI and minimum temperature cycles are negatively correlated (S17 Tabe, S86 Fig).

Fig 21. Smoothed quadrivariate integrated random walk trends for monthly average rainfall, total monthly rainfall, average monthly minimum and maximum temperatures for Narok Town, Kenya.

Discussion

We detected strongly deterministic and persistent bivariate cycles in both wet and dry season rainfall components across the GMSE, encompassing the Masai Mara Ecosystem and Narok Town in Kenya and the Serengeti (Seronera) and Ngorongoro in Tanzania. These bivariate cycles showed a consistent compensatory pattern: low wet season rainfall was typically offset by higher dry season rainfall and vice versa, with dominant cycle periods of about 20 years. In Ngorongoro, despite a positive correlation between the wet and dry season rainfall cycles, a negative correlation between their levels led to a similar compensatory pattern as for the other regions. Notably, only in Seronera, Serengeti, did the bivariate rainfall components display a shorter cycle period of about 10.4 years. The 34-year time series from Seronera may not have been long enough to detect the longer-term oscillations observed in other GMSE rainfall data. This pattern of compensatory bivariate oscillations in the wet and dry season rainfall components is likely crucial for the ecosystem's stability.

This manuscript is a preprint and has not been peer reviewed. The copyright holder has made the manuscript available under a Creative Commons Attribution 4.0 International (CC BY) license and consented to have it forwarded to EarthArXiv for public posting.

The bivariate cycle periods, ranging between about 10 and 20 years, are considerably longer than the dominant cycle periods of 2.3 and 10.1 years identified in univariate analyses of wet and dry season rainfall components (Bartzke et al. 2016). These bivariate cycle periods also exceed those of the Indian Ocean Dipole (3.2 years) and the El Niño-Southern Oscillation (ENSO-SOI, 4.4 years), both of which are well known to significantly influence East African rainfall, especially during the wet season (Nicholson 1996, Latif et al. 1999, Webster et al. 1999, Mutai and Ward 2000, Mistry and Conway 2003, Behera et al. 2005, Shongwe et al. 2011, Tierney et al. 2013). Despite the variable amplitudes and phases of the ENSO-SOI and the Indian Ocean Dipole oscillations, the consistent, deterministic and persistent pattern of bivariate rainfall oscillations suggests that factors other than these known climate phenomena may be driving the observed long-term bivariate oscillations.

The long cycle periods of the bivariate rainfall cycle may reflect the influence of the Atlantic Multidecadal Oscillation (AMO). Oscillations in Atlantic ocean temperatures can significantly influence East African rainfall (Nicholson 1996, Mutai et al. 1998, Mutai and Ward 2000, McHugh 2004) through their teleconnections with the West African monsoon and the El Niño Southern Oscillation (Hills 1979, Shanahan et al. 2009, Rodríguez-Fonseca et al. 2011, Lopez et al. 2016). Additionally, the location and intensity of the Mascarene High (Ogwang et al. 2015), low-level jet streams, pressure cells over the Sahara and Saudi Arabia, and local topography, also contribute to rainfall variation in East Africa (Nicholson 1996, 2015) and hence to the rainfall oscillations in the GMSE.

The amplitudes of the rainfall oscillations in Narok was rather stable despite rising temperatures. This is inconsistent with global observations of more extreme weather events, such as droughts and floods, associated with rising temperatures (IPCC 2007). Furthermore, in the Serengeti and Narok regions, the amplitude of the dry season rainfall oscillations

This manuscript is a preprint and has not been peer reviewed. The copyright holder has made the manuscript available under a Creative Commons Attribution 4.0 International (CC BY) license and consented to have it forwarded to EarthArXiv for public posting.

exceeded that of the wet season. This heightened variability in the dry season rainfall, crucial for the survival of plants and animals during resource-scarce periods (Sinclair 1975, Mduma et al. 1999, Owen-Smith et al. 2005), may have significant implications for biodiversity and animal population dynamics.

The seasonality of minimum and maximum temperatures and rainfall in Narok was strongly persistent and deterministic. This was indicated by the extremely low stochastic disturbance variances within the seasonal components in the trivariate state space models. Additionally, there was also weak positive correlation between the seasonal cycles of temperature and rainfall. This pattern is consistent with the deterministic movements of the Intertropical Convergence Zone. This belt of rising and convecting air masses around the equator is the major driver of seasonality in temperature and rainfall in East Africa, including in the GMSE (Norton-Griffiths et al. 1975, Anyah and Semazzi 2007; Mahony et al. 2021). The movement of the Intertropical Convergence zone is therefore likely an extremely stable factor generating alternating wet and dry seasons each climatic year.

In contrast to the deterministic (predictable) intra-annual seasonal cycles we found highly transient (unpredictable) trivariate multiannual cycles in monthly minimum and maximum temperatures and rainfall with a period of about 1.8 years. The multiannual cycles were highly transient, primarily due to significant variability in temperature cycles. This variability was evident from the much higher stochastic disturbance variances in the temperature cycles, compared to those in the multiannual rainfall cycle.

Interestingly, the cycles of minimum and maximum temperatures were positively correlated with each other but both were negatively correlated with the rainfall cycle. This pattern was particularly noticeable in 1972 when the rainfall was at its lowest and the maximum

This manuscript is a preprint and has not been peer reviewed. The copyright holder has made the manuscript available under a Creative Commons Attribution 4.0 International (CC BY) license and consented to have it forwarded to EarthArXiv for public posting.

temperature peaked. Similarly, during 1974-1985, periods of above-average minimum temperatures coincided with below-average rainfall. For Narok Town, the persistent decline in rainfall during 1960-2020 coincided with an increase in minimum temperatures, echoing our earlier findings (Bartzke et al. 2016) and observations for other parts of East Africa (Ogutu et al. 2012a, 2012b, 2013, 2016). These results indicate that rising temperatures generally lead to reduced, rather than increasing rainfall and enhanced evaporative cooling.

Overall, rainfall levels during the wet and dry season across the GMSE remained relatively stable. However, some declines were apparent in the monthly, wet and dry season rainfall in Narok during 1960-2020, and in the dry season rainfall in Ngorongoro during 1963-2014. These decreases in rainfall, potentially linked to increases in temperatures, might be offset by an increasing influx of moisture from the Indian Ocean to East Africa. This moisture increase could be a result of the strengthening of the Indian Ocean Dipole (Dore 2005, Cai et al. 2014). Similarly, the El Niño Southern Oscillation phenomenon, which is often in phase with a positive Indian Ocean Dipole (Saji et al. 1999), has historically brought rain to East Africa (Hastenrath et al. 1993, Indeje and Semazzi 2000). Earlier studies suggested that this phenomenon might be intensifying with rising temperatures (Vecchi et al. 2006, Lu et al. 2007). Our results support this trend. Thus, even though the signal for the strengthening of the El Niño phenomenon still remains controversial (Fedorov and Philander 2000, Collins et al. 2010), our results support the notion that El Niño is strengthening.

Similarly to the monthly rainfall, vegetation productivity was largely invariant in terms of its cyclical, level and seasonal components. The level of NDVI increased slightly during 1999-2014 concurrent with increases in the levels of rainfall and maximum temperatures. There were also weak positive associations between the NDVI cycle and those for rainfall and maximum temperatures. This increase apparently accelerated from 2010, mirroring the effect

This manuscript is a preprint and has not been peer reviewed. The copyright holder has made the manuscript available under a Creative Commons Attribution 4.0 International (CC BY) license and consented to have it forwarded to EarthArXiv for public posting.

of increasing rainfall. It appears that the combination of high rainfall and high temperatures during daytime enhances the photosynthetic activity of plants (Lotsch et al. 2003). Previously, we found that extremely high rainfall increased significantly during 1990-2000 in the Mara (Bartzke et al. 2016). The 1998 flood was the worst on instrumental record for the GMSE (Bartzke et al. 2016). This extreme rainfall event likely facilitated the recruitment of woody plants from seedlings (Kraaij and Ward 2006) with consequent densification of woody cover and increase in NDVI. However, confirming these findings would require a longer NDVI time series than the current 15-year dataset.

The rising temperatures contribute to increased evaporation, which might result in a net negative water balance. This is despite the possibility of more intense oceanic and hemispheric oscillations bringing more moisture to East African. Such a scenario raises concerns about the potential for increasing habitat desiccation in the GMSE. This drying could adversely affect plants and animals (Ogutu et al. 2008).

In conclusion, understanding regional climate and vegetation trends and variation and how these are influenced by large-scale oceanic and atmospheric oscillations is crucial for predicting future climatic behaviours, environmental planning and conservation efforts. The results highlight the complexity of the regional climatic and environmental dynamics, emphasizing the impact of global climate phenomena like the DMI and SOI on local weather patterns. This impact is evident in rising temperatures and changing rainfall patterns. The findings underscore the crucial need for integrative approaches to understand and address the challenges posed by climate change to biodiversity, ecosystems and human wellfare.

This manuscript is a preprint and has not been peer reviewed. The copyright holder has made the manuscript available under a Creative Commons Attribution 4.0 International (CC BY) license and consented to have it forwarded to EarthArXiv for public posting.

Conclusions

The univariate patterns produced several intefesting insights. The Greater Mara-Serengeti Ecosystem experiences recurrent severe droughts and erratic wet conditions and recorded a substantial rise in temperatures over six decades. The monthly minimum temperature showed a striking increase, while the trends in maximum temperature were more subdued. Notably, monthly minimum temperatures increased by 4.2 °C during wet seasons and 3.3 °C in dry seasons, while maximum temperatures also increased, though with greater variability. Rainfall showed quasi-periodic oscillations with cycle periods of between 2.5 and 5.3 years. The SOI declined slightly but was generally stable. The DMI increased persistently and significantly and had a stochastic cycle period of about 2.7 years. The bivariate and multivariate patterns also yielded several key findings. These include negative correlations between wet and dry season rainfall, marked by opposing oscillations, and consistent increases in DMI and temperature trends, with notable correlations among them. The SOI and DMI trends were negatively correlated and influenced rainfall patterns. Rainfall trends were often correlated more strongly with DMI than with SOI variations. The models also identified many significant structural breaks and outliers in the series. These insights have implications for designing strategies to mitigate climate change impacts on ecosystems, biodiversity, and human wellbeing.

Acknowledgements

We thank the Kenya Meteorological Department (KMD), Prof. Kay E. Holekamp (Michigan State University) and the World Wildlife Fund for Nature (WWF) for providing the rainfall

This manuscript is a preprint and has not been peer reviewed. The copyright holder has made the manuscript available under a Creative Commons Attribution 4.0 International (CC BY) license and consented to have it forwarded to EarthArXiv for public posting.

data. We are greatly indebted to Ms Christine Mahonga for her patience and support in making the data available and coordinating the verification of the rainfall data at KMD. The Maasai Mara Ecological Monitoring Programme (MMEMP) was designed and supervised by Dr. Holly T. Dublin, supported by Professor A.R.E. Sinclair (University of British Columbia), and executed by Messrs. Paul Chara (July 1989–1992), John Naiyoma (1989–1993), Alex Obara (1995–1997) and Charles Matankory (1991–2003). Many other individuals and organizations, too many to list individually, also helped in various ways over the last 40 years. We are grateful to Mr. Gordon Ojwang (Directorate of Resource Surveys and Remote Sensing of Kenya) for his assistance in acquiring the rainfall data for Narok for 1970–2014 from KMD.

References

Anyah, R. O., and F. H. M. Semazzi. 2007. Variability of East African rainfall based on multiyear RegCM3 simulations. Int J Climatol 27:357–371.

Bartzke, G. S., J. O. Ogutu, D. Mtui, S. Mukhopadhyay, and H.-P. Piepho. 2016. Modelled trends in climate and vegetation. University of Hohenheim, Baden-Württemberg, Germany.

Bartzke, G. S., Ogutu, J. O., Mukhopadhyay, S., Mtui, D., Dublin, H. T., and Piepho, H. P. 2018. Rainfall trends and variation in the Maasai Mara ecosystem and their implications for animal population and biodiversity dynamics. PloS one, 13(9), e0202814.

Behera, S. K., J.-J. Luo, S. Masson, P. Delecluse, S. Gualdi, A. Navarra, and T. Yamagata. 2005. Paramount impact of the Indian Ocean dipole on the East African short rains: A CGCM study. J Climate 18:4514–4530.

This manuscript is a preprint and has not been peer reviewed. The copyright holder has made the manuscript available under a Creative Commons Attribution 4.0 International (CC BY) license and consented to have it forwarded to EarthArXiv for public posting.

Boone, R. B., S. J. Thirgood, and J. G. C. Hopcraft. 2006. Serengeti Wildebeest Migratory Patterns Modeled from Rainfall and New Vegetation Growth. Ecology 87:1987–1994.

Boutton, T. W., Tieszen, L. L., & Imbaba, S. K. 1988a. Seasonal changes in the nutrient content of East African grassland vegetation. African Journal of Ecology 26: 103-115.

Boutton, T. W., Tieszen, L. L., & Imbamba, S. K. 1988b. Biomass dynamics of grassland vegetation in Kenya. African Journal of Ecology, 26(2), 89-101.

Brown, L.H. & Cocheme, J. 1973. A study of the agroclimatology of the highlands of eastern Africa. Technical Note No. 125 (WMO 339). World Meteorological Organization, Geneva.

Cai, W., S. Borlace, M. Lengaigne, P. Van Rensch, M. Collins, G. Vecchi, A. Timmermann, A. Santoso, M. J. McPhaden, L. Wu, and others. 2014. Increasing frequency of extreme El Niño events due to greenhouse warming. Nat Clim Chang 4:111–116.

Climate Hazards Centre (2016) CHIRPS Diagnostics—Global Station Density—0.25 Degrees. Available at: https://data.chc.ucsb.
edu/products/CHIRPS-2.0/diagnostics/global_monthly_station _density/tifs/p25/ (Accessed: August 21, 2017).

Collins, M., S.-I. An, W. Cai, A. Ganachaud, E. Guilyardi, F.-F. Jin, M. Jochum, M. Lengaigne, S. Power, A. Timmermann, and others. 2010. The impact of global warming on the tropical Pacific Ocean and El Niño. Nat Geosci 3:391–397.

De Jong, P., and Chu-Chun-Lin, S. (2003). "Smoothing with an Unknown Initial Condition." *Journal of Time Series Analysis* 24:141–148.

Dore, M. H. I. 2005. Climate change and changes in global precipitation patterns: What do we know? Environ Int 31:1167–1181.

Dublin, H. T., and J. O. Ogutu. 2015. Population regulation of African buffalo in the Mara–Serengeti ecosystem. Wildl Res 42:382–393.

This manuscript is a preprint and has not been peer reviewed. The copyright holder has made the manuscript available under a Creative Commons Attribution 4.0 International (CC BY) license and consented to have it forwarded to EarthArXiv for public posting.

Fedorov, A. V., and S. G. Philander. 2000. Is El Niño changing? Science 288:1997–2002.

Griffiths, J. F., and Gwynne, M. D. (1962). The climate of Kenya Masailand. East African Agricultural and Forestry Journal 28: 1-6.

Hastenrath, S., A. Nicklis, and L. Greischar. 1993. Atmospheric-hydrospheric mechanisms of climate anomalies in the western equatorial Indian Ocean. J Geophys Res Oceans 98:20219–20235.

Harvey, A. C. (1989). *Forecasting, Structural Time Series Models, and the Kalman Filter*. Cambridge: Cambridge University Press.

Harvey, A. C. (2001). "Testing in Unobserved Components Models." *Journal of Forecasting* 20:1–19.

Hills, R. C. 1979. The structure of the Inter-Tropical Convergence Zone in Equatorial Africa and its relationship to East African rainfall. Trans Inst Br Geogr 4:329–352.

Hoffmann, W. A., and R. B. Jackson. 2000. Vegetation-Climate Feedbacks in the Conversion of Tropical Savanna to Grassland. J Climate 13:1593–1602.

Holdo, R. M., K. A. Galvin, E. Knapp, S. Polasky, R. Hilborn, and R. D. Holt. 2010. Responses to alternative rainfall regimes and antipoaching in a migratory system. Ecol Appl 20:381–397.

Indeje, M., and F. H. M. Semazzi. 2000. Relationships Between QBO in the Lower Equatorial Stratospheric Zonal Winds and East African Seasonal Rainfall. Meteorol Atmos Phys 73:227–244.

IPCC. 2007. Climate Change 2007: The Physical Science Basis. Page 996 (S. Solomon, D. Qin, M. Manning, Z. Chen, M. Marquis, K. B. Averyt, M. Tignor, and H. L. Miller, Eds.) Agenda. . Cambridge University Press, Cambridge, United Kingdom and New York, NY, USA.

This manuscript is a preprint and has not been peer reviewed. The copyright holder has made the manuscript available under a Creative Commons Attribution 4.0 International (CC BY) license and consented to have it forwarded to EarthArXiv for public posting.

King'Uyu, S. M., L. A. Ogallo, and E. K. Anyamba. 2000. Recent Trends of Minimum and Maximum Surface Temperatures over Eastern Africa. J Climate 13:2876–2886.

Knight, J. R., C. K. Folland, and A. A. Scaife. 2006. Climate impacts of the Atlantic Multidecadal Oscillation. Geophys Res Lett 33:L17706.

Kraaij, T., and D. Ward. 2006. Effects of rain, nitrogen, fire and grazing on tree recruitment and early survival in bush-encroached savanna, South Africa. Plant Ecol 186:235–246.

Latif, M., D. Dommenget, M. Dima, and A. Grötzner. 1999. The Role of Indian Ocean Sea Surface Temperature in Forcing East African Rainfall Anomalies during December-January 1997/98. J Climate 12:3497–3504.

Lopez, H., S. Dong, S.-K. Lee, and G. Goni. 2016. Decadal Modulations of Interhemispheric Global Atmospheric Circulations and Monsoons by the South Atlantic Meridional Overturning Circulation. J Climate 29:1831–1851.

Lotsch, A., M. A. Friedl, B. T. Anderson, and C. J. Tucker. 2003. Coupled vegetation-precipitation variability observed from satellite and climate records. Geophys Res Lett 30:1774, doi:10.1029/2003GL017506.

Lu, J., G. A. Vecchi, and T. Reichler. 2007. Expansion of the Hadley cell under global warming. Geophys Res Lett 34:L06805.

Mahony, J., Dyer, E., & Washington, R. 2021. The precipitation patterns and atmospheric dynamics of the Serengeti National Park. International Journal of Climatology, 41, E2051-E2072.

McHugh, M. J. 2004. Near-Surface Zonal Flow and East African Precipitation Receipt during Austral Summer. J Climate 17:4070–4079.

McHugh, M. J. 2006. Impact of South Pacific circulation variability on east African rainfall. Int J Climatol 26:505–521.

This manuscript is a preprint and has not been peer reviewed. The copyright holder has made the manuscript available under a Creative Commons Attribution 4.0 International (CC BY) license and consented to have it forwarded to EarthArXiv for public posting.

Mduma, S. A. R., A. R. E. Sinclair, and R. Hilborn. 1999. Food regulates the Serengeti wildebeest: a 40-year record. J Anim Ecol 68:1101–1122.

Mills, M. G. L., H. C. Biggs, and I. J. Whyte. 1995. The relationship between rainfall, lion predation and population trends in African herbivores. Wildl Res 22:75–87.

Mistry, V. V., and D. Conway. 2003. Remote Forcing of East African Rainfall and Relationships with Fluctuations in Levels of Lake Victoria. Int J Climatol 23:67–89.

Mtewele, Z. F., Jia, G., & Xu, X. 2023. Serengeti–Masai Mara ecosystem dynamics inferred from rainfall extremes. Environmental Research Letters, 18(11), 114026.

Mukhopadhyay, S., Ogutu, J. O., Bartzke, G., Dublin, H. T., and Piepho, H. P. 2019. Modelling spatio-temporal variation in sparse rainfall data using a hierarchical Bayesian regression model. Journal of Agricultural, Biological and Environmental Statistics, 24(2), 369-393.

Musiega, D. E., and S.-N. Kazadi. 2004. Simulating the East African wildebeest migration patterns using GIS and remote sensing. African Journal of Ecology 42:355–362.

Mutai, C. C., and M. N. Ward. 2000. East African Rainfall and the Tropical Circulation/Convection on Intraseasonal to Interannual Timescales. J Climate 13:3915–3939.

Mutai, C. C., M. N. Ward, and A. W. Colman. 1998. Towards the Prediction of the East Africa short rains based on sea-surface temperature-atmosphere coupling. Int J Climatol 18:975–997.

Mwale, D., and T. Y. Gan. 2005. Wavelet Analysis of Variability, Teleconnectivity, and Predictability of the September-November East African Rainfall. J Appl Meteorol 44:256–269.

Nicholson, S. 2015. The Turkana low-level jet: mean climatology and association with regional aridity. Int J Climatol 36:2598–2614.

This manuscript is a preprint and has not been peer reviewed. The copyright holder has made the manuscript available under a Creative Commons Attribution 4.0 International (CC BY) license and consented to have it forwarded to EarthArXiv for public posting.

Nicholson, S. E. 1996. A Review of Climate Dynamics and Climate Variability in Eastern Africa. Pages 25–56 *in* T. C. Johnson and E. O. Odada, editors. The Limnology, Climatology and Paleoclimatology of the East African Lakes. . Gordon and Breach Amsterdam, Amsterdam, Netherlands.

Nicholson, S. E. 2000. The nature of rainfall variability over Africa on time scales of decades to millenia. Global and planetary change 26:137–158.

Norton-Griffiths, M., D. Herlocker, and L. Pennycuick. 1975. The patterns of rainfall in the Serengeti ecosystem, Tanzania. Afr J Ecol 13:347–374.

Ogallo, L. 1984. Temporal fluctuations of seasonal rainfall patterns in East Africa. Mausam 35:175–180.

Ogallo, L. J. 1982. Quasi-periodic patterns in the East African rainfall records. Kenya Journal of Science and Technology(A) 3:43–54.

Ogutu, J. O., B. Kuloba, H.-P. Piepho, and E. Kanga. 2017. Wildlife Population Dynamics in Human-Dominated Landscapes under Community-Based Conservation: The Example of Nakuru Wildlife Conservancy, Kenya. PLoS One 12:e0169730.

Ogutu, J. O., and N. Owen-Smith. 2005. Oscillations in large mammal populations: are they related to predation or rainfall? Afr J Ecol 43:332–339.

Ogutu, J. O., N. Owen-Smith, H.-P. Piepho, B. Kuloba, and J. Edebe. 2012a. Dynamics of ungulates in relation to climatic and land use changes in an insularized African savanna ecosystem. Biodivers Conserv 21:1033–1053.

Ogutu, J. O., N. Owen-Smith, H.-P. Piepho, M. Y. Said, S. Kifugo, R. S. Reid, H. Gichohi, P. Kahumbu, and S. Andanje. 2013. Changing wildlife populations in Nairobi National Park and Adjoining Athi-Kaputiei Plains: Collapse of the Migratory Wildebeest. Open Conservation Biology Journal 7:11–26.

This manuscript is a preprint and has not been peer reviewed. The copyright holder has made the manuscript available under a Creative Commons Attribution 4.0 International (CC BY) license and consented to have it forwarded to EarthArXiv for public posting.

Ogutu, J. O., H.-P. Piepho, and H. T. Dublin. 2014a. Reproductive seasonality in African ungulates in relation to rainfall. Wildl Res 41:323–342.

Ogutu, J. O., Piepho, H. P., & Dublin, H. T. 2014b. Responses of phenology, synchrony and fecundity of breeding by African ungulates to interannual variation in rainfall. Wildlife Research, 40(8), 698-717.

Ogutu, J. O., H.-P. Piepho, H. T. Dublin, N. Bhola, and R. S. Reid. 2008. El Niño-Southern Oscillation, rainfall, temperature and Normalized Difference Vegetation Index fluctuations in the Mara-Serengeti ecosystem. Afr J Ecol 46:132–143.

Ogutu, J. O., H.-P. Piepho, and E. Kanga. 2012b. Dynamics of an Insularized and Compressed Impala Population: Rainfall, Temperature and Density Influences. Open Ecol J 5:1–17.

Ogutu, J. O., Owen-Smith, N., Piepho, H. P., & Dublin, H. T. (2015). How rainfall variation influences reproductive patterns of African savanna ungulates in an equatorial region where photoperiod variation is absent. PloS one, 10(8), e0133744.

Ogutu, J. O., H.-P. Piepho, M. Y. Said, G. O. Ojwang, L. W. Njino, S. C. Kifugo, and P. W. Wargute. 2016. Extreme Wildlife Declines and Concurrent Increase in Livestock Numbers in Kenya: What Are the Causes? PLoS One 11:e0163249.

Ogutu, J. O., Kuloba, B., Piepho, H. P., and Kanga, E. 2017. Wildlife population dynamics in human-dominated landscapes under community-based conservation: the example of Nakuru Wildlife Conservancy, Kenya. PloS one, 12(1), e0169730.

Ogwang, B. A., V. Ongoma, L. Xing, and F. K. Ogou. 2015. Influence of Mascarene high and Indian Ocean dipole on East African extreme weather events. Geogr Pannon 19:64–72.

Omondi, P., L. A. Ogallo, R. Anyah, J. M. Muthama, and J. Ininda. 2013. Linkages between global sea surface temperatures and decadal rainfall variability over Eastern Africa region. Int J Climatol 33:2082–2104.

This manuscript is a preprint and has not been peer reviewed. The copyright holder has made the manuscript available under a Creative Commons Attribution 4.0 International (CC BY) license and consented to have it forwarded to EarthArXiv for public posting.

Owen-Smith, N., D. R. Mason, and J. O. Ogutu. 2005. Correlates of survival rates for 10 African ungulate populations: density, rainfall and predation. J Anim Ecol 74:774–788.

Oyama, M. D., and C. A. Nobre. 2004. Climatic Consequences of a Large-Scale Desertification in Northeast Brazil: A GCM Simulation Study. Journal of Climate 17:3203–3213.

Pennycuick, L. 1975. Movements of the migratory wildebeest population in the Serengeti area between 1960 and 1973. Afr J Ecol 13:65–87.

Pennycuick, L., and M. Norton-Griffiths. 1976. Fluctuations in the rainfall of the Serengeti Ecosystem, Tanzania. J Biogeogr 3:125–140.

Prins, H. H. T., and P. E. Loth. 1988. Rainfall patterns as background to plant phenology in northern Tanzania. J Biogeogr 15:451–463.

Ritchie, M. E. 2008. Global environmental changes and their impact on the Serengeti. Serengeti III: human impacts on ecosystem dynamics, 209-240.

Rodríguez-Fonseca, B., S. Janicot, E. Mohino, T. Losada, J. Bader, C. Caminade, F. Chauvin, B. Fontaine, J. García-Serrano, S. Gervois, M. Joly, I. Polo, P. Ruti, P. Roucou, and A. Voldoire. 2011. Interannual and decadal SST-forced responses of the West African monsoon. Atmos Sci Lett 12:67–74.

SAS Institute Inc. (2022). SAS/ETS user's guide, 152. System for Statistical Analysis, Version 9.4, SAS Institute, NC, USA.

Saji, N. H., B. N. Goswami, P. N. Vinayachandran, and T. Yamagata. 1999. A dipole mode in the tropical Indian Ocean. Nature 401:360–363.

Shanahan, T. M., J. T. Overpeck, K. J. Anchukaitis, J. W. Beck, J. E. Cole, D. L. Dettman, J. A. Peck, C. A. Scholz, and J. W. King. 2009. Atlantic Forcing of Persistent Drought in West Africa. Science 324:377–380.

This manuscript is a preprint and has not been peer reviewed. The copyright holder has made the manuscript available under a Creative Commons Attribution 4.0 International (CC BY) license and consented to have it forwarded to EarthArXiv for public posting.

Shongwe, M. E., G. J. van Oldenborgh, B. van den Hurk, and M. van Aalst. 2011. Projected Changes in Mean and Extreme Precipitation in Africa under Global Warming. Part II: East Africa. J Climate 24:3718–3733.

Sinclair, A. R. E. 1975. The Resource Limitation of Trophic Levels in Tropical Grassland Ecosystems. J Anim Ecol 44:497–520.

Tierney, J. E., J. E. Smerdon, K. J. Anchukaitis, and R. Seager. 2013. Multidecadal variability in East African hydroclimate controlled by the Indian Ocean. Nature 493:389–392.

Trenberth, K. E., and D. J. Shea. 2005. Relationships between precipitation and surface temperature. Geophys Res Lett 32:L14703.

Vecchi, G. A., B. J. Soden, A. T. Wittenberg, I. M. Held, A. Leetmaa, and M. J. Harrison. 2006. Weakening of tropical Pacific atmospheric circulation due to anthropogenic forcing. Nature 441:73–76.

Webster, P. J., A. M. Moore, J. P. Loschnigg, and R. R. Leben. 1999. Coupled ocean–atmosphere dynamics in the Indian Ocean during 1997–98. Nature 401:356–360.

Supporting Information

S1 Text. Supplementary figures and tables.

S2 Text. SAS Program codes for fitting UCMs and SSMs.docx

S3 Text. SAS Program codes for fitting UCMs and SSMs.sas

S1 Data. Total monthly (Month1 to Month12) rainfall in milimeters for Narok Town Meteorological Station from April 1913 to July2020. The rainfall values were verified against the original monthly paper cards at the Kenya Meteoreological Department.

S2 Data. The monthly average (of daily records) minimum and maximum surface air temperature in degrees celsius at Narok Town Meteorological Station for the period January 1960 to July 2020.

This manuscript is a preprint and has not been peer reviewed. The copyright holder has made the manuscript available under a Creative Commons Attribution 4.0 International (CC BY) license and consented to have it forwarded to EarthArXiv for public posting.

S3 Data. The total monthly rainfall in milimeters (Rain) for 15 rain gauges located within or near (Cottars) the Masai Mara National Reserve for the period January 1965 to August 2020. Predicted is the model predicted rainfall. Rain_imp is the measured rain (Rain) and imputed (predicted) missing values.

S4 Data. The total monthly rainfall averaged over all 5 × 5 km grids in Narok County of Kenya based on blended station-satellite rainfall data (rain) and on rainfall data predicted by a spatio-temporal hierarchical Bayesian model (rain_Bayes) (Mukhopadhyay, S., Ogutu, J. O., Bartzke, G., Dublin, H. T., & Piepho, H. P. (2019). Modelling spatio-temporal variation in sparse rainfall data using a hierarchical Bayesian regression model. Journal of Agricultural, Biological and Environmental Statistics, 24(2), 369-393.). Min (minimum) and max (maximum) are the average monthly temperatures based on blended Station-Satellite data. The NOAA and SPOT Normalized Difference Vegetation Index (NDVI) (minimum, maximum, mean, range and standard deviation) averaged over the 5 × 5 km grid in Narok County. Rain_1 to Rain_6 are lagled rain values whereas rain_Bayes_1 to rain_Bayes_6 are lagged rain_Bayes values.

S5 Data. The total monthly rainfall in milimiters (rain) for Seronera Research Station in Serengeti National Park in Tanzania for the period January 1980 to December 2015. Rain_imp are the measured rainfall records and imputed missing values.

S6 Data. The total monthly rainfall in milimiters (rain) for Ngorongor Crater in in Tanzania for the period January 1963 to December 2014. Rain_imp are the measured rainfall records and imputed missing values.

S7 Data. The monthly Indian Ocean Dipole Mode Index (DMI) for January 1870 to March 2021.

S8 Data. The monthly Southern Oscillation Index (SOI) for January 1866 to December 2021.

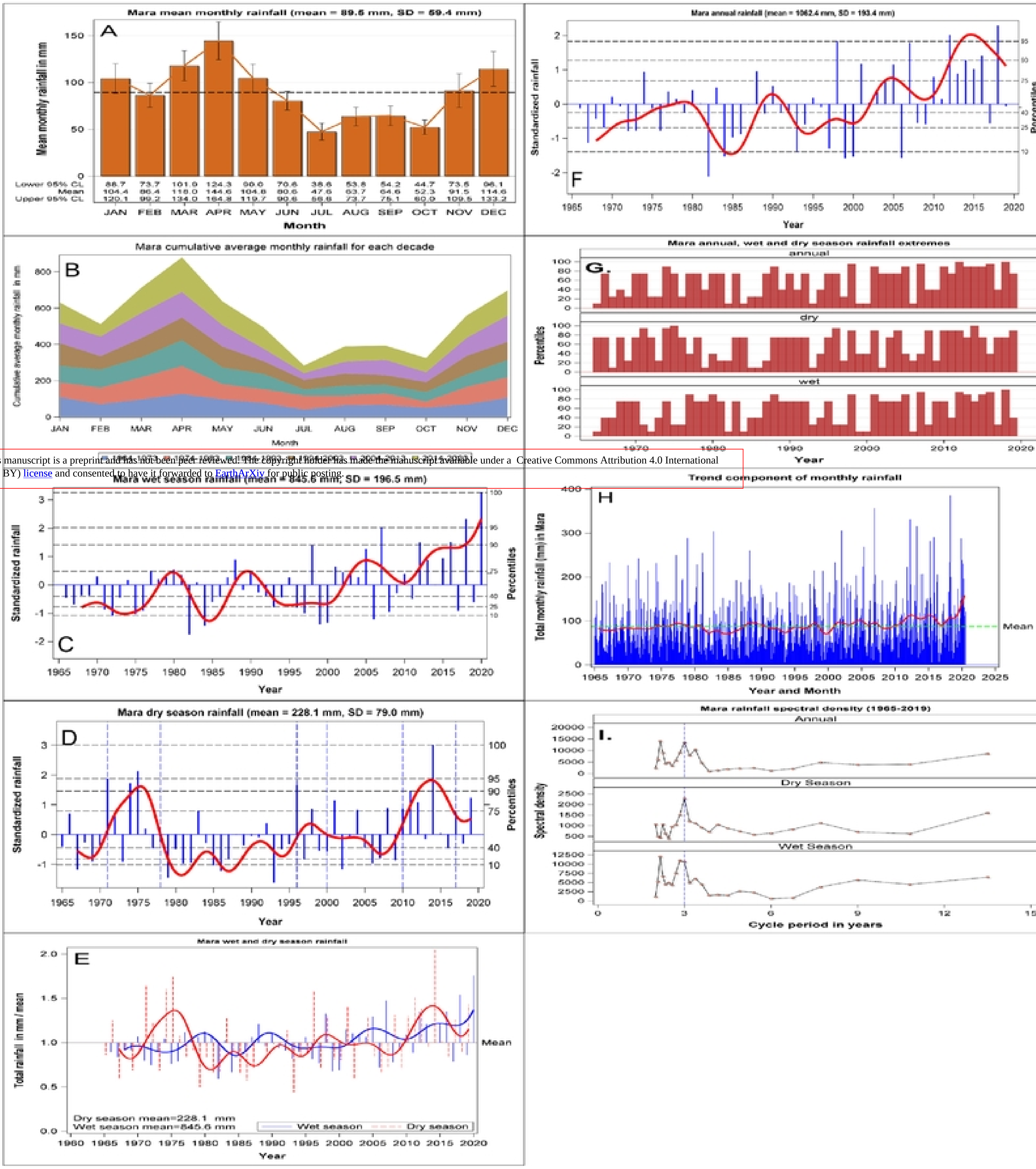

This manuscript is a preprint and has not been peer reviewed. The copyright holder has made the manuscript available under a Creative Commons Attribution 4.0 International (CC BY) license and consented to have it forwarded to EarthArXiv for public posting.

Figure 1

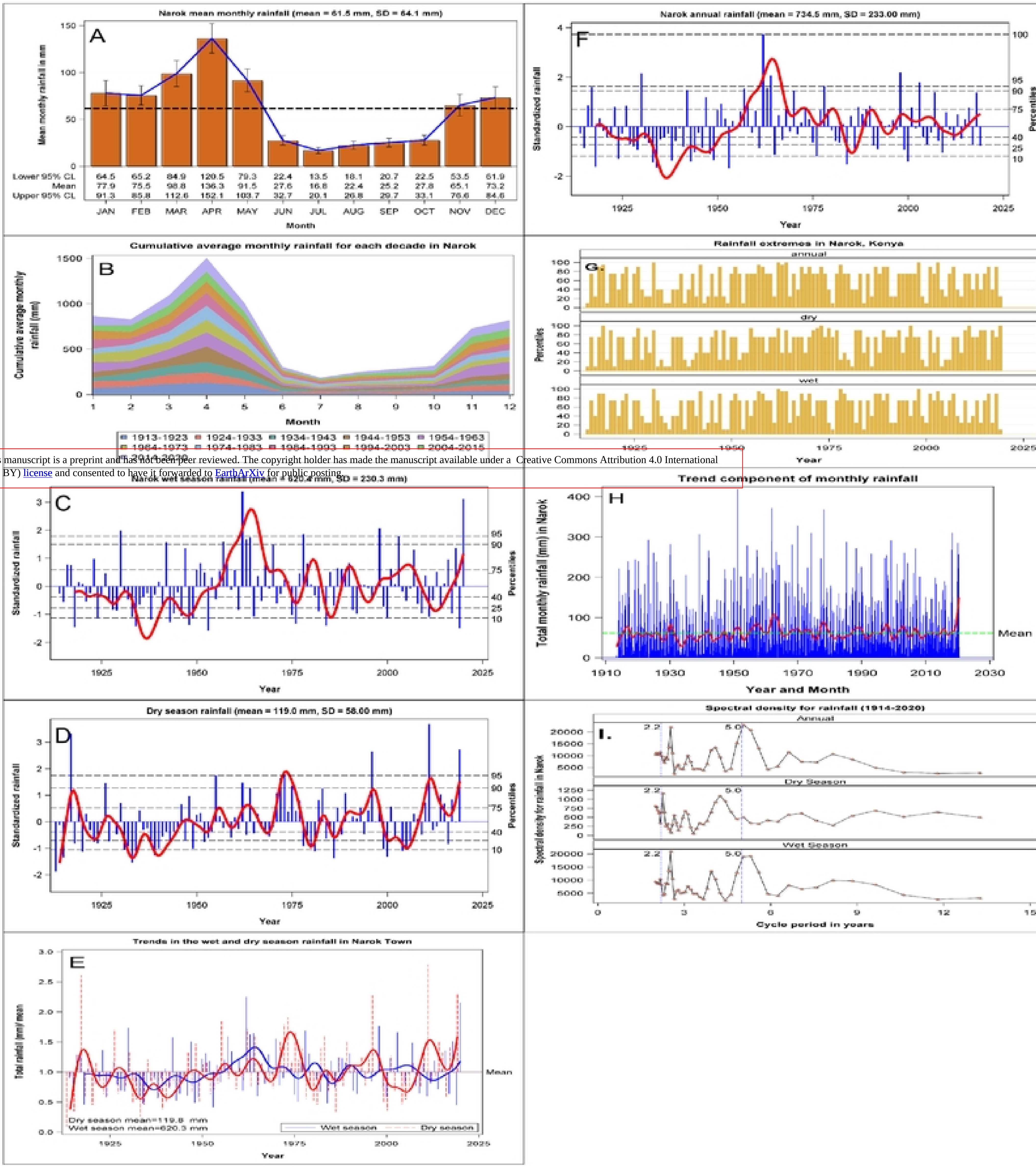

This manuscript is a preprint and has not been peer reviewed. The copyright holder has made the manuscript available under a Creative Commons Attribution 4.0 International (CC BY) license and consented to have it forwarded to EarthArXiv for public posting.

Figure 2

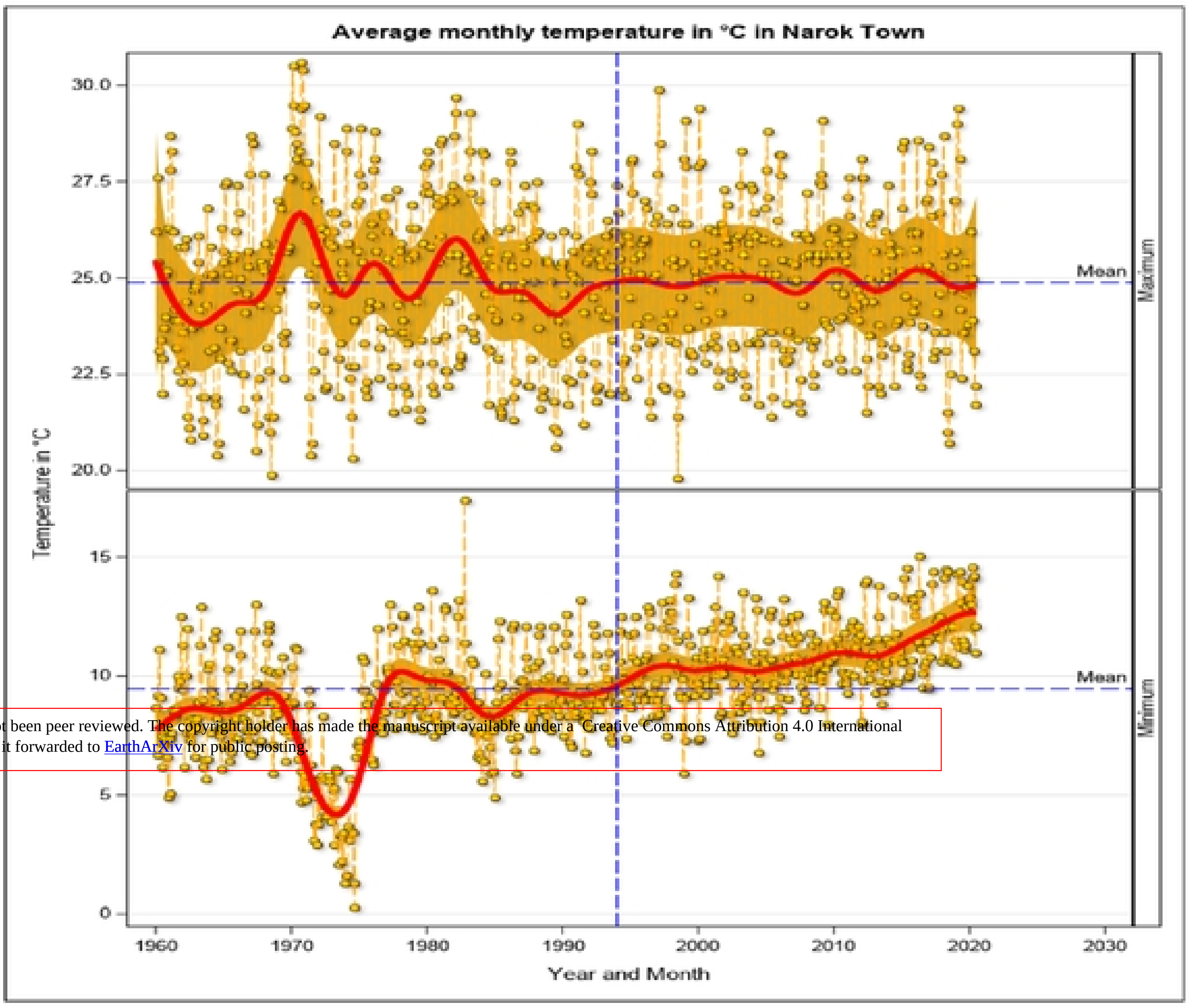

This manuscript is a preprint and has not been peer reviewed. The copyright holder has made the manuscript available under a Creative Commons Attribution 4.0 International (CC BY) license and consented to have it forwarded to EarthArXiv for public posting.

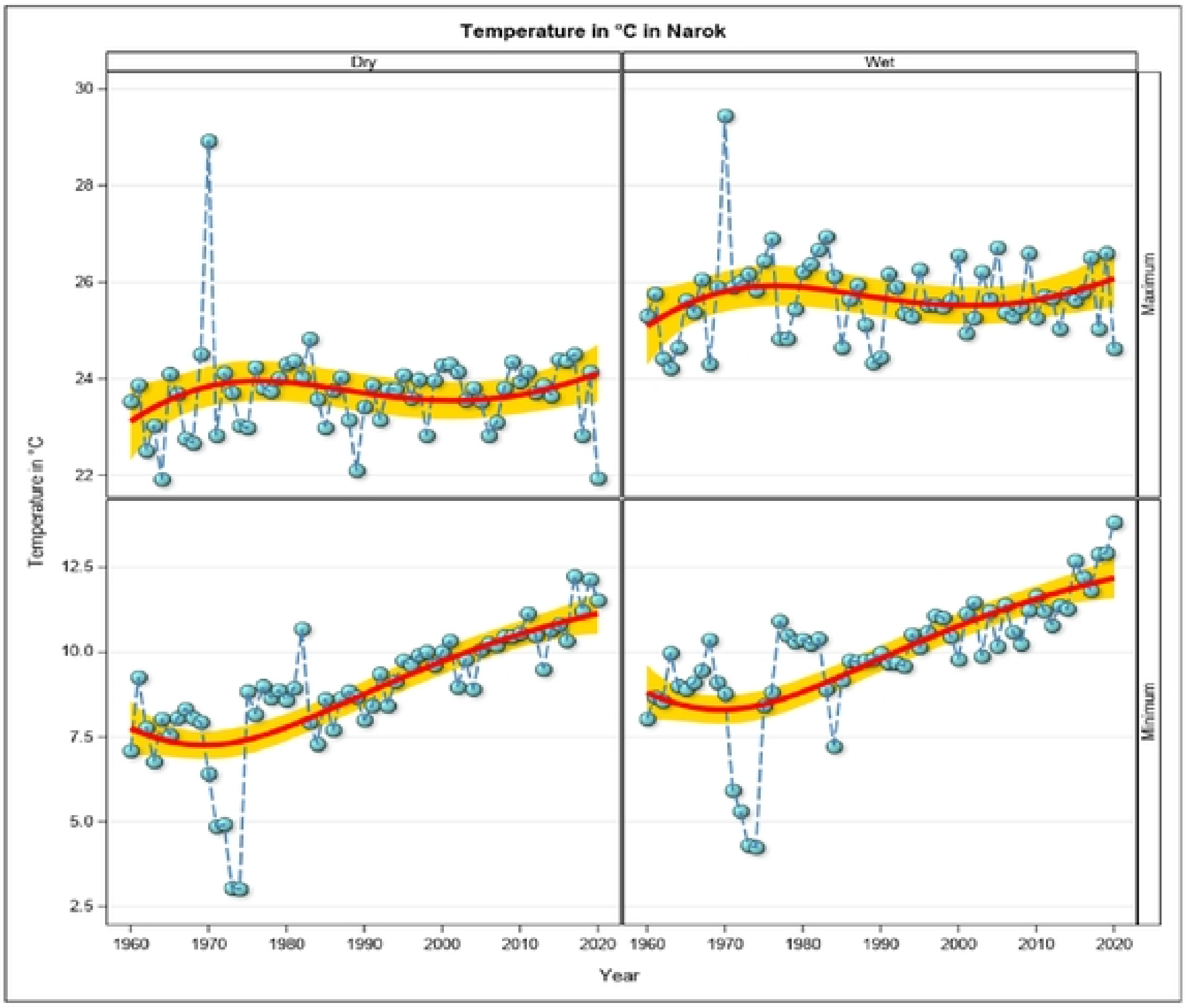

Figure 3

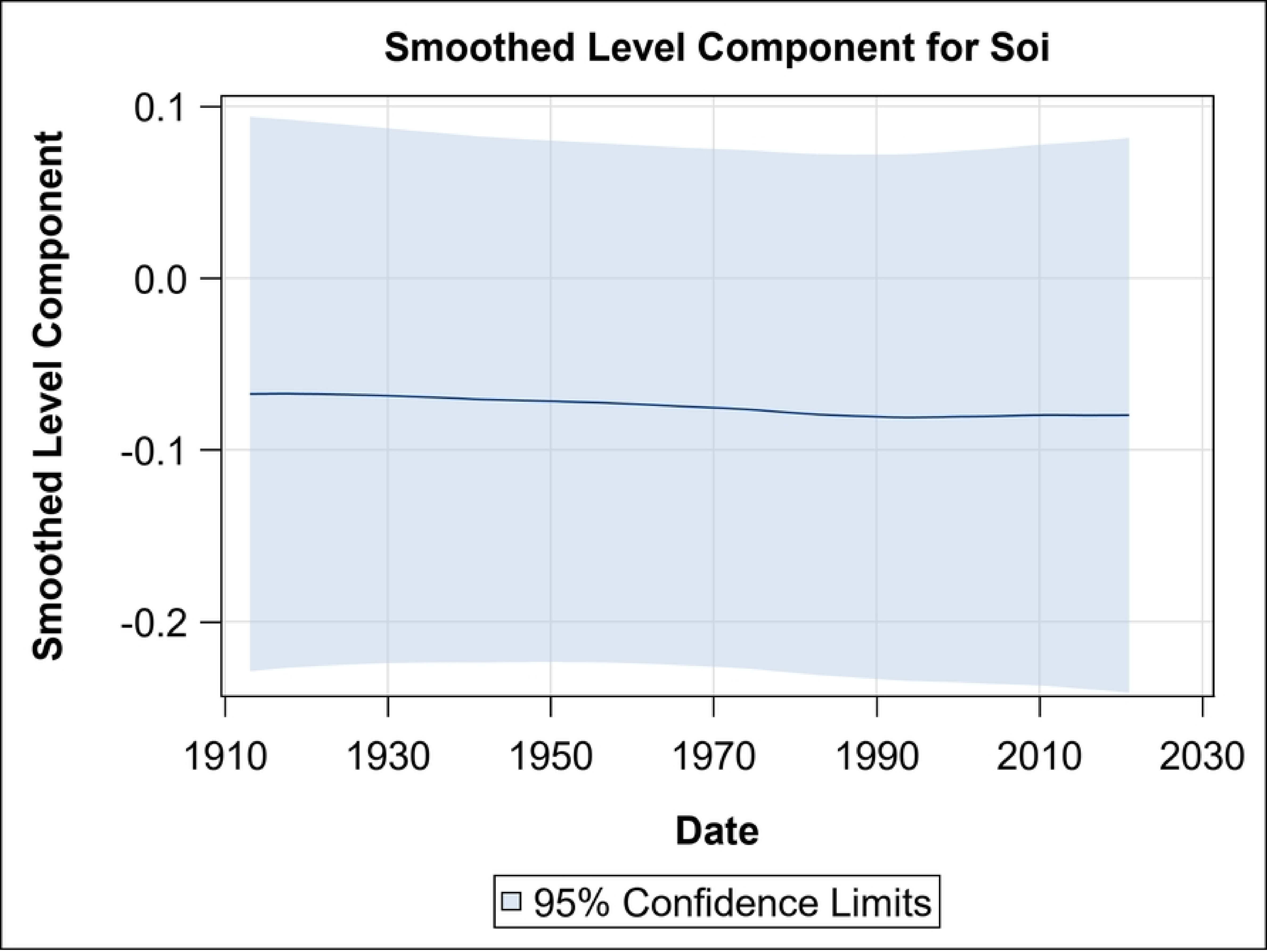

Smoothed Level Component for Soi
Smoothed Level Component
0.1
0.0
-0.1
-0.2
1910
1930
1950
1970
1990
2010
2030
Date
95% Confidence Limits

Figure 4a

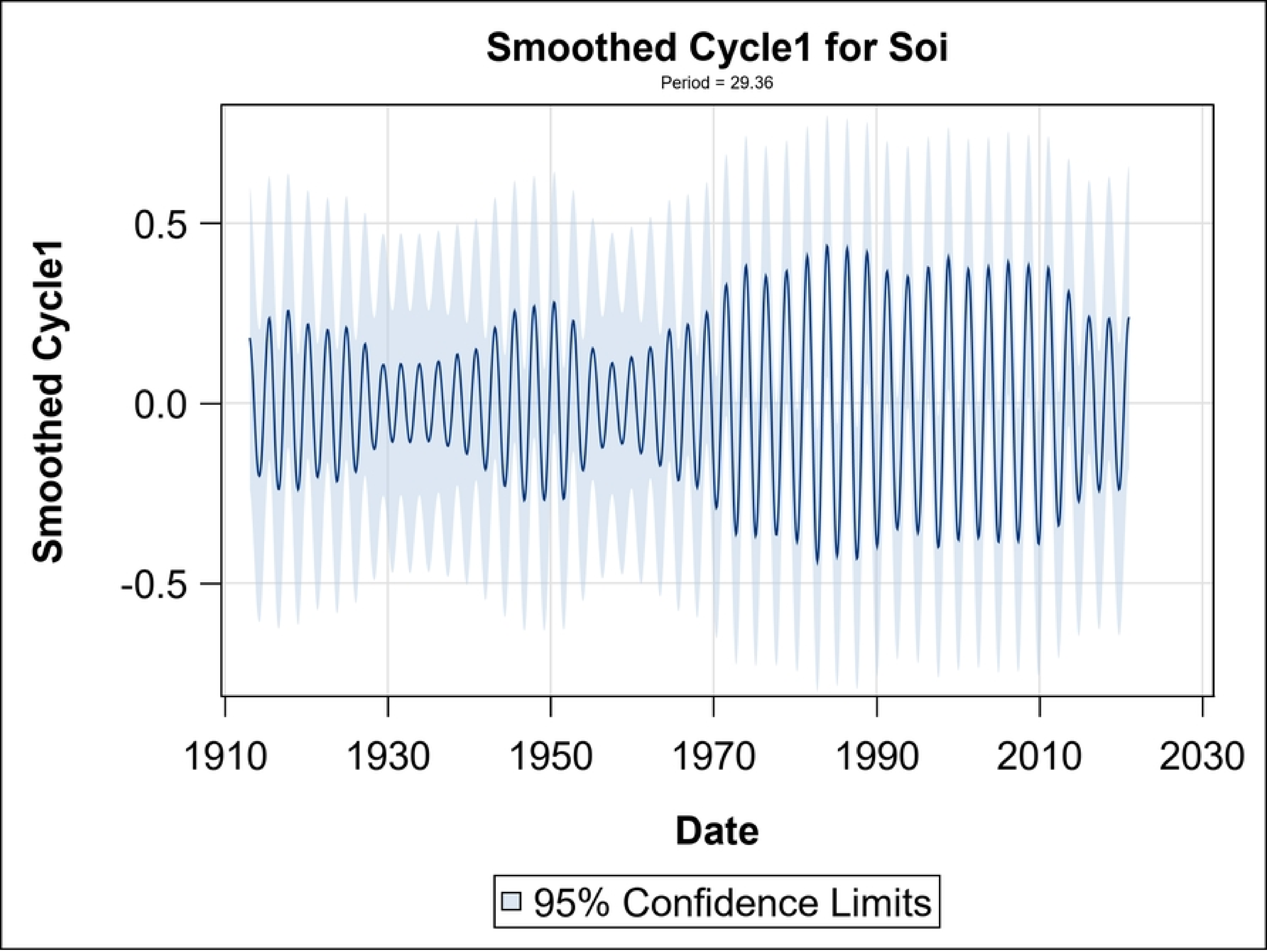
Smoothed Cycle1 for Soi
Period = 29.36
Smoothed Cycle1
0.5
0.0
-0.5
1910
1930
1950
1970
1990
2010
2030
Date
95% Confidence Limits

Figure 4b

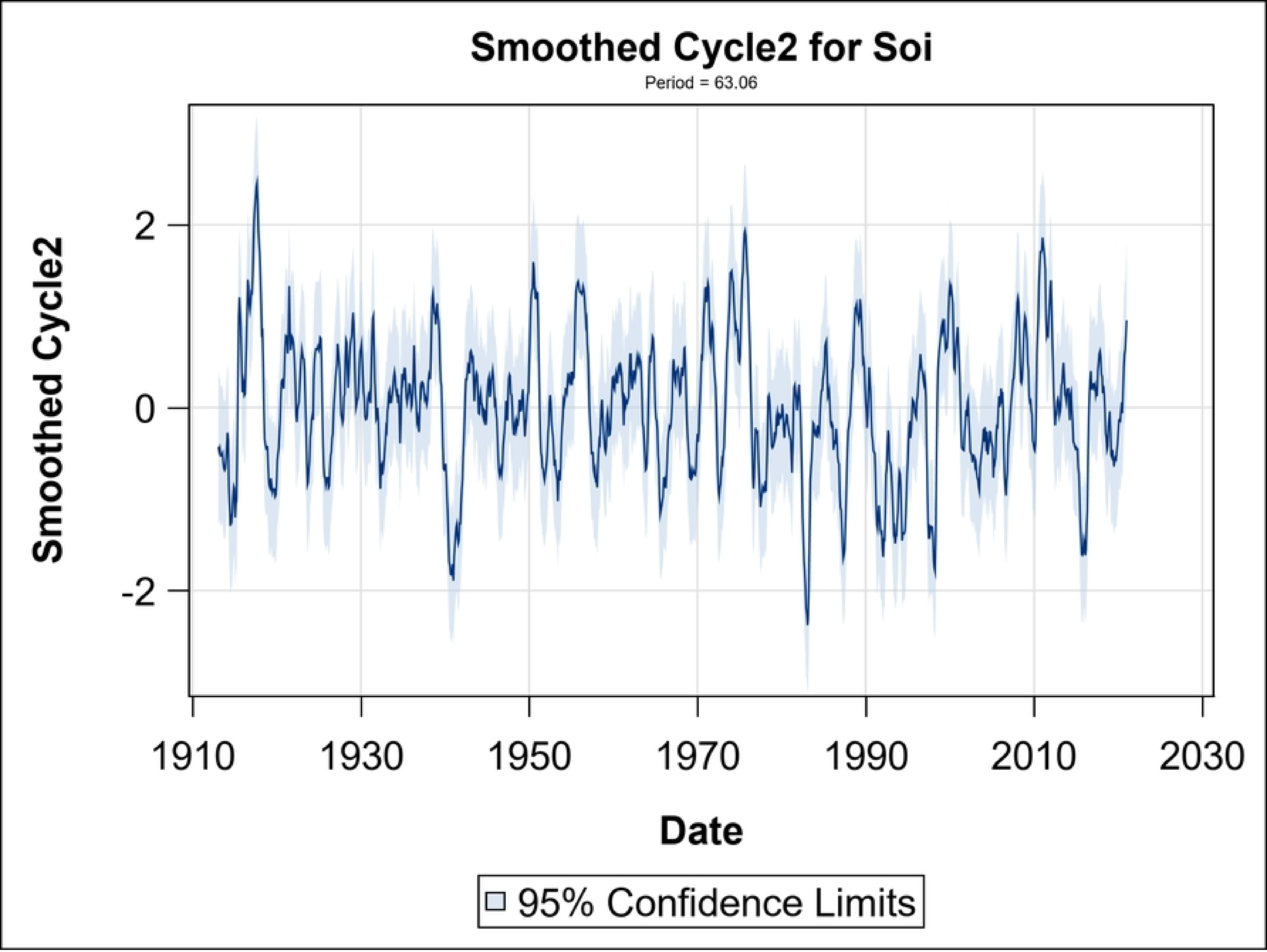
Smoothed Cycle2 for Soi
Period = 63.06
Smoothed Cycle2
2
0
-2
1910
1930
1950
1970
1990
2010
2030
Date
95% Confidence Limits

Figure 4c

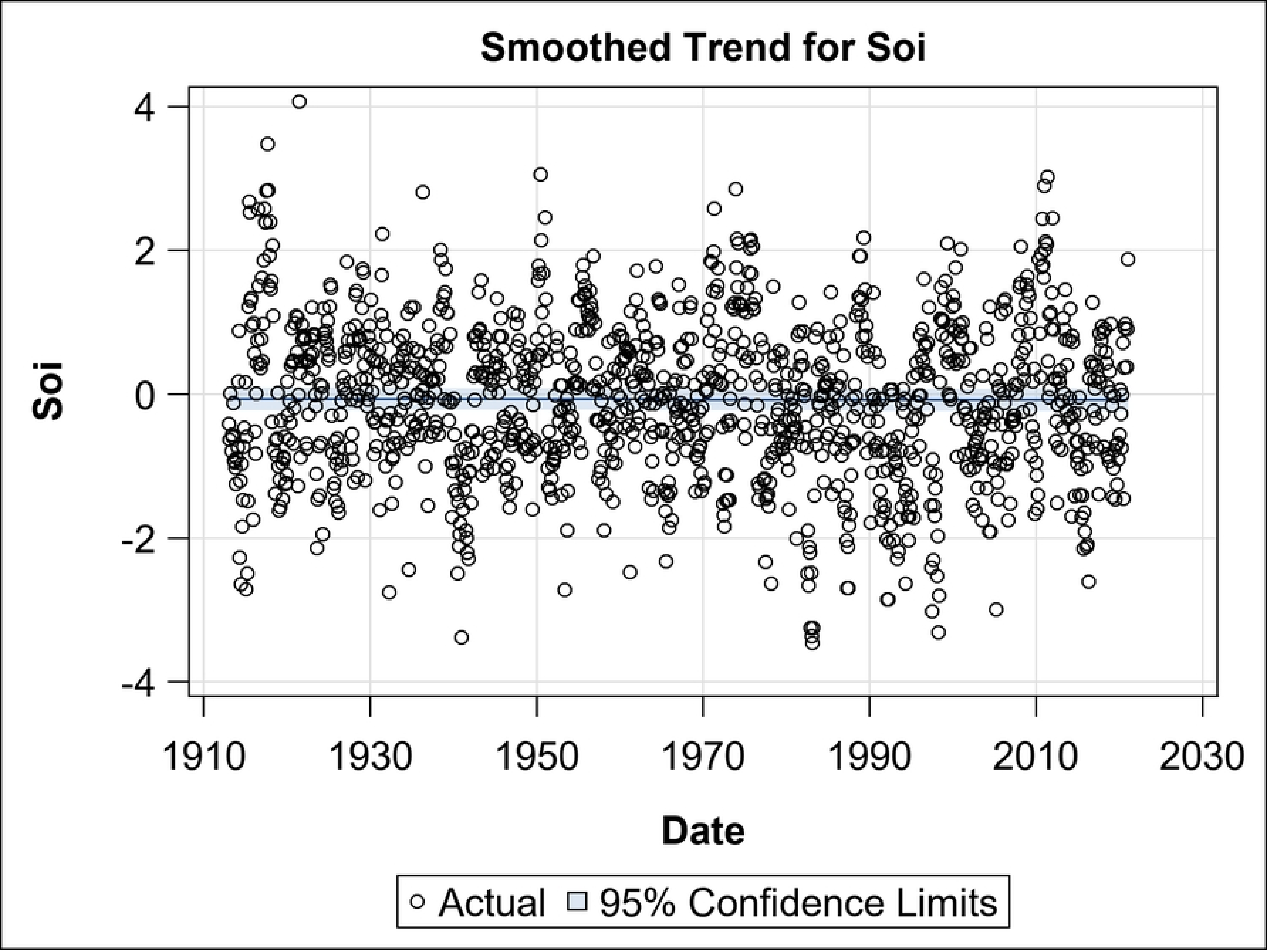
Smoothed Trend for Soi
4
2
0
-2
-4
Soi
1910
1930
1950
1970
1990
2010
2030
Date
Actual
95% Confidence Limits
Figure 4d

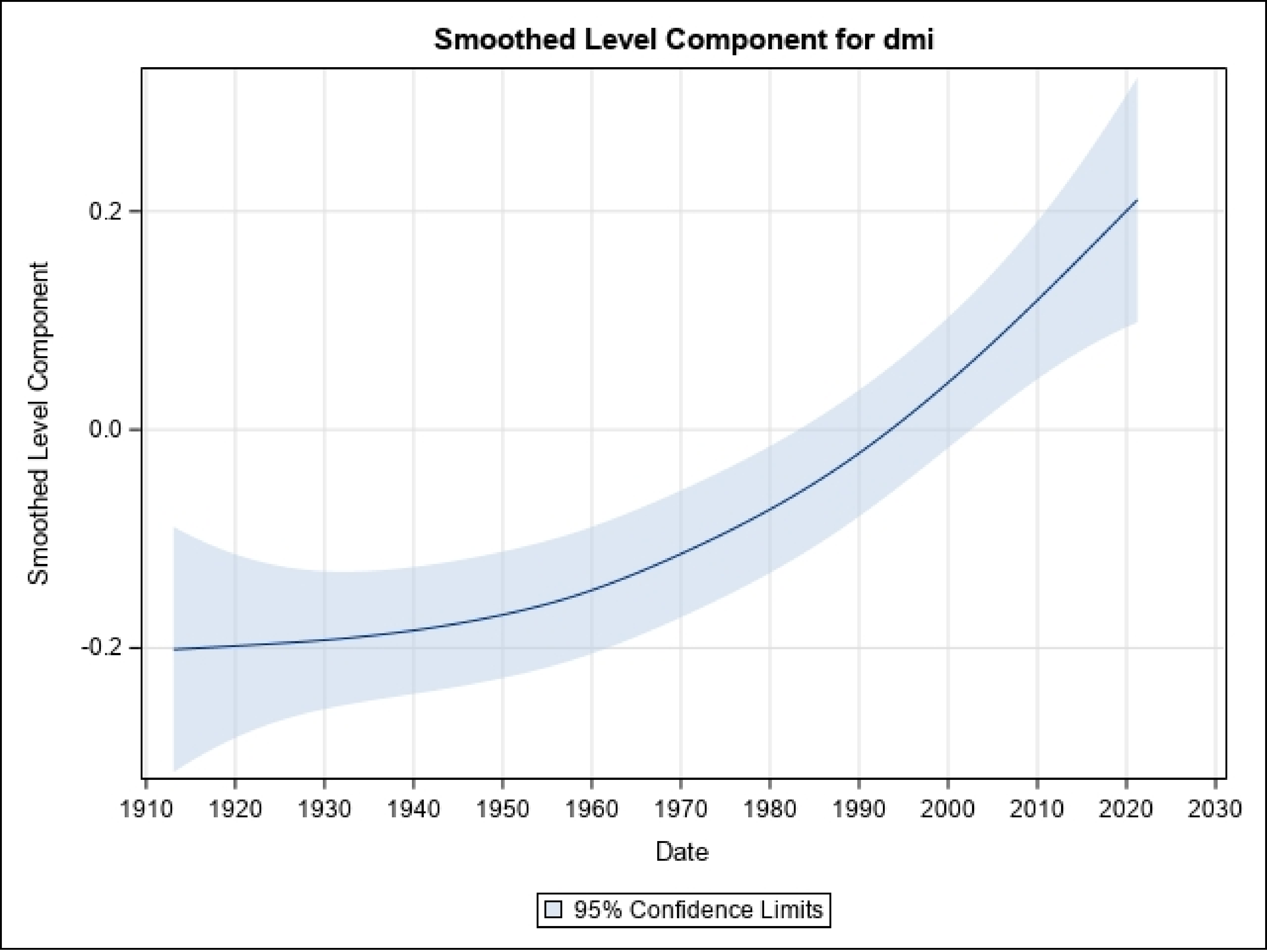

Smoothed Level Component for dmi
Smoothed Level Component
0.2
0.0
-0.2
1910
1920
1930
1940
1950
1960
1970
1980
1990
2000
2010
2020
2030
Date
95% Confidence Limits

Figure 5a

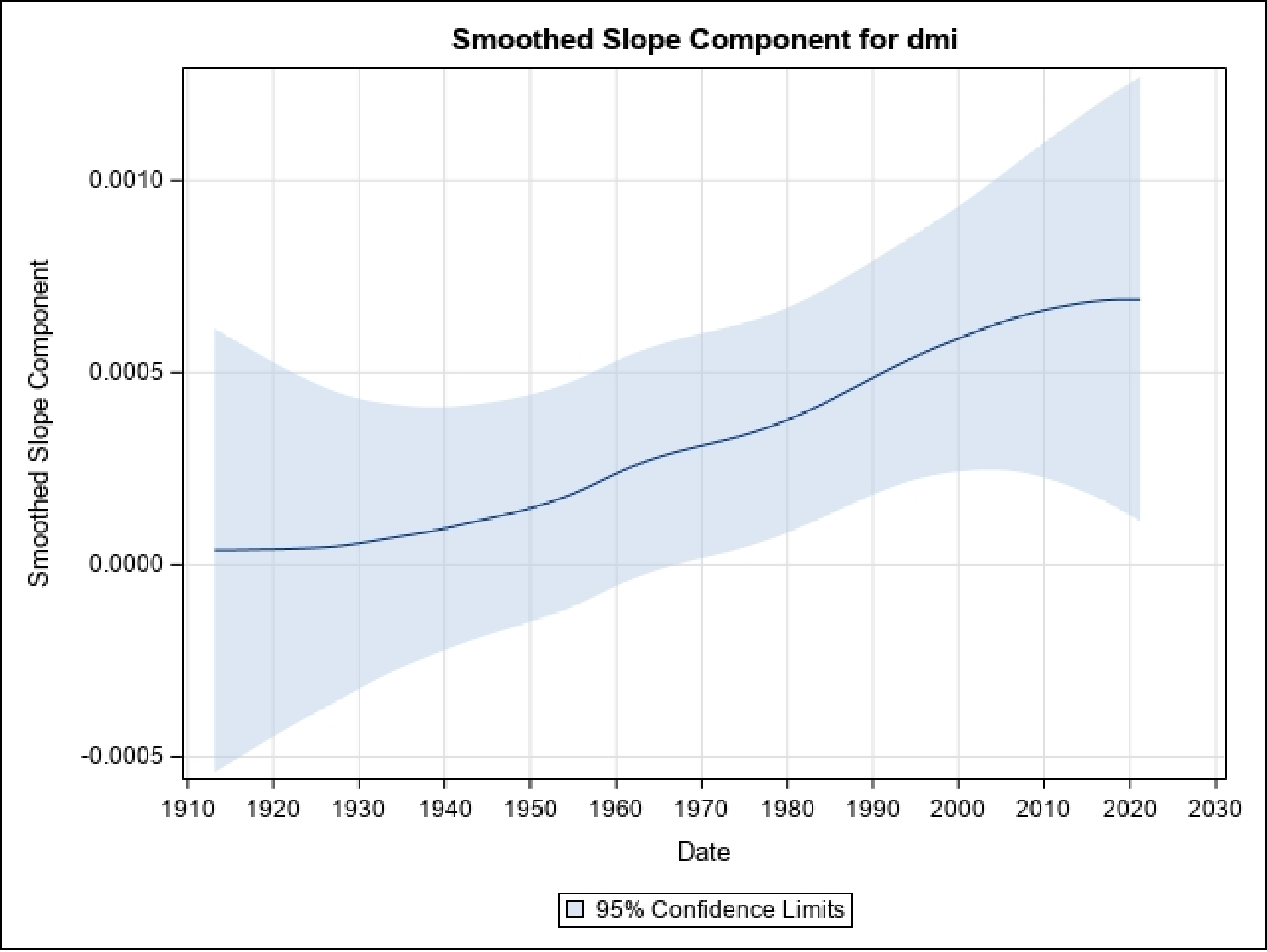
Smoothed Slope Component for dmi
Smoothed Slope Component
0.0010
0.0005
0.0000
-0.0005
1910
1920
1930
1940
1950
1960
1970
1980
1990
2000
2010
2020
2030
Date
95% Confidence Limits

Figure 5b

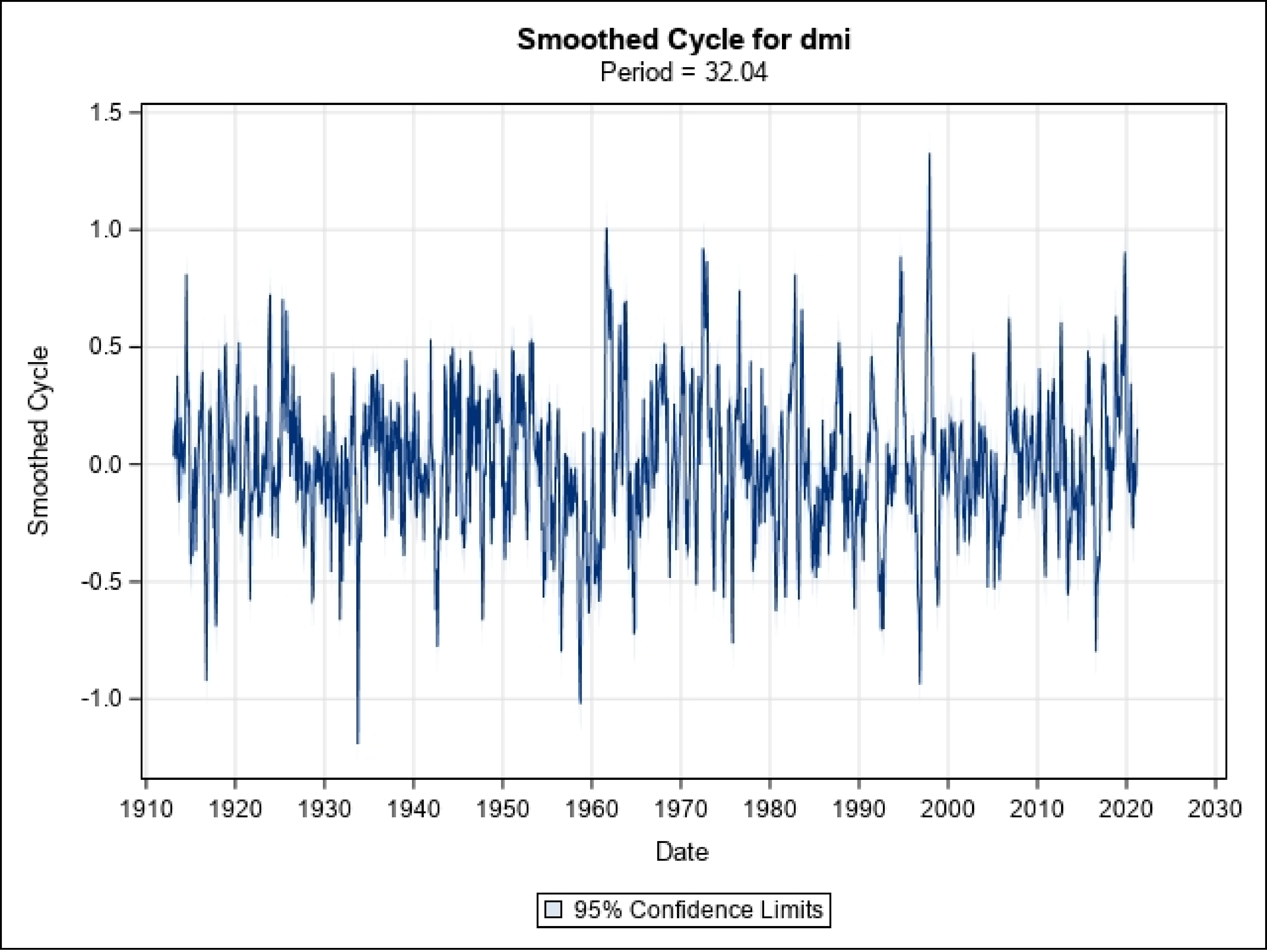
Smoothed Cycle for dmi
Period = 32.04
Smoothed Cycle
1.5
1.0
0.5
0.0
-0.5
-1.0
1910
1920
1930
1940
1950
1960
1970
1980
1990
2000
2010
2020
2030
Date
95% Confidence Limits

Figure 5c

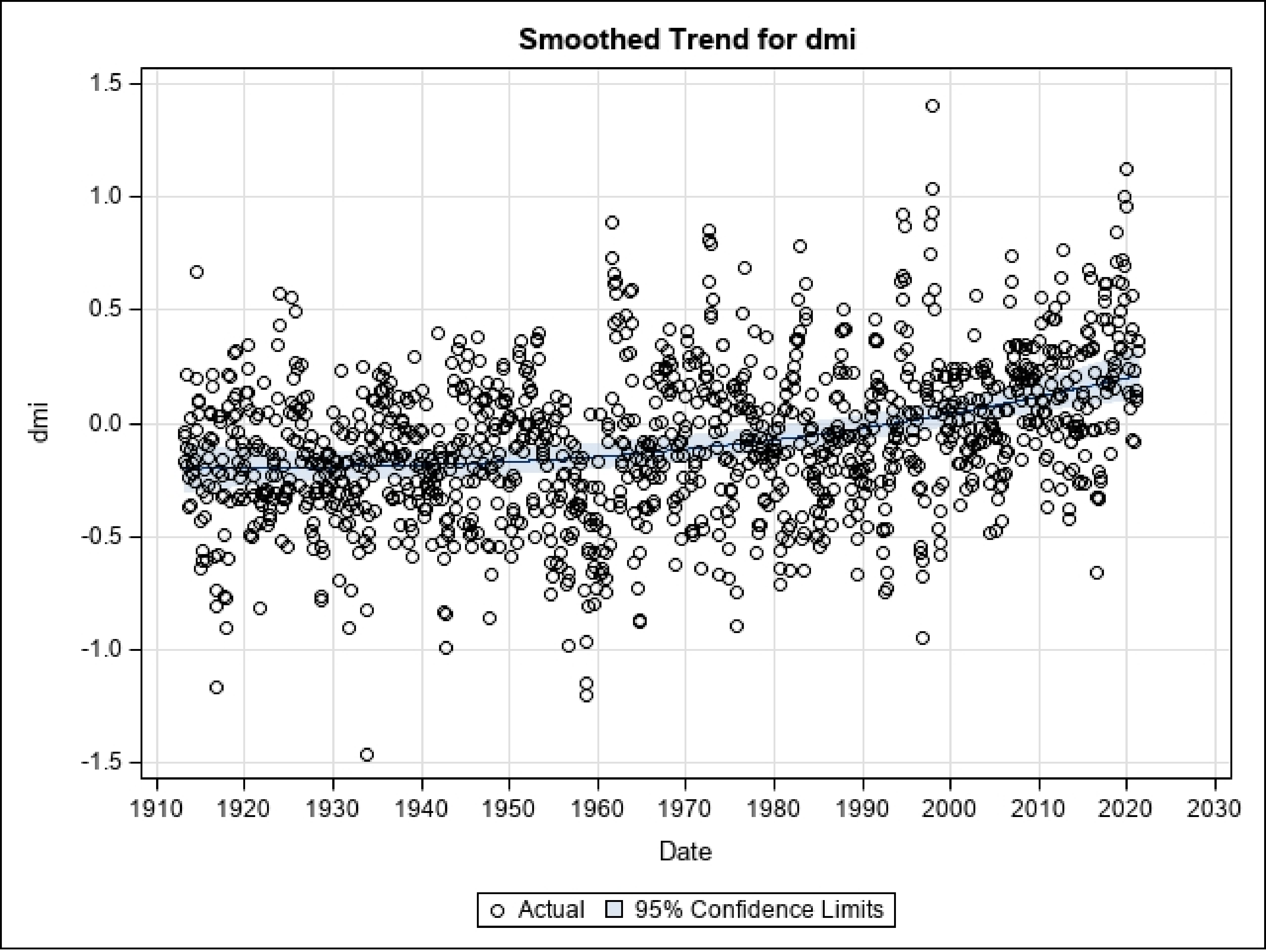
Smoothed Trend for dmi
dmi
1.5
1.0
0.5
0.0
-0.5
-1.0
-1.5
1910
1920
1930
1940
1950
1960
1970
1980
1990
2000
2010
2020
2030
Date
Actual
95% Confidence Limits

Figure 5d

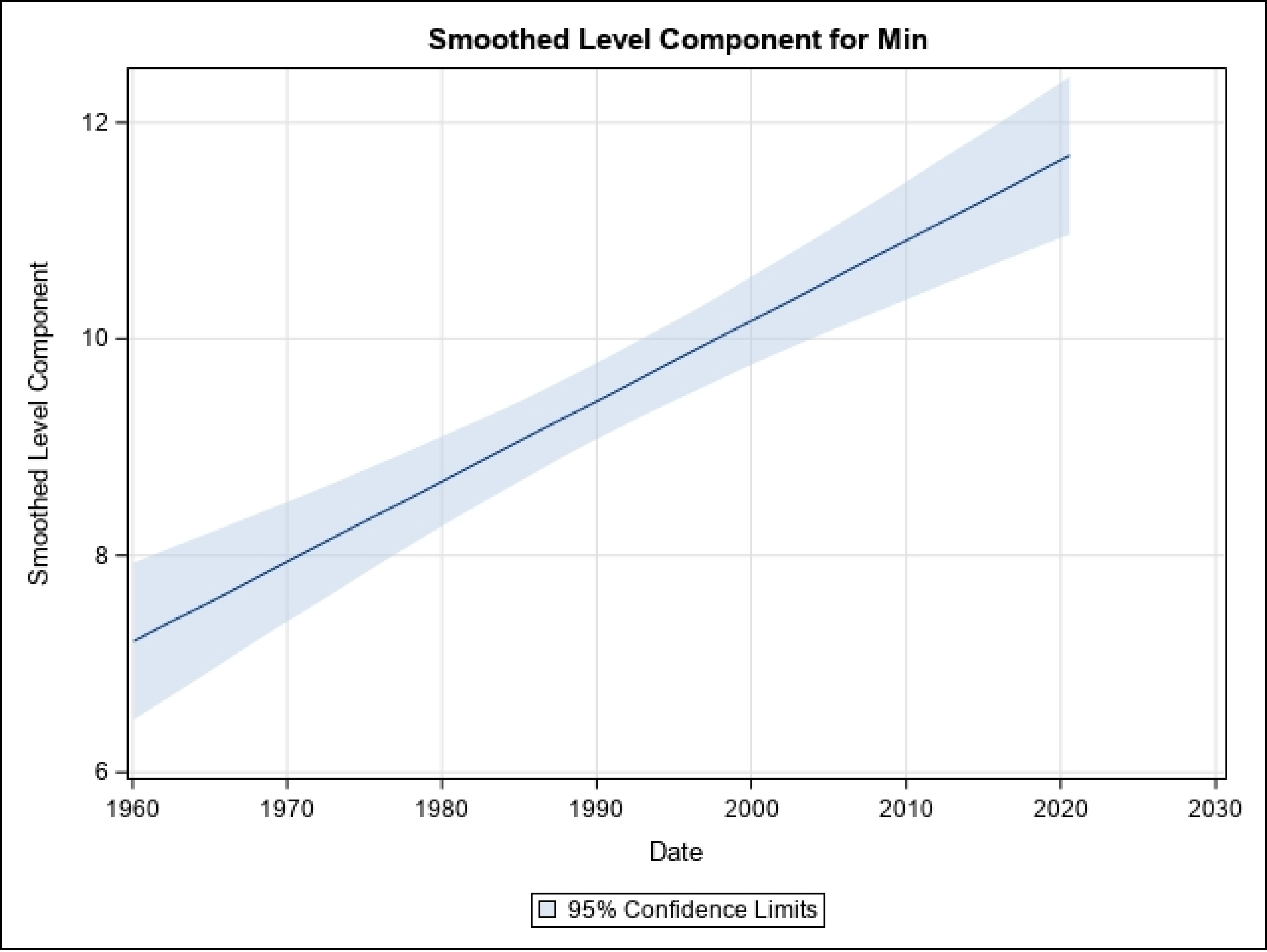
Smoothed Level Component for Min
Smoothed Level Component
12
10
8
6
1960
1970
1980
1990
2000
2010
2020
2030
Date
95% Confidence Limits

Figure 6a

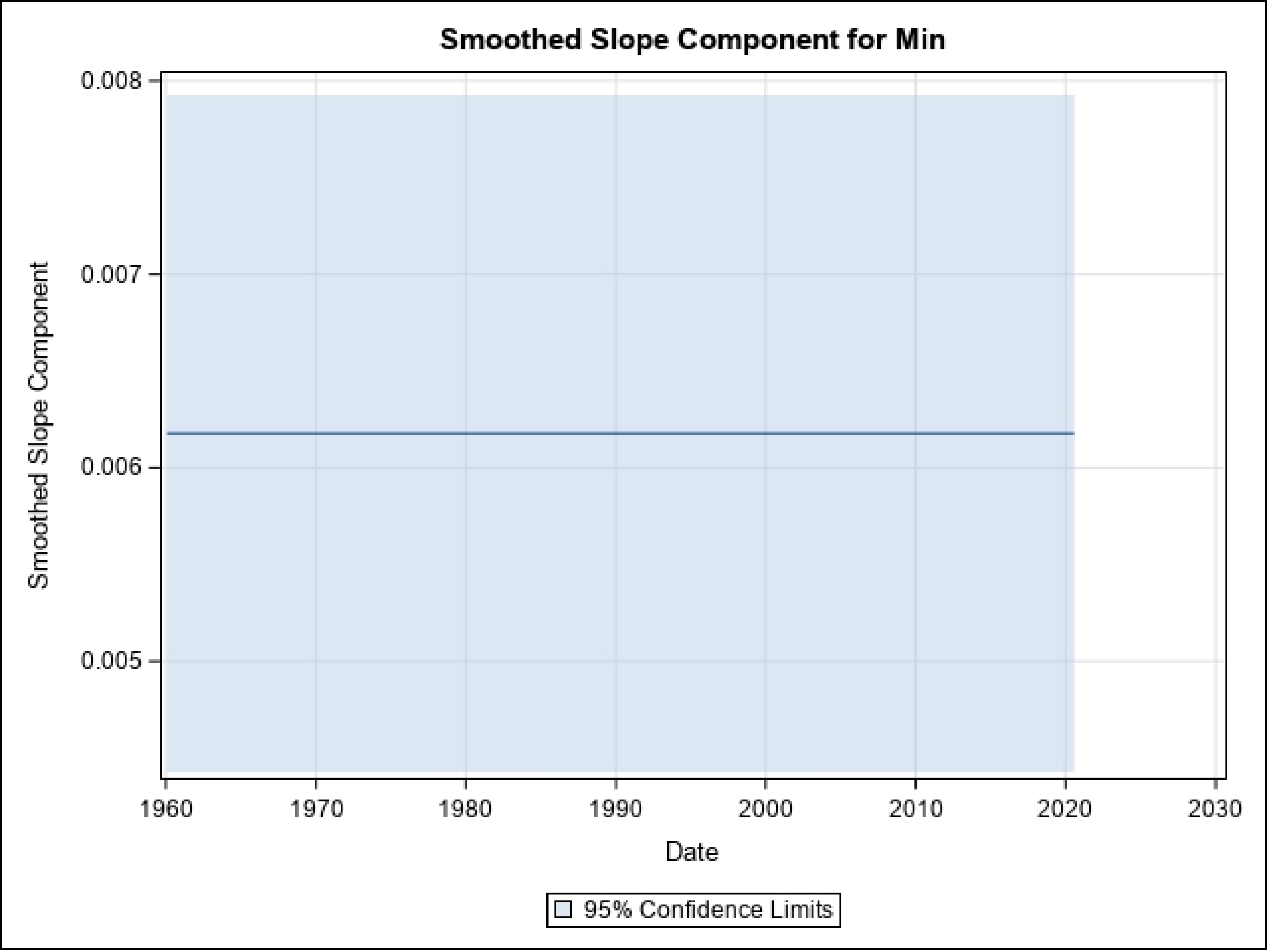

Smoothed Slope Component for Min
0.008
0.007
0.006
0.005
Smoothed Slope Component
1960
1970
1980
1990
2000
2010
2020
2030
Date
95% Confidence Limits

Figure 6b

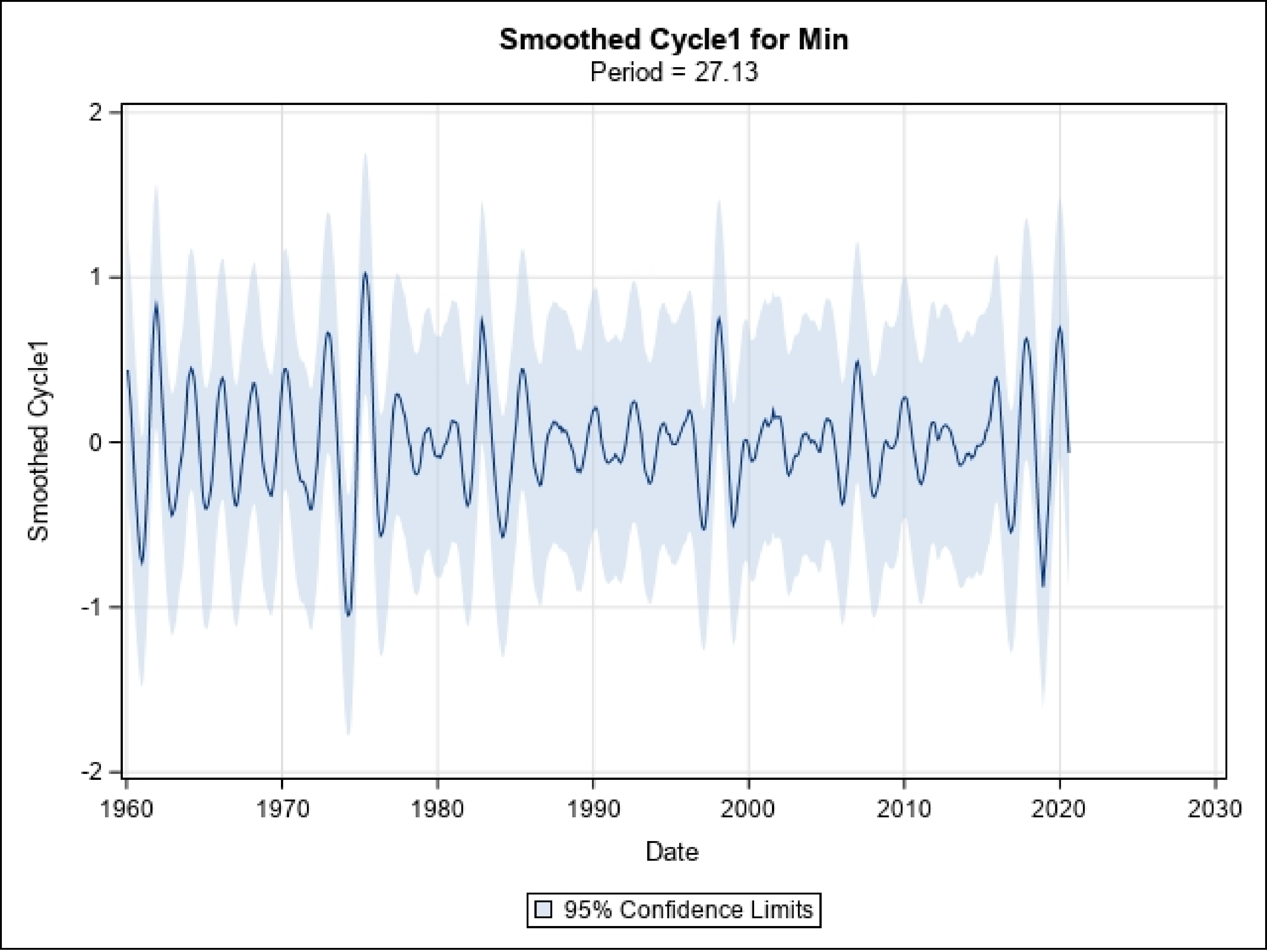
Smoothed Cycle1 for Min
Period = 27.13
Smoothed Cycle1
2
1
0
-1
-2
1960
1970
1980
1990
2000
2010
2020
2030
Date
95% Confidence Limits

Figure 6c

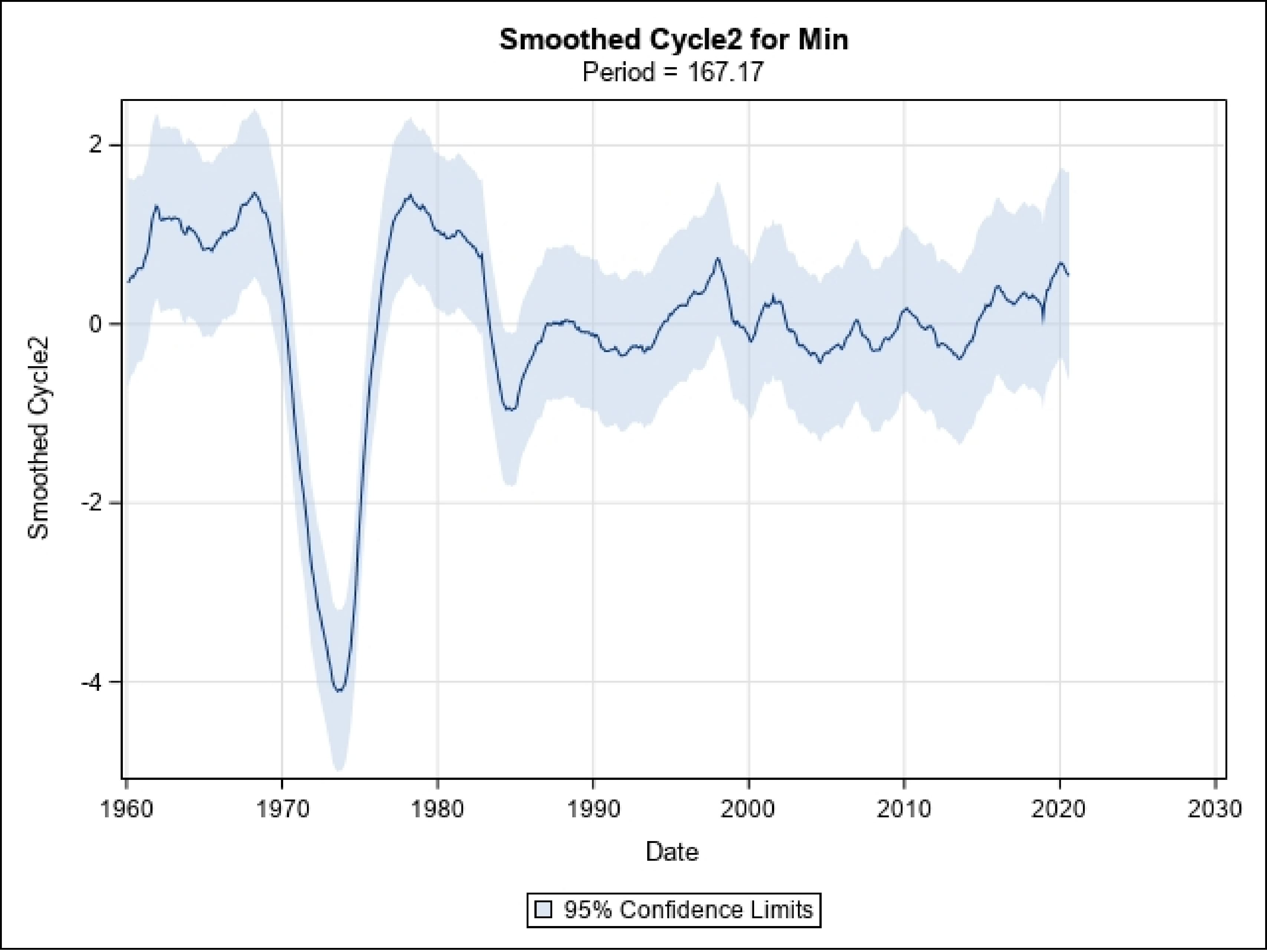
Smoothed Cycle2 for Min
Period = 167.17
Smoothed Cycle2
2
0
-2
-4
1960
1970
1980
1990
2000
2010
2020
2030
Date
95% Confidence Limits

Figure 6d

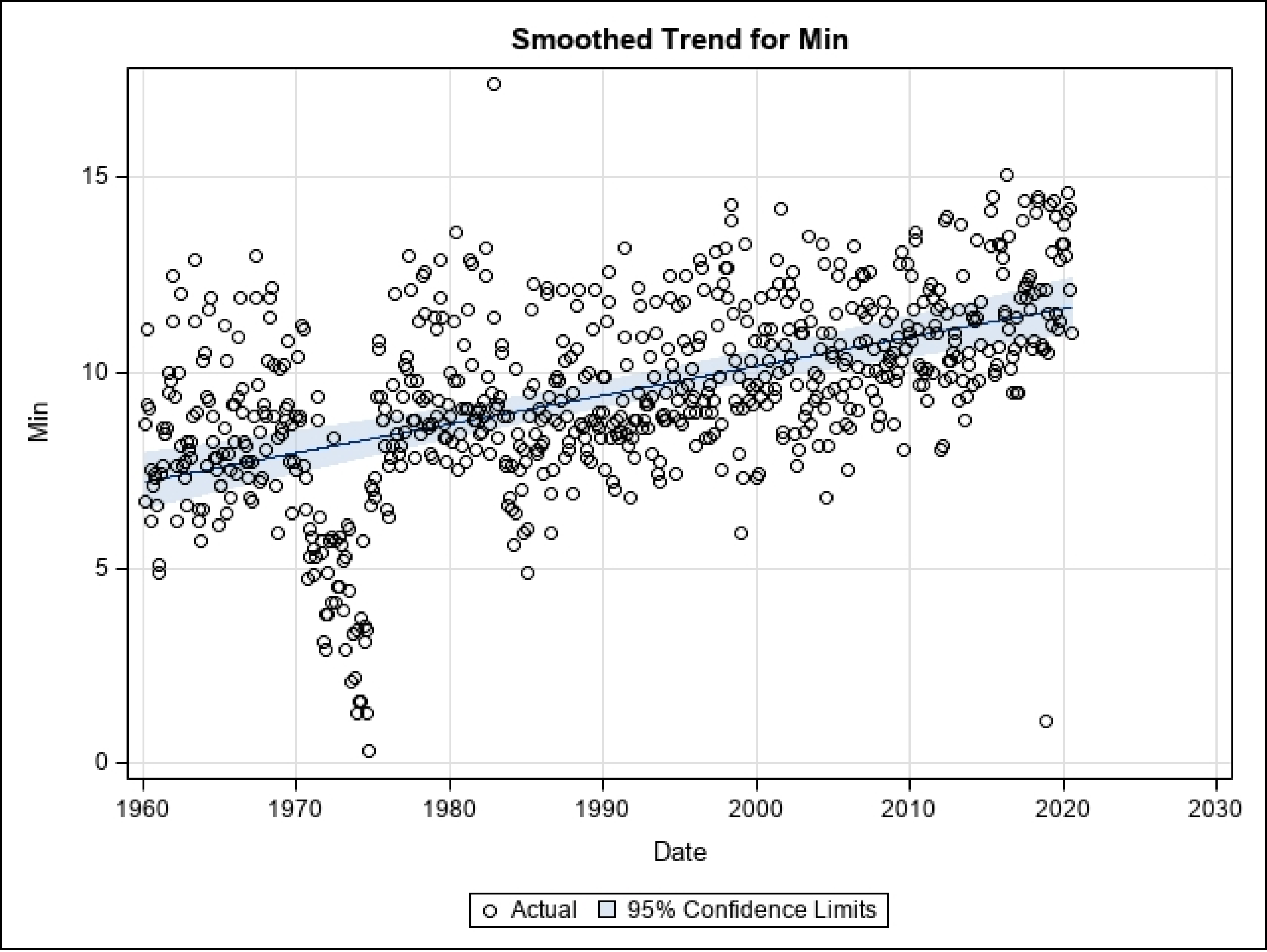

Smoothed Trend for Min
15
10
5
0
Min
1960
1970
1980
1990
2000
2010
2020
2030
Date
Actual
95% Confidence Limits

Figure 6e

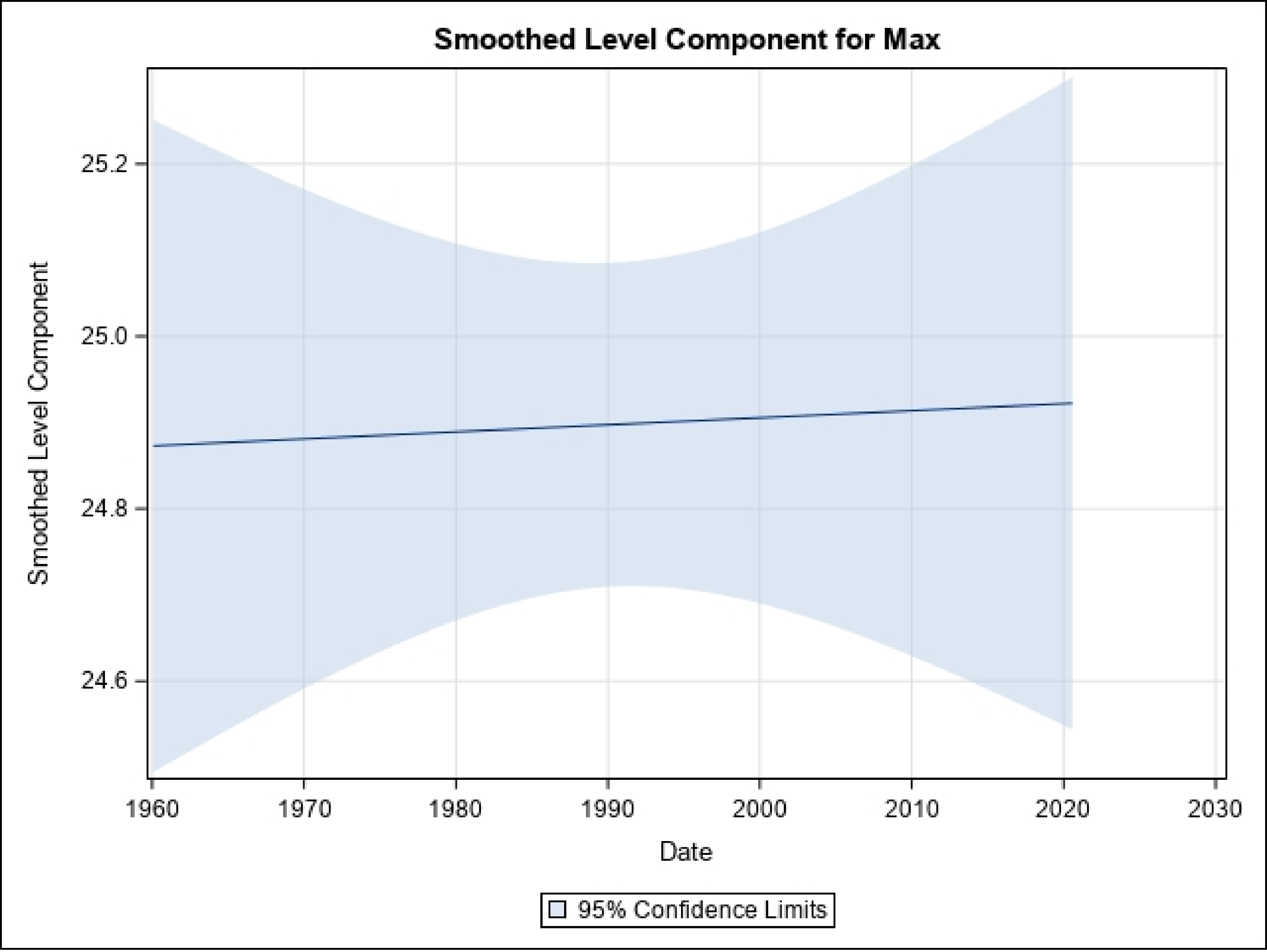

Smoothed Level Component for Max
Smoothed Level Component
25.2
25.0
24.8
24.6
1960
1970
1980
1990
2000
2010
2020
2030
Date
95% Confidence Limits

Figure 7a

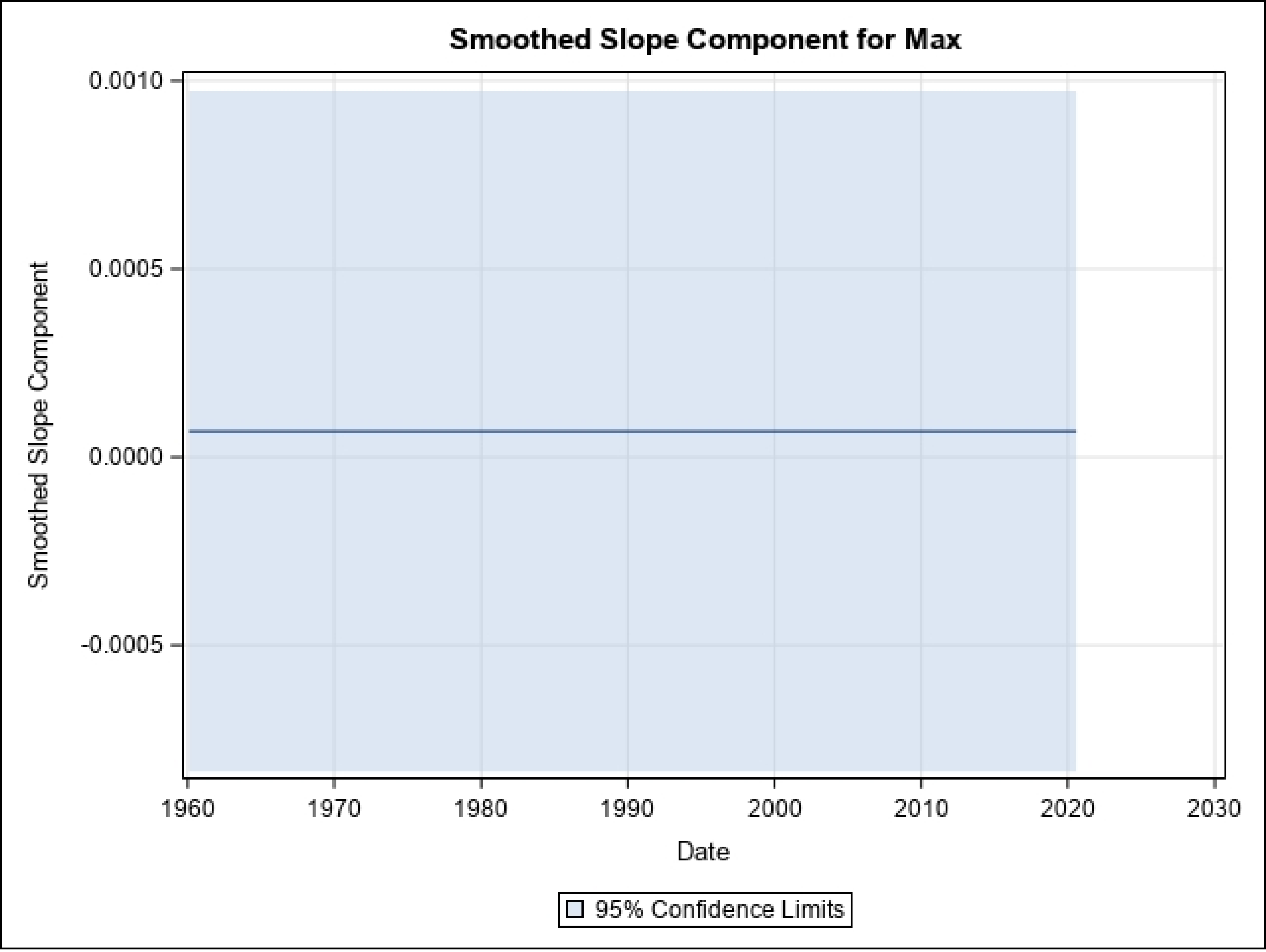

Smoothed Slope Component for Max
Smoothed Slope Component
0.0010
0.0005
0.0000
-0.0005
1960
1970
1980
1990
2000
2010
2020
2030
Date
95% Confidence Limits

Figure 7b

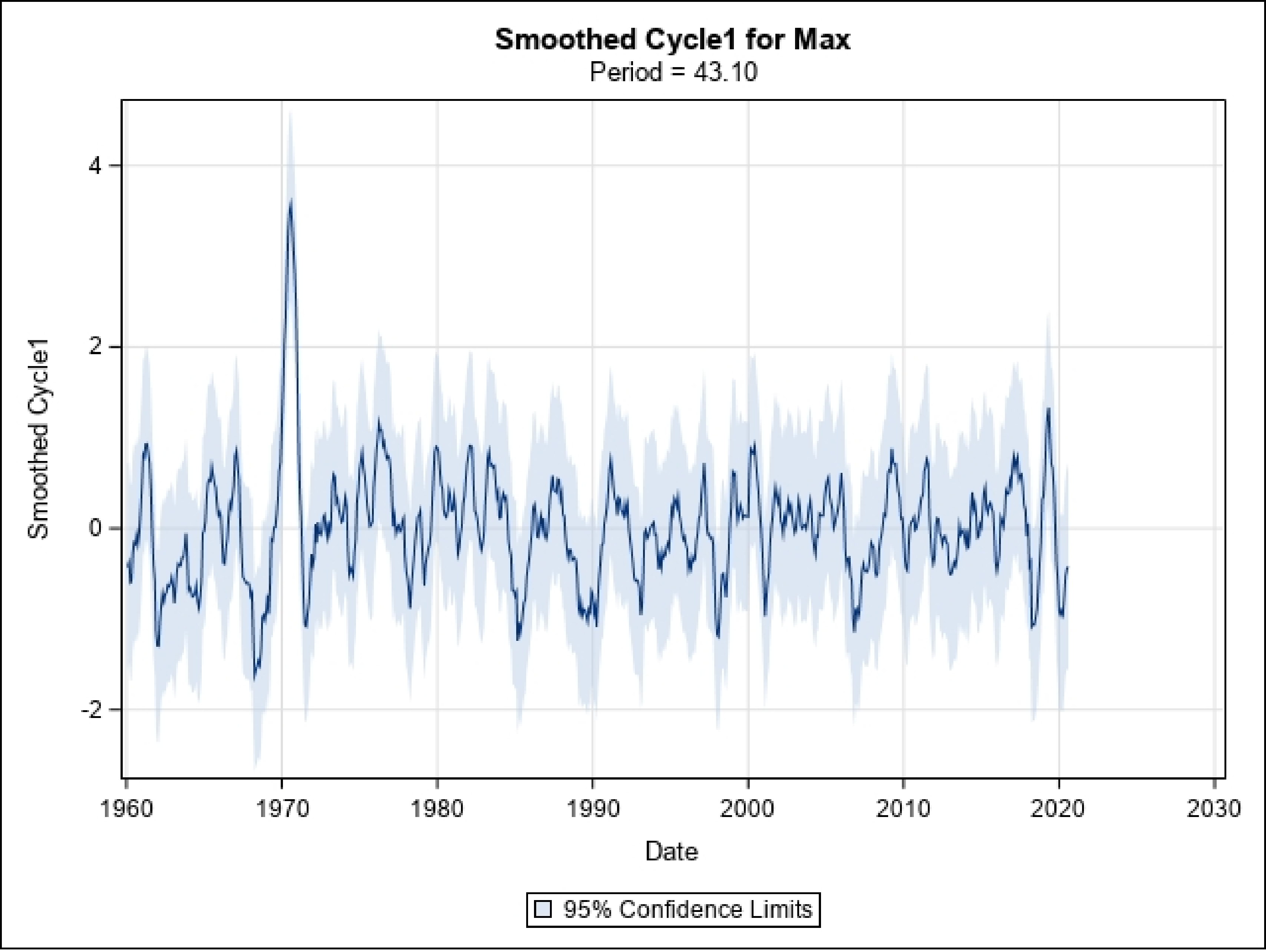

Smoothed Cycle1 for Max
Period = 43.10
4
2
0
-2
Smoothed Cycle1
1960
1970
1980
1990
2000
2010
2020
2030
Date
95% Confidence Limits

Figure 7c

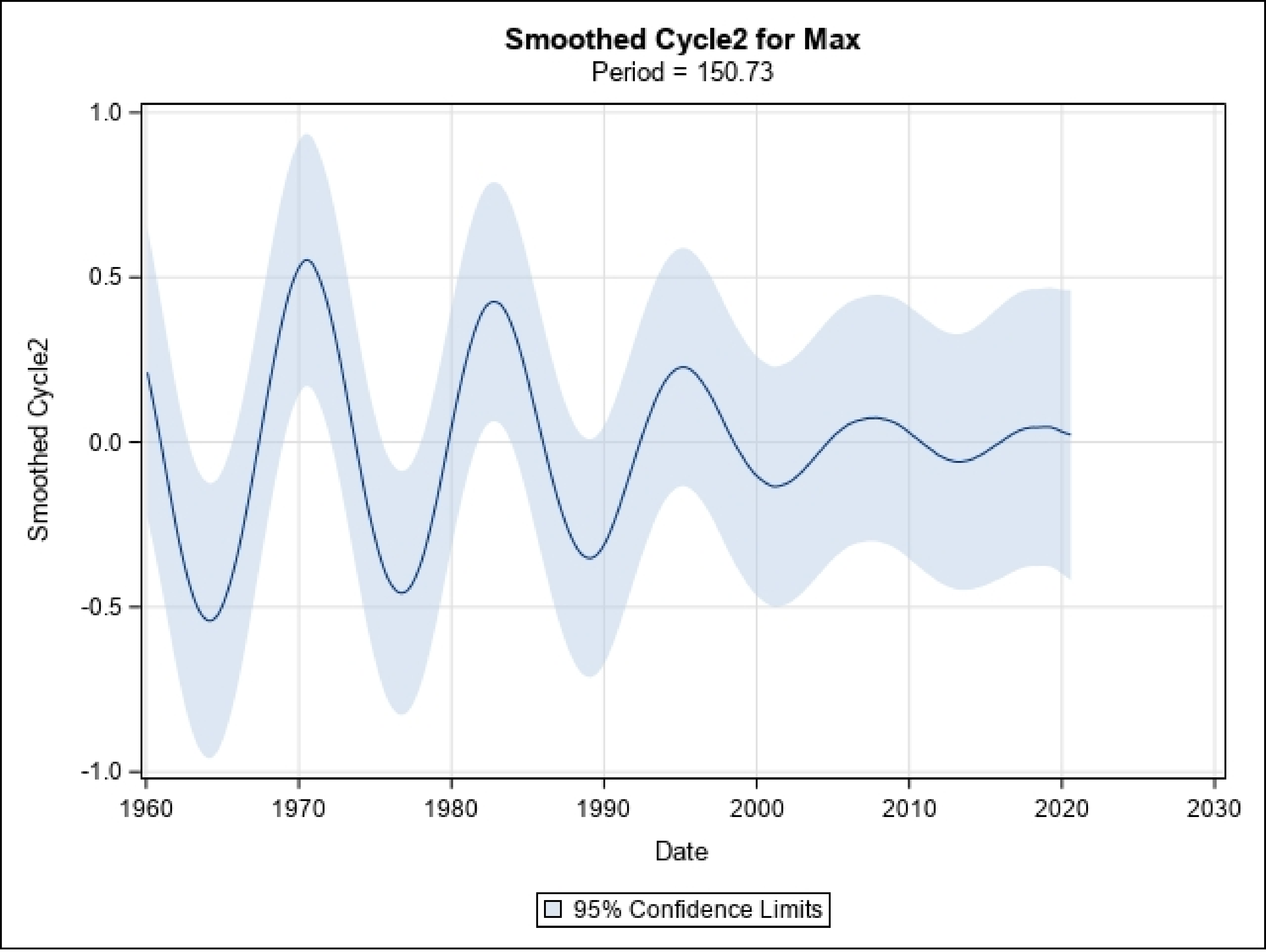
Smoothed Cycle2 for Max
Period = 150.73
Smoothed Cycle2
1.0
0.5
0.0
-0.5
-1.0
1960
1970
1980
1990
2000
2010
2020
2030
Date
95% Confidence Limits

Figure 7d

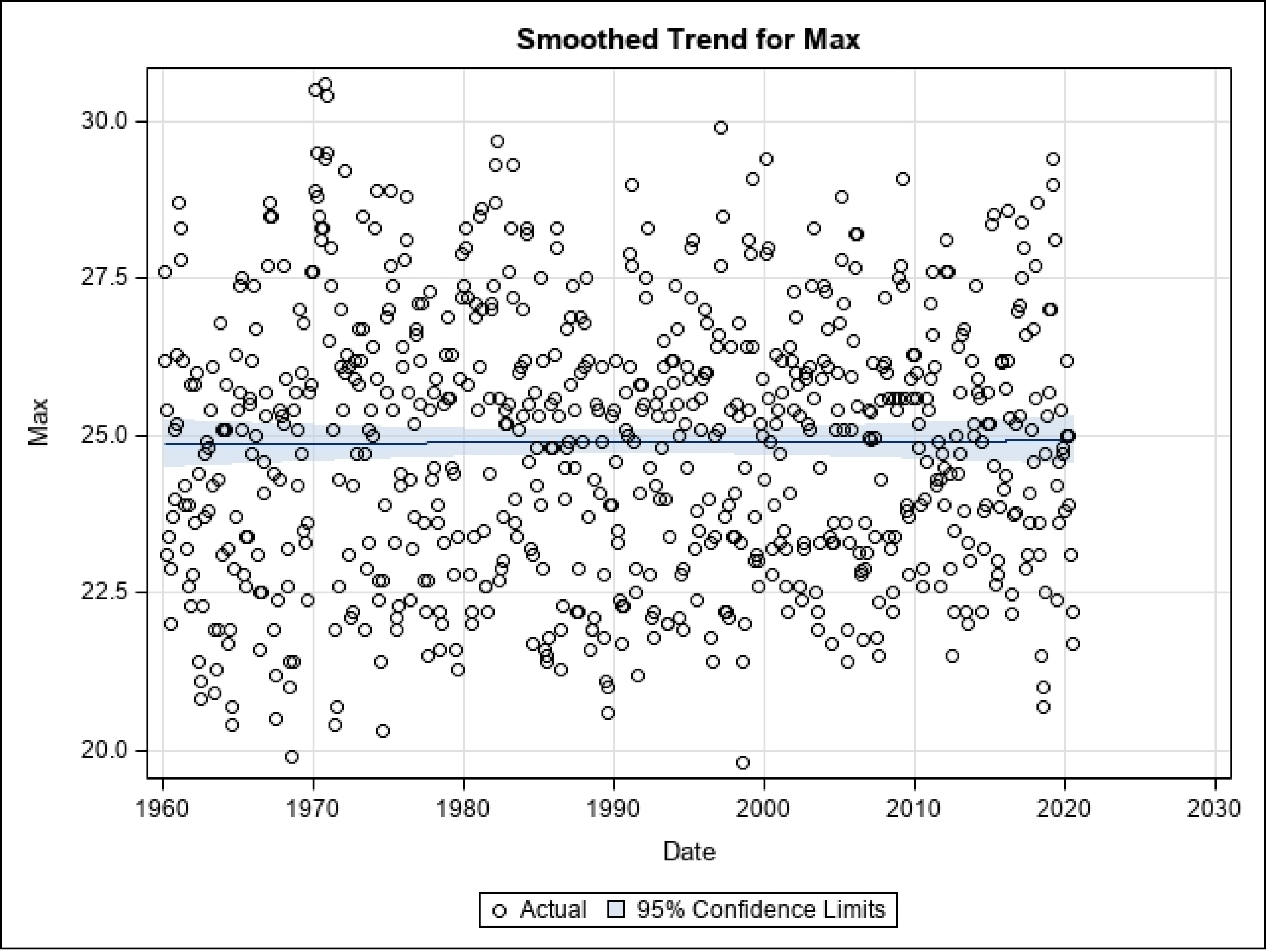
Smoothed Trend for Max
Max
30.0
27.5
25.0
22.5
20.0
1960
1970
1980
1990
2000
2010
2020
2030
Date
Actual
95% Confidence Limits

Figure 7e

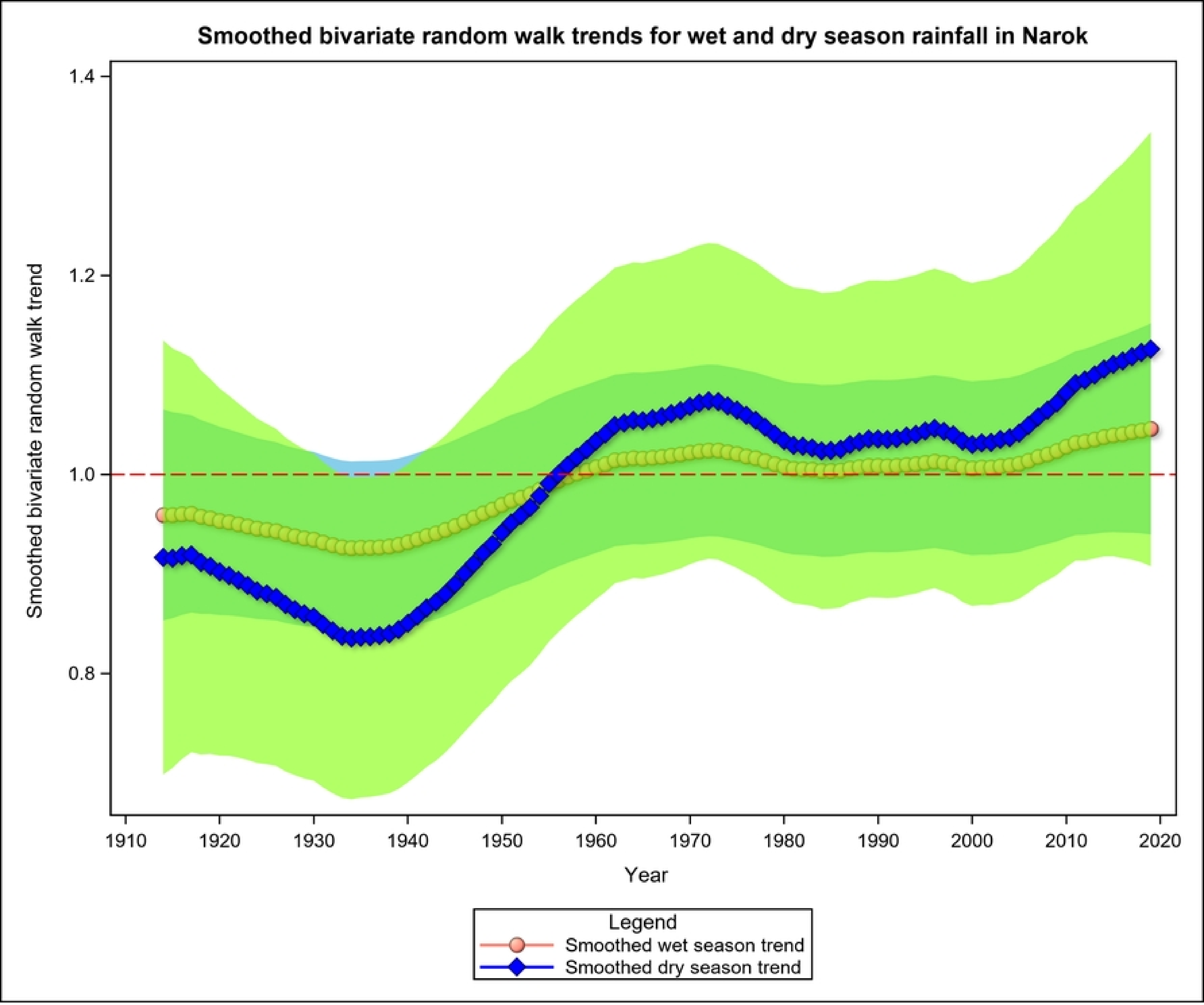
Smoothed bivariate random walk trends for wet and dry season rainfall in Narok
Smoothed bivariate random walk trend
1.4
1.2
1.0
0.8
1910
1920
1930
1940
1950
1960
1970
1980
1990
2000
2010
2020
Year
Legend
Smoothed wet season trend
Smoothed dry season trend

Figure 8a

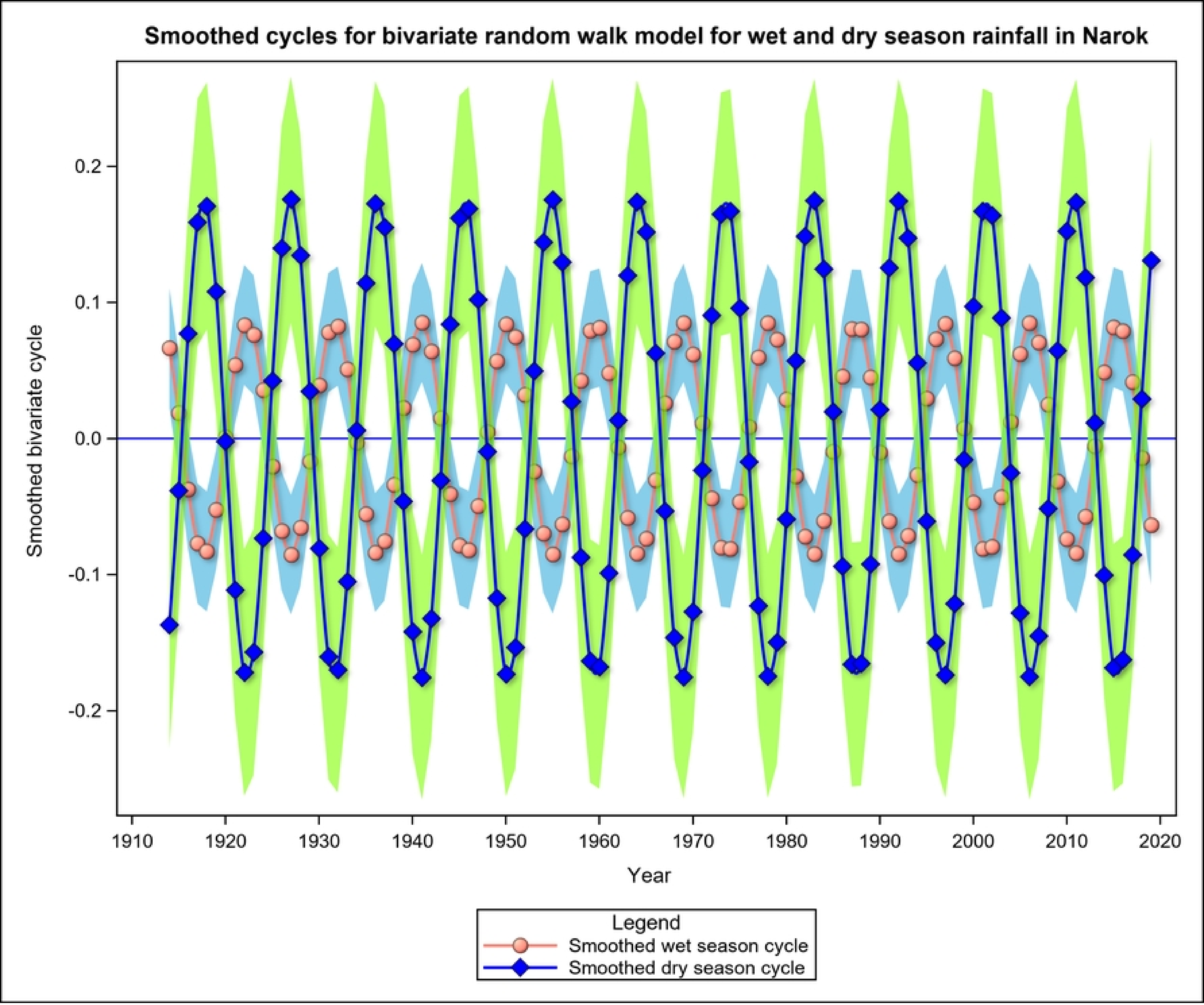
Smoothed cycles for bivariate random walk model for wet and dry season rainfall in Narok
Smoothed bivariate cycle
0.2
0.1
0.0
-0.1
-0.2
1910
1920
1930
1940
1950
1960
1970
1980
1990
2000
2010
2020
Year
Legend
Smoothed wet season cycle
Smoothed dry season cycle

Figure 8b

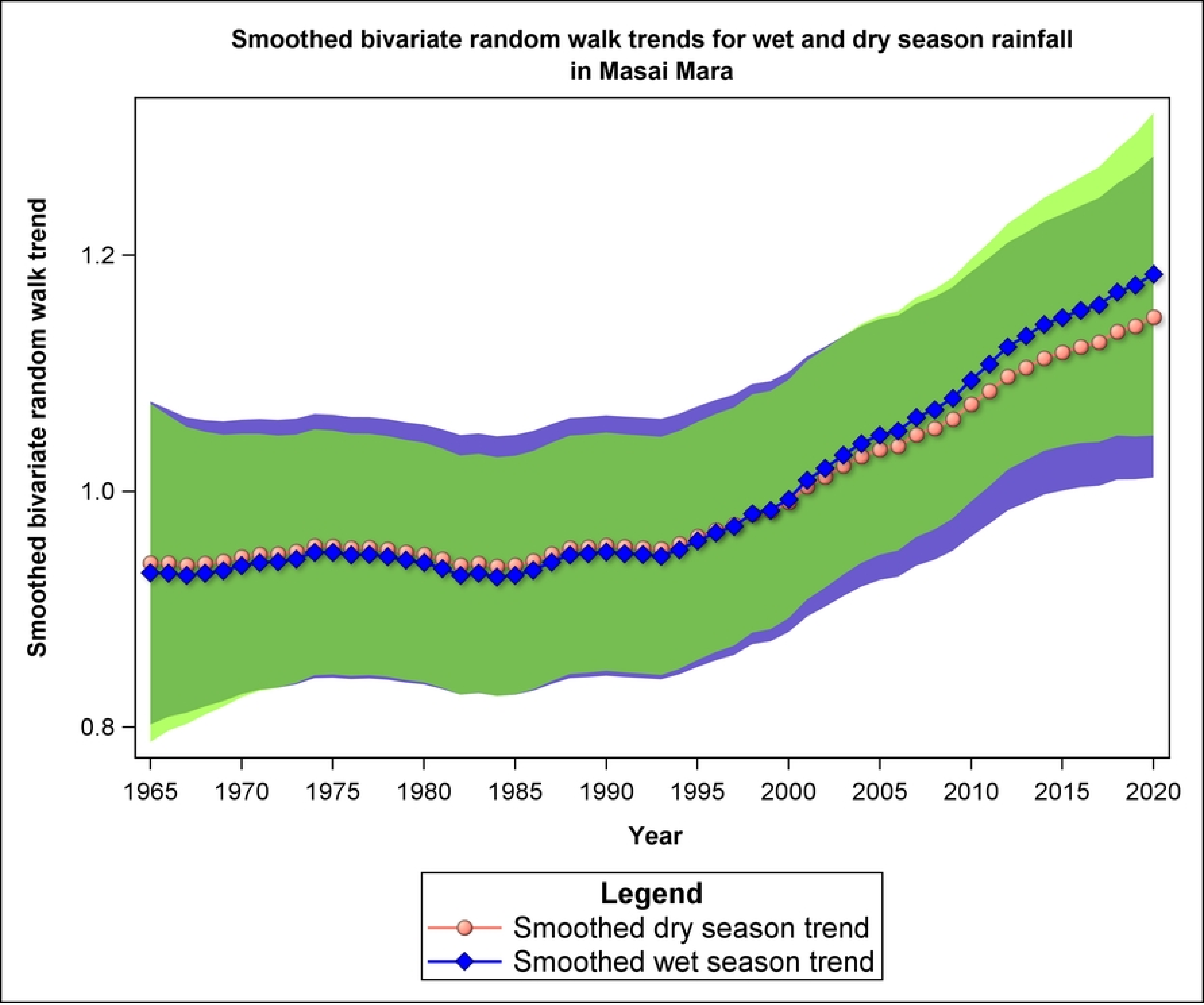
Smoothed bivariate random walk trends for wet and dry season rainfall
in Masai Mara
Smoothed bivariate random walk trend
1.2
1.0
0.8
1965
1970
1975
1980
1985
1990
1995
2000
2005
2010
2015
2020
Year
Legend
Smoothed dry season trend
Smoothed wet season trend

Figure 9a

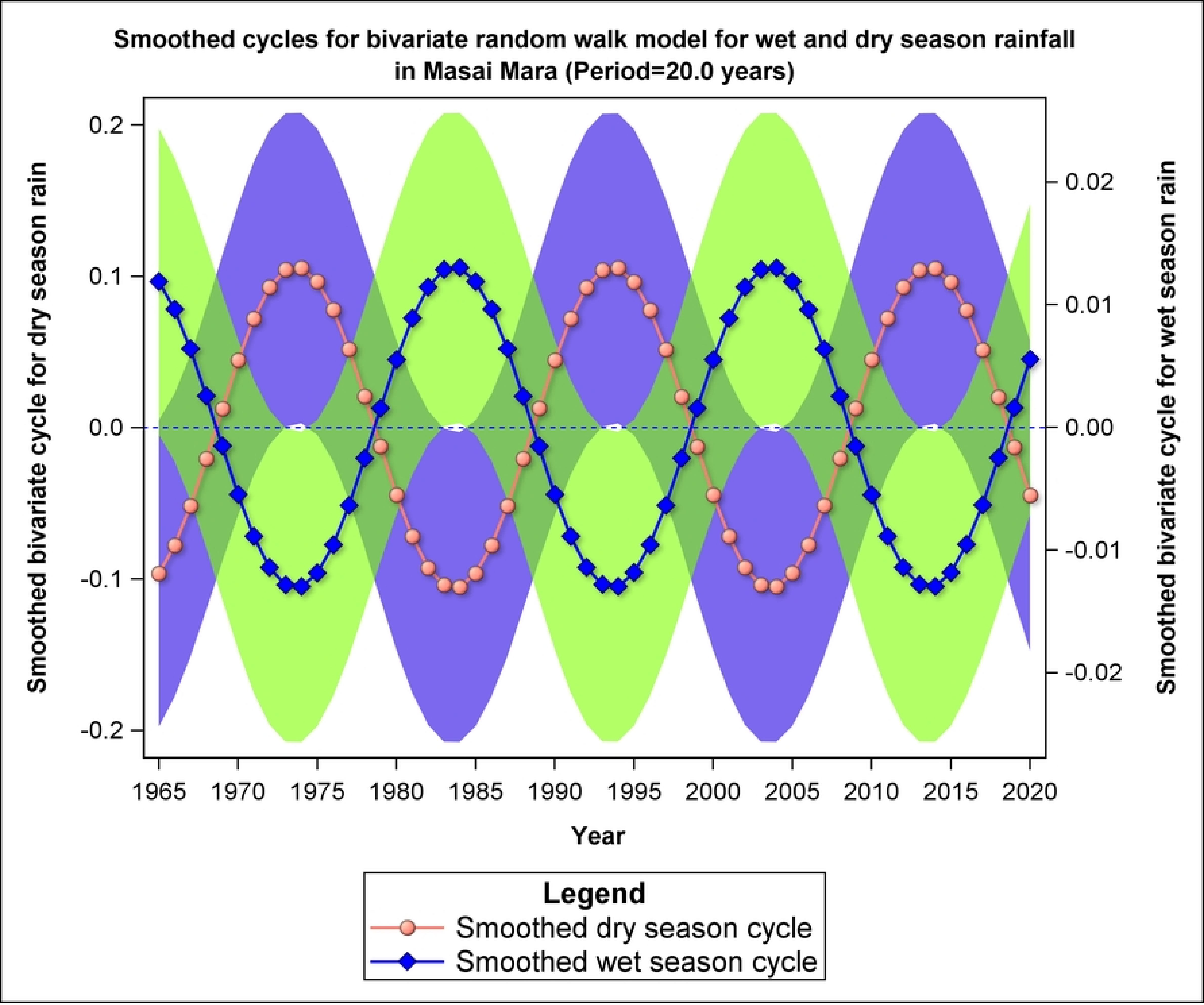
Smoothed cycles for bivariate random walk model for wet and dry season rainfall
in Masai Mara (Period=20.0 years)
0.2
0.1
0.0
-0.1
-0.2
Smoothed bivariate cycle for dry season rain
0.02
0.01
0.00
-0.01
-0.02
Smoothed bivariate cycle for wet season rain
1965
1970
1975
1980
1985
1990
1995
2000
2005
2010
2015
2020
Year
Legend
Smoothed dry season cycle
Smoothed wet season cycle

Figure 9b

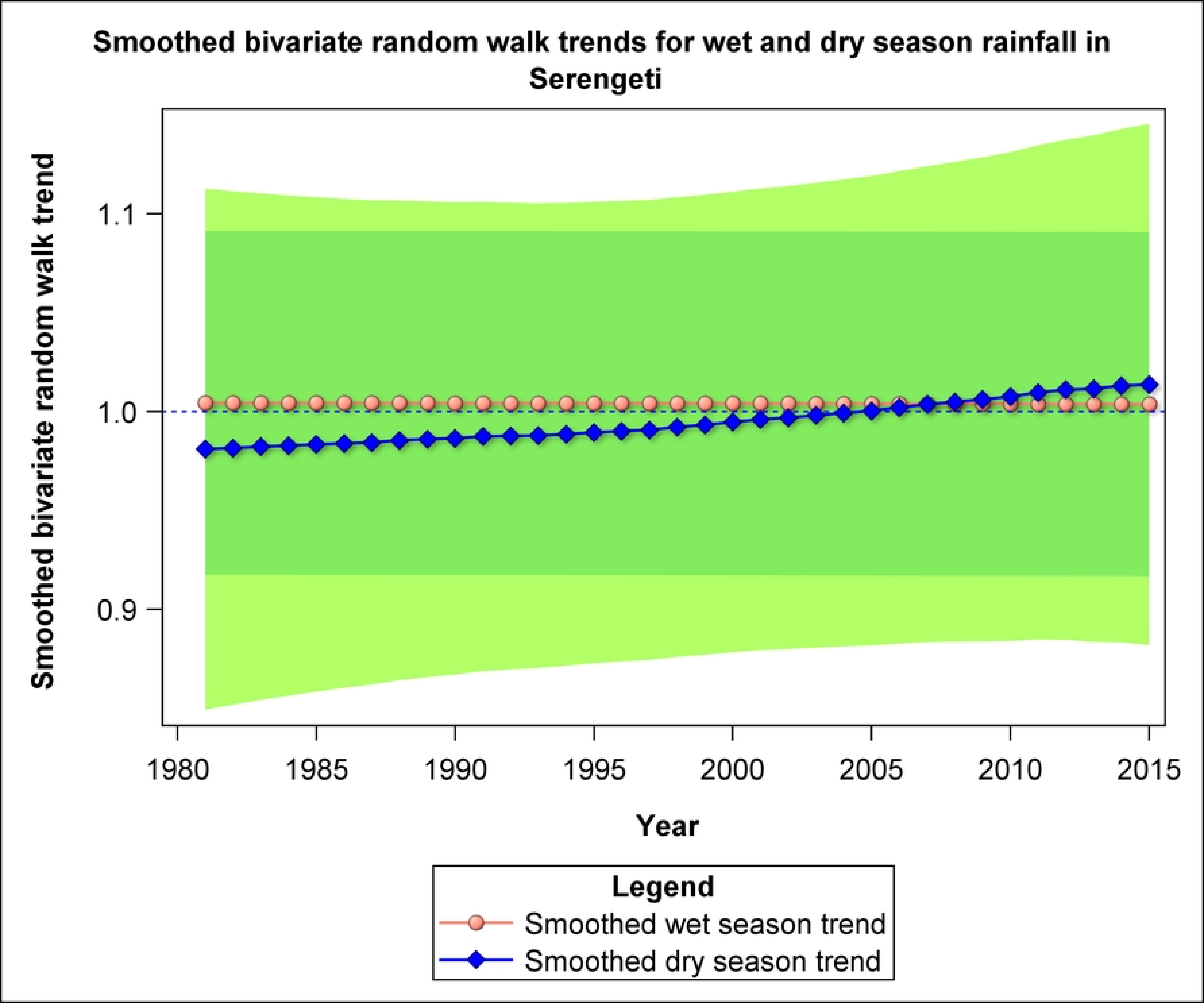

Smoothed bivariate random walk trends for wet and dry season rainfall in Serengeti
Smoothed bivariate random walk trend
1.1
1.0
0.9
1980
1985
1990
1995
2000
2005
2010
2015
Year
Legend
Smoothed wet season trend
Smoothed dry season trend

Figure 10a

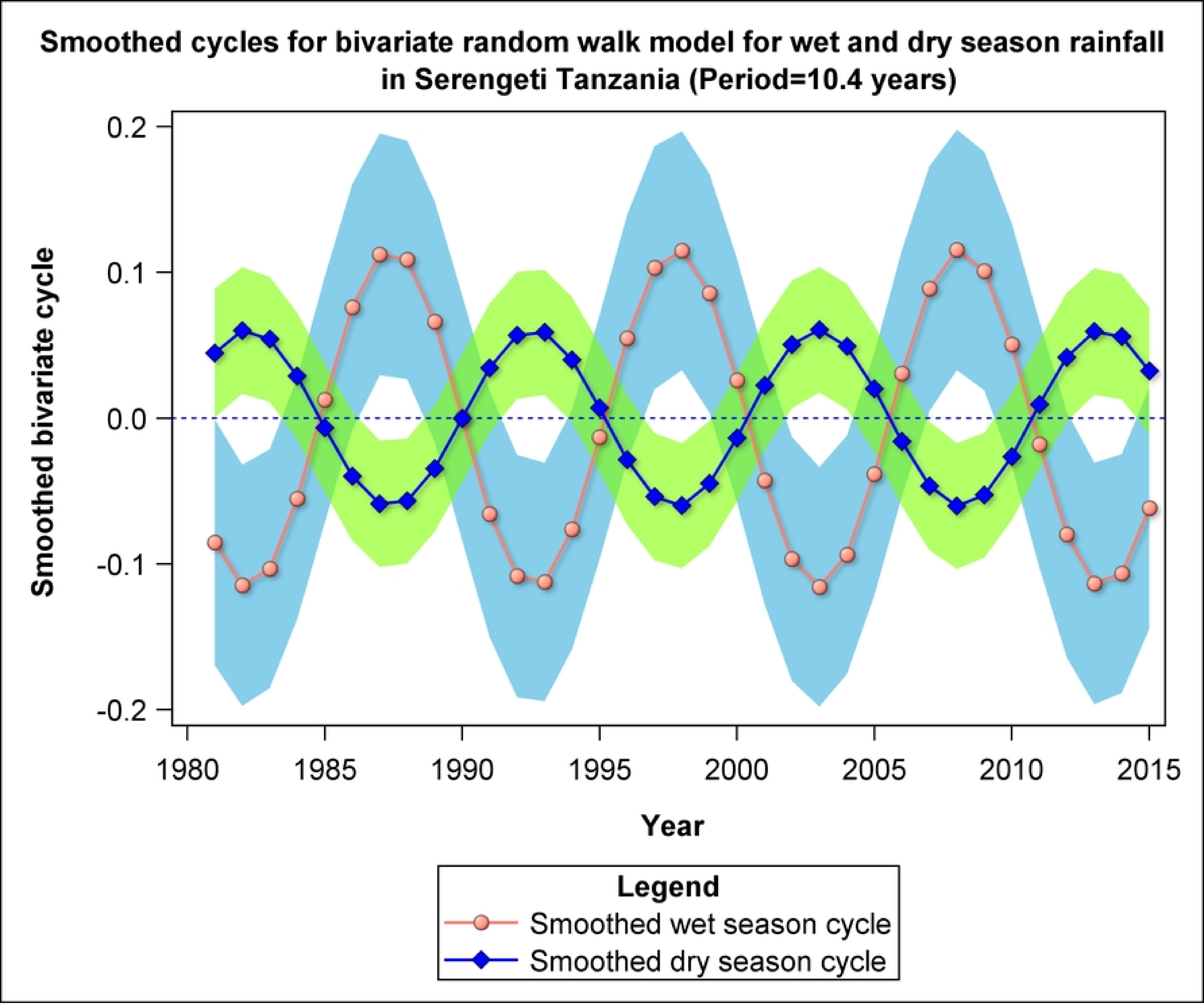

Smoothed cycles for bivariate random walk model for wet and dry season rainfall in Serengeti Tanzania (Period=10.4 years)
0.2
0.1
0.0
-0.1
-0.2
Smoothed bivariate cycle
1980
1985
1990
1995
2000
2005
2010
2015
Year
Legend
Smoothed wet season cycle
Smoothed dry season cycle

Figure 10b

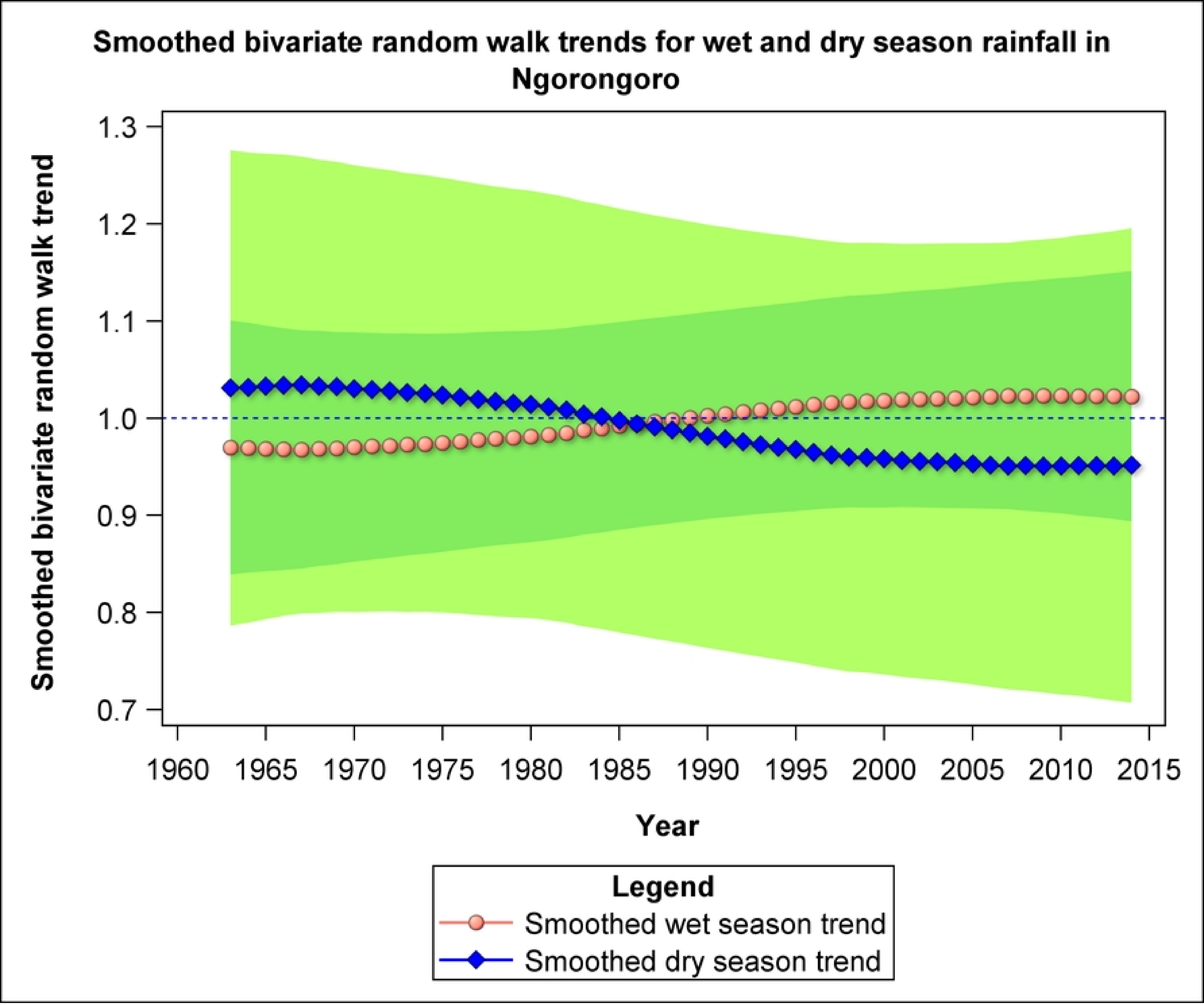
Smoothed bivariate random walk trends for wet and dry season rainfall in Ngorongoro
Smoothed bivariate random walk trend
1.3
1.2
1.1
1.0
0.9
0.8
0.7
1960
1965
1970
1975
1980
1985
1990
1995
2000
2005
2010
2015
Year
Legend
Smoothed wet season trend
Smoothed dry season trend

Figure 11a

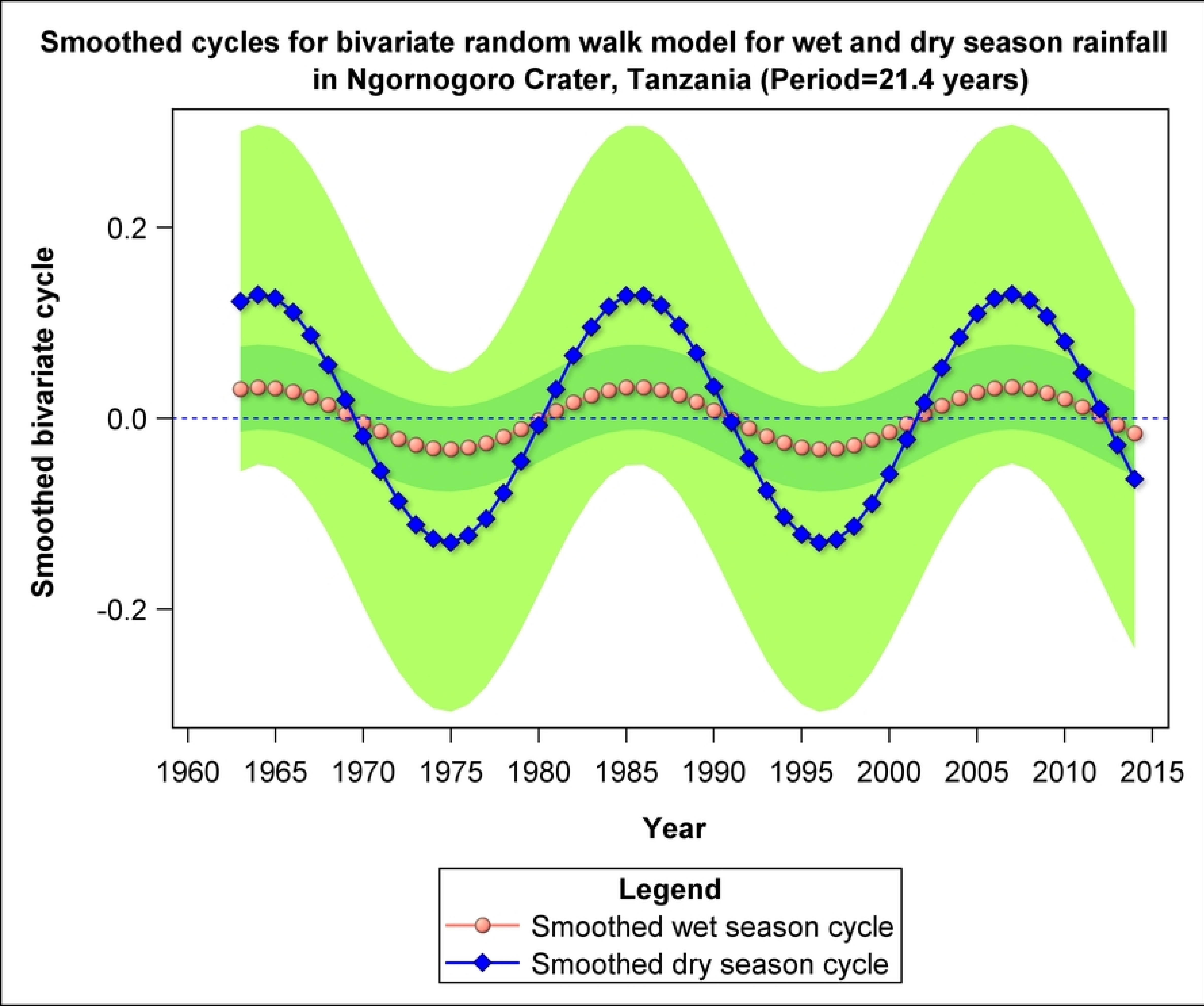

Smoothed cycles for bivariate random walk model for wet and dry season rainfall in Ngornogoro Crater, Tanzania (Period=21.4 years)
Smoothed bivariate cycle
0.2
0.0
-0.2
1960
1965
1970
1975
1980
1985
1990
1995
2000
2005
2010
2015
Year
Legend
Smoothed wet season cycle
Smoothed dry season cycle

Figure 11b

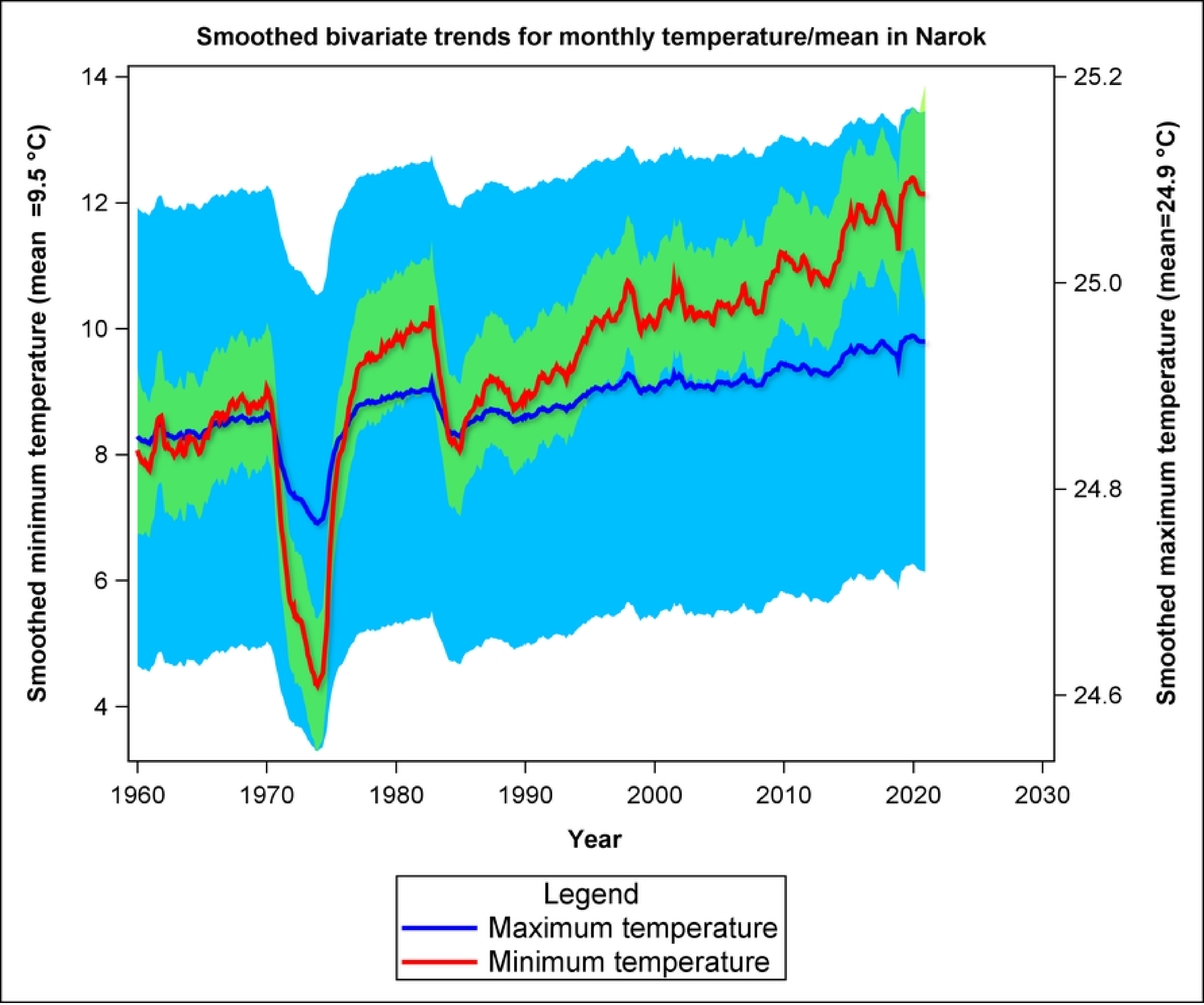
Smoothed bivariate trends for monthly temperature/mean in Narok
Smoothed minimum temperature (mean =9.5 °C)
Smoothed maximum temperature (mean=24.9 °C)
Year
14
12
10
8
6
4
25.2
25.0
24.8
24.6
1960
1970
1980
1990
2000
2010
2020
2030
Legend
Maximum temperature
Minimum temperature

Figure 12

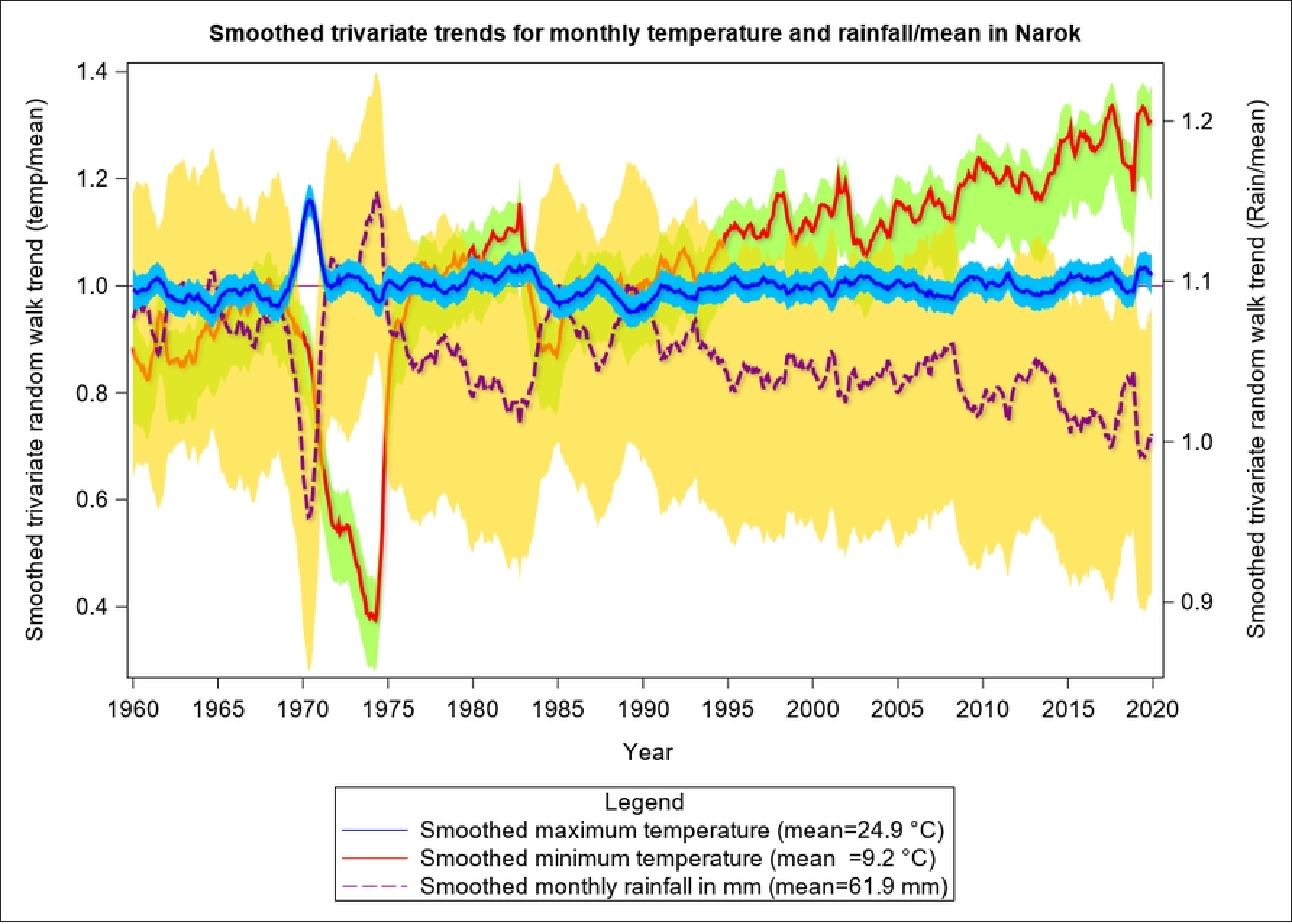

Smoothed trivariate trends for monthly temperature and rainfall/mean in Narok
Smoothed trivariate random walk trend (temp/mean)
Smoothed trivariate random walk trend (Rain/mean)
1.4
1.2
1.0
0.8
0.6
0.4
1.2
1.1
1.0
0.9
1960
1965
1970
1975
1980
1985
1990
1995
2000
2005
2010
2015
2020
Year
Legend
Smoothed maximum temperature (mean=24.9 °C)
Smoothed minimum temperature (mean =9.2 °C)
Smoothed monthly rainfall in mm (mean=61.9 mm)

Figure 13

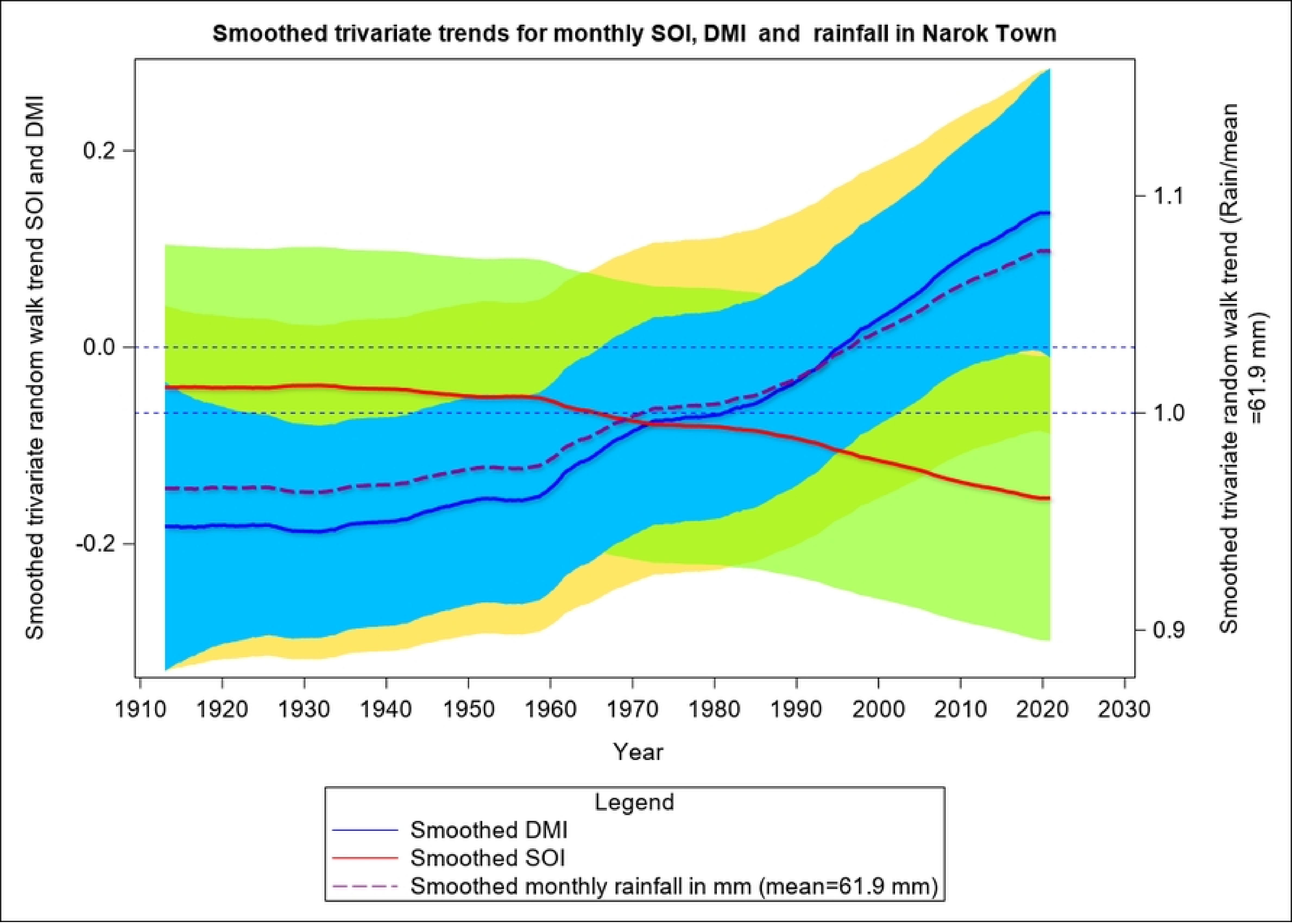
Smoothed trivariate trends for monthly SOI, DMI and rainfall in Narok Town
Smoothed trivariate random walk trend SOI and DMI
0.2
0.0
-0.2
Smoothed trivariate random walk trend (Rain/mean =61.9 mm)
1.1
1.0
0.9
1910
1920
1930
1940
1950
1960
1970
1980
1990
2000
2010
2020
2030
Year
Legend
Smoothed DMI
Smoothed SOI
Smoothed monthly rainfall in mm (mean=61.9 mm)

Figure 14

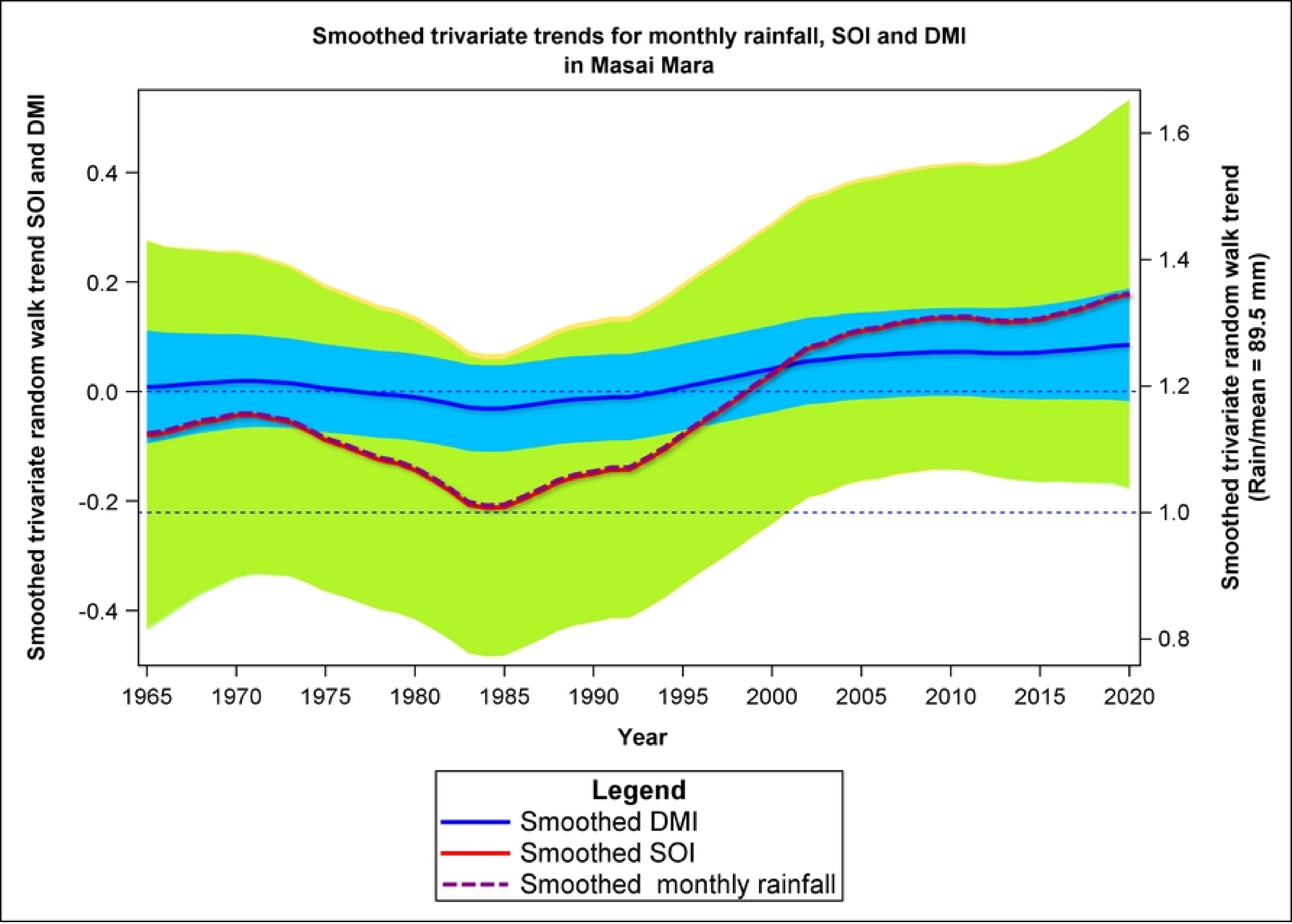

Smoothed trivariate trends for monthly rainfall, SOI and DMI
in Masai Mara
Smoothed trivariate random walk trend SOI and DMI
Smoothed trivariate random walk trend
(Rain/mean = 89.5 mm)
0.4
0.2
0.0
-0.2
-0.4
1.6
1.4
1.2
1.0
0.8
1965
1970
1975
1980
1985
1990
1995
2000
2005
2010
2015
2020
Year
Legend
Smoothed DMI
Smoothed SOI
Smoothed monthly rainfall

Figure 15

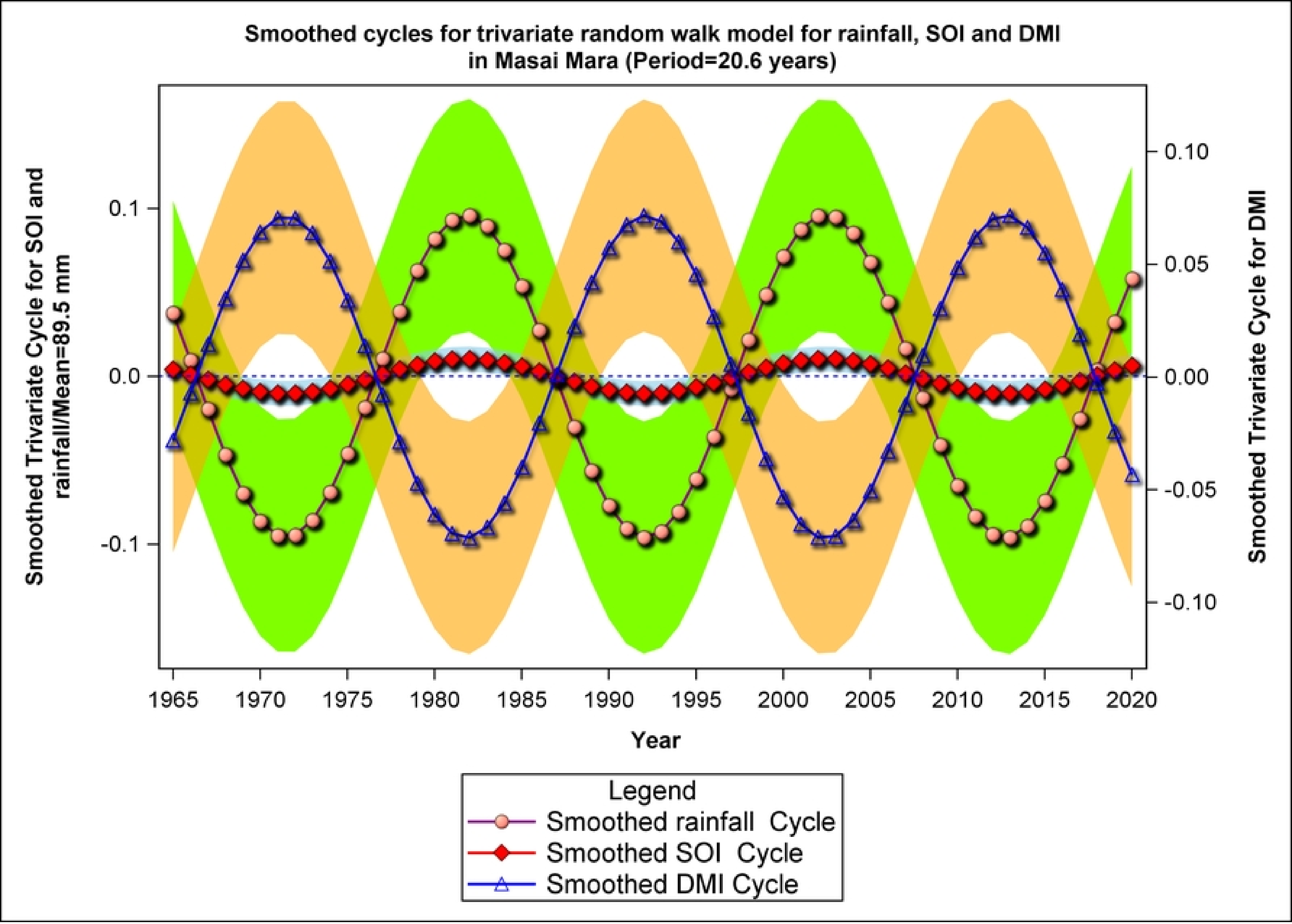
Smoothed cycles for trivariate random walk model for rainfall, SOI and DMI
in Masai Mara (Period=20.6 years)
Smoothed Trivariate Cycle for SOI and rainfall/Mean=89.5 mm
Smoothed Trivariate Cycle for DMI
0.1
0.0
-0.1
0.10
0.05
0.00
-0.05
-0.10
1965
1970
1975
1980
1985
1990
1995
2000
2005
2010
2015
2020
Year
Legend
Smoothed rainfall Cycle
Smoothed SOI Cycle
Smoothed DMI Cycle

Figure 16

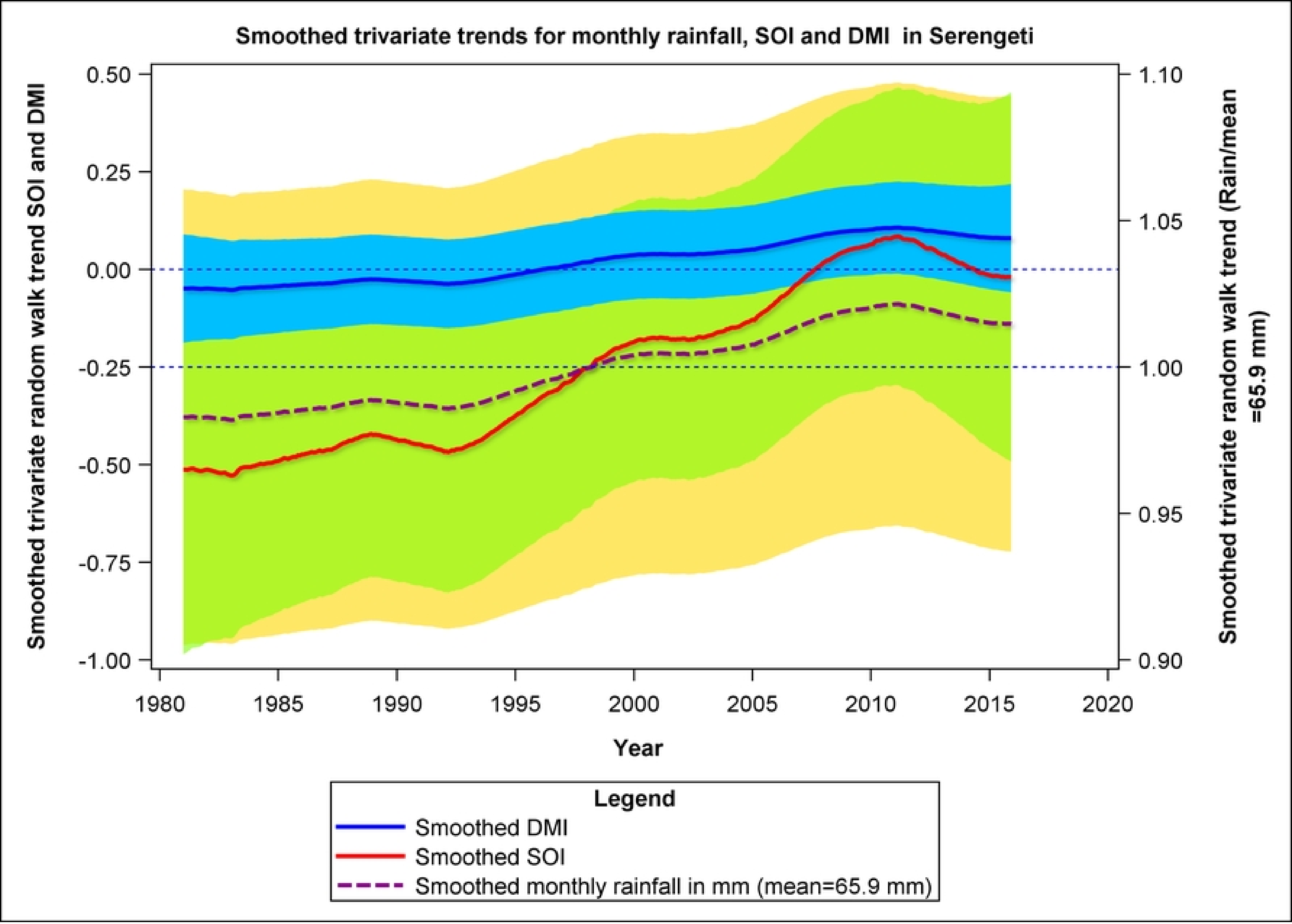

Smoothed trivariate trends for monthly rainfall, SOI and DMI in Serengeti
Smoothed trivariate random walk trend SOI and DMI
Smoothed trivariate random walk trend (Rain/mean =65.9 mm)
0.50
0.25
0.00
-0.25
-0.50
-0.75
-1.00
1.10
1.05
1.00
0.95
0.90
1980
1985
1990
1995
2000
2005
2010
2015
2020
Year
Legend
Smoothed DMI
Smoothed SOI
Smoothed monthly rainfall in mm (mean=65.9 mm)

Figure 17

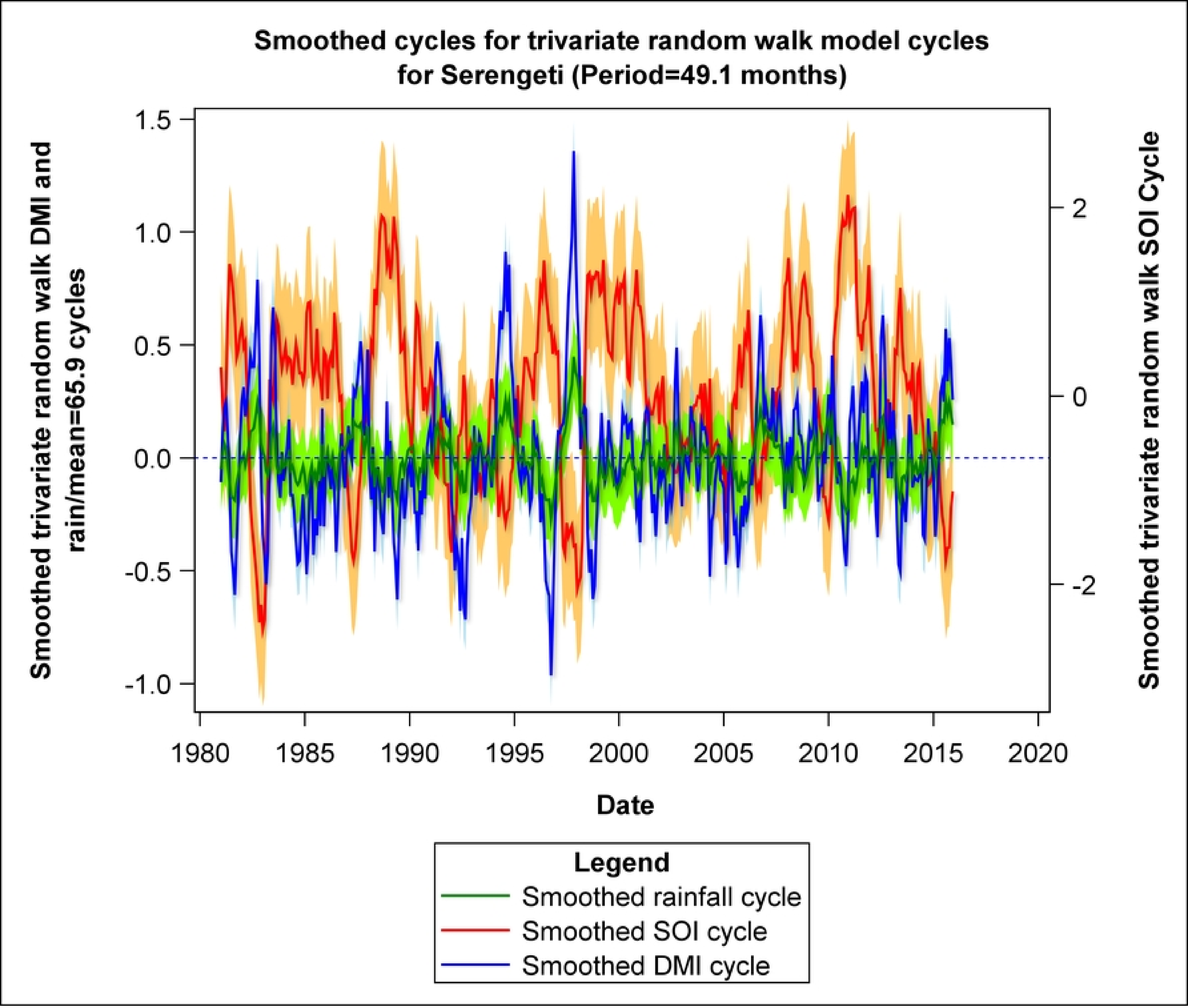
Smoothed cycles for trivariate random walk model cycles
for Serengeti (Period=49.1 months)
Smoothed trivariate random walk DMI and rain/mean=65.9 cycles
Smoothed trivariate random walk SOI Cycle
1.5
1.0
0.5
0.0
-0.5
-1.0
2
0
-2
1980
1985
1990
1995
2000
2005
2010
2015
2020
Date
Legend
Smoothed rainfall cycle
Smoothed SOI cycle
Smoothed DMI cycle

Figure 18

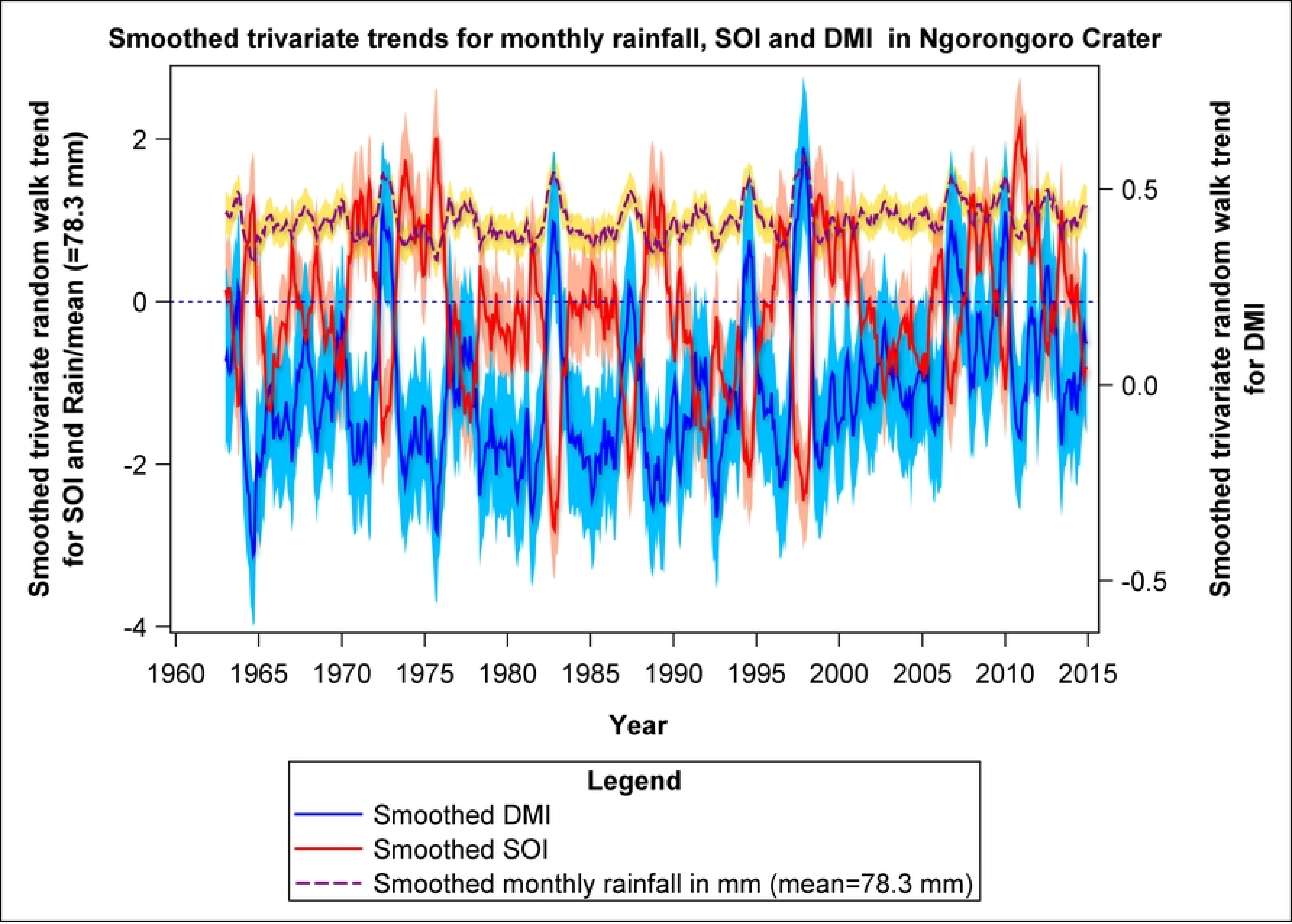
Smoothed trivariate trends for monthly rainfall, SOI and DMI in Ngorongoro Crater
Smoothed trivariate random walk trend for SOI and Rain/mean (=78.3 mm)
Smoothed trivariate random walk trend for DMI
2
0
-2
-4
0.5
0.0
-0.5
1960
1965
1970
1975
1980
1985
1990
1995
2000
2005
2010
2015
Year
Legend
Smoothed DMI
Smoothed SOI
Smoothed monthly rainfall in mm (mean=78.3 mm)

Figure 19

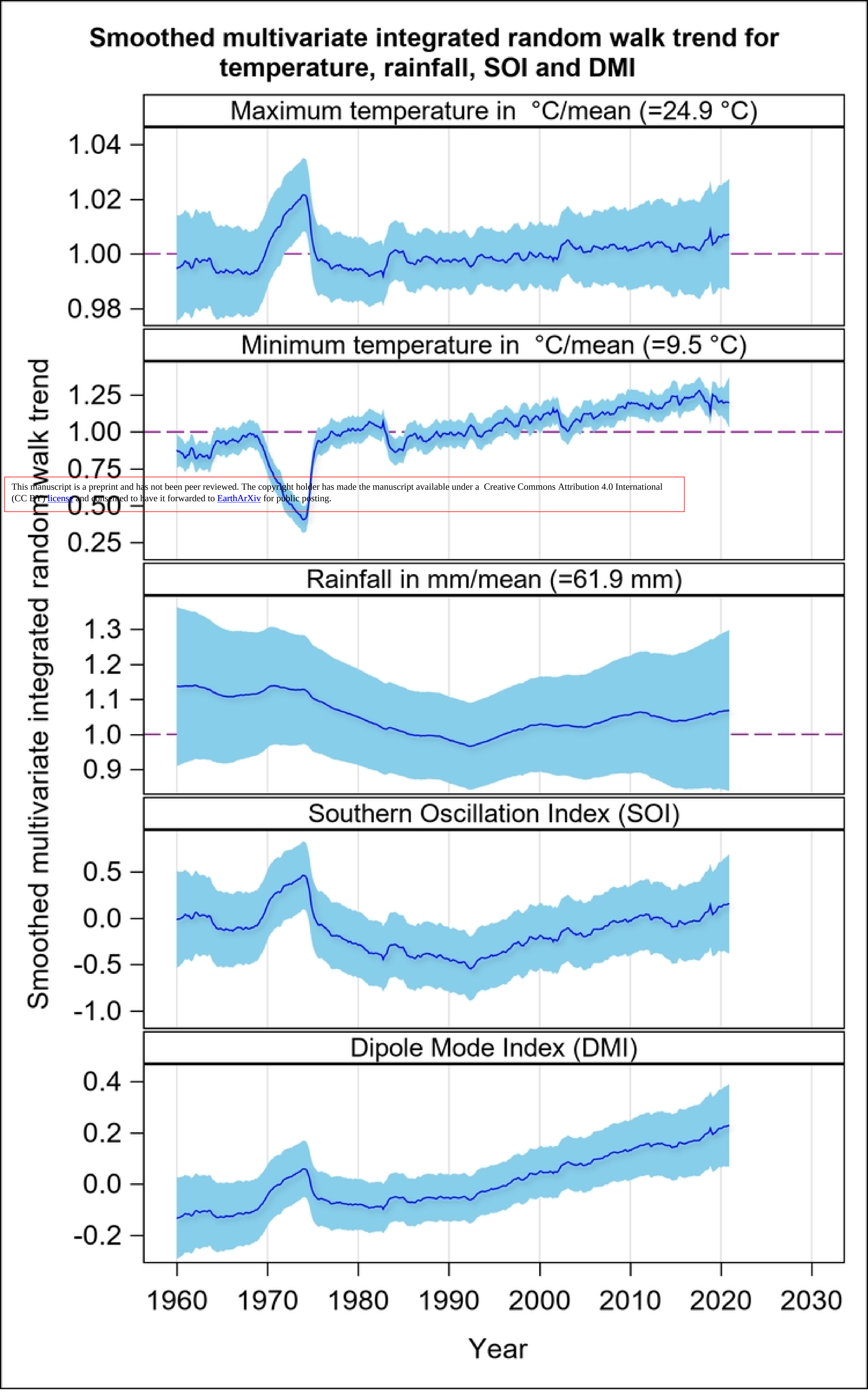

This manuscript is a preprint and has not been peer reviewed. The copyright holder has made the manuscript available under a Creative Commons Attribution 4.0 International (CC BY) license and consented to have it forwarded to EarthArXiv for public posting.

Figure 20

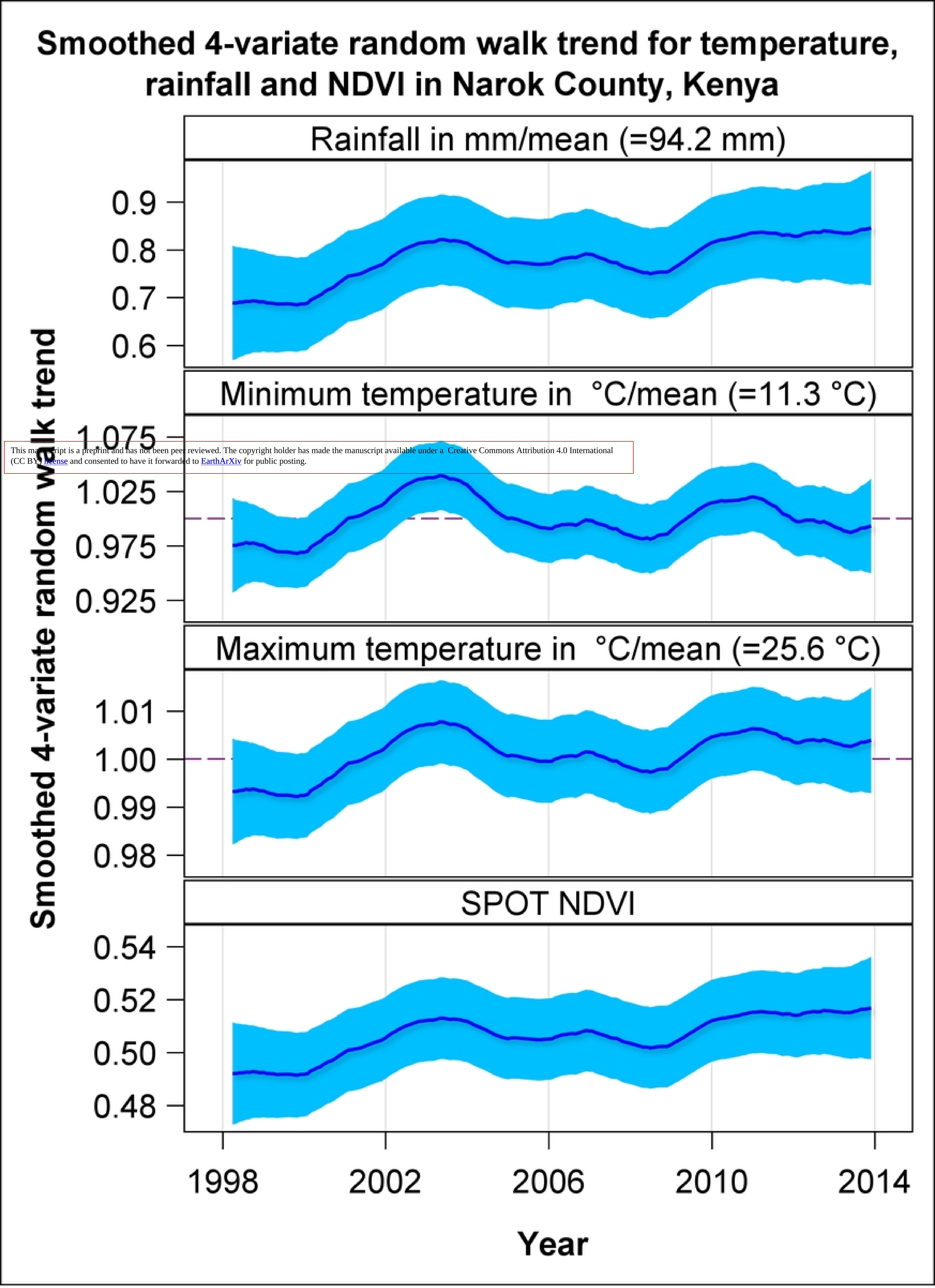

This manuscript is a preprint and has not been peer reviewed. The copyright holder has made the manuscript available under a Creative Commons Attribution 4.0 International (CC BY) license and consented to have it forwarded to EarthArXiv for public posting.

Figure 21